TECH LIBRARY KAFB, NM
0060639

NASA CONTRACTOR REPORT

NASA CR-1426
c. 1

LOAN COPY: RETURN TO
AFWL (WLOL-2)
KIRTLAND AFB, N MEX

FLIGHT TEST RESULTS OF A TRAILING EDGE FLAP DESIGNED FOR DIRECT-LIFT CONTROL

by Charles R. Taylor, Jr.

Prepared by
THE BOEING COMPANY
Seattle, Wash.
for Ames Research Center

NATIONAL AERONAUTICS AND SPACE ADMINISTRATION • WASHINGTON, D. C. • OCTOBER 1969

NASA CR-1426
TECH LIBRARY KAFB, NM
0060639

FLIGHT TEST RESULTS OF A TRAILING EDGE FLAP DESIGNED FOR DIRECT-LIFT CONTROL

By Charles R. Taylor, Jr.

Distribution of this report is provided in the interest of information exchange. Responsibility for the contents resides in the author or organization that prepared it.

Prepared under Contract No. NAS 2-4200 by
THE BOEING COMPANY
Seattle, Wash.

for Ames Research Center

NATIONAL AERONAUTICS AND SPACE ADMINISTRATION

For sale by the Clearinghouse for Federal Scientific and Technical Information
Springfield, Virginia 22151 – CFSTI price $3.00

CONTENTS

FIGURES

FLIGHT TEST RESULTS OF A TRAILING EDGE FLAP DESIGNED FOR DIRECT-LIFT CONTROL

by Charles R. Taylor, Jr.
The Boeing Company
Seattle, Washington

SUMMARY

A flight test investigation was conducted with the Boeing 707 prototype to obtain the performance characteristics of a trailing edge flap for direct-lift control (DLC). The flap was designed and tested by The Boeing Company for the National Aeronautics and Space Administration.

The flap system consisted of a main flap with blowing boundary layer control (BLC) and a slotted aft auxiliary flap for DLC. The auxiliary flap had a deflection range of 10^{o} up and 30^{o} down with respect to a faired position with the main flap. The DLC-null angle was 10^{o} down from the faired position.

Steady-state aerodynamic characteristics of the flap system were obtained from steady trimmed flight at several speeds plus slow deceleration to the stall. Airplane response and dynamics were obtained from step inputs to the auxiliary flap from their null setting. Similar maneuvers using wing spoilers for DLC also were accomplished.

The steady-state results showed that lift coefficient increments (ΔC_L) of about 0.30 to 0.40 generally were obtained with 40^{o} of auxiliary flap travel, while increments of 0.52 to 0.60 were noted with 15^{o} of spoiler travel. Thrust impingement and BLC both tended to increase the ΔC_L's of the flaps, whereas higher main flap settings decreased them. Incremental normal accelerations on the order of +0.10 and -0.12 g were obtained with $\pm 20^{\circ}$ flap steps from the null flap. Spoiler steps of $\pm 8^{\circ}$ from the null spoiler gave +0.22 and -0.10 g increments.

INTRODUCTION

A flight test program was conducted to investigate a trailing edge flap system designed for direct-lift control (DLC). The investigation was part of a program to develop and evaluate systems designed for noise abatement approaches to landing using low-power settings and/or steeper than conventional flight paths. The Boeing 367-80 airplane (KC-135/707 prototype) was used as the test vehicle for the program.

DLC has been proposed (refs. 1 and 2) as a means of improving longitudinal flight-path control and response. Direct control of lift at constant pitch attitude angle and/or airspeed requires the modulation of a control surface that will vary the lift on an airplane without a corresponding large pitching moment change. Two control surfaces that have been considered for DLC are trailing edge flaps and spoilers. Lowering the flaps or closing the spoilers from a DLC-null deflection angle will increase the lift. Conversely, raising the flaps or opening the spoilers from the null angle will reduce the lift. Thus, DLC enhances the handling qualities of an airplane by quickening its response in vertical motion to pilot or autopilot commands.

The test program was conducted in three phases. Phase I consisted of initial DLC flap design using NASA data from the Ames full-scale wind tunnel and preliminary flight investigation of noise abatement approaches. During a portion of the flight investigation, initial flap design characteristics of the DLC flap were simulated on the airplane. Phase II consisted of installation, airworthiness checks, and the initiation of inflight performance testing of the DLC flap system. Phase III consisted of additional flap performance testing and evaluation of DLC and other systems while performing normal and noise abatement approaches to landing. This report presents the results of the DLC flap performance testing accomplished in Phases II and III. Performance data obtained during Phase III using spoiler DLC are also included. A report of the systems evaluation conducted in Phases I and III of the program is presented in ref. 3. Reference 4 presents a comparison of the flight data presented in this report with wind tunnel results acquired by NASA in the Ames 40- by 80-foot tunnel using a 1/3-scale model of the 367-80. The wind tunnel results are documented in ref. 5.

SYMBOLS

C_D	Drag coefficient
C_L	Lift coefficient
$C_{L_{max}}$	Maximum lift coefficient
$C\mu$	Momentum coefficient
D	Drag, lb
dh/dt	Altitude change with time, ft/sec
dv/dt	Velocity change with time, ft/sec^2
F_G	Gross thrust, lb
F_N	Net thrust, lb
g	Acceleration due to gravity, ft/sec^2
h_i	Indicated altitude, ft
N_{CG}	Acceleration normal to body axis at center of gravity, g units
N_2	High-pressure compressor speed, percent

q	Freestream dynamic pressure, lb/ft^2
S	Wing area, ft^2
V	True airspeed, kn
V_e	Equivalent airspeed, kn
V_s	One g stall speed, kn
W	Gross weight, lb
W_a	Engine airflow rate, lb/sec
α	Body angle of attack, deg
δ_{am}	Ambient pressure ratio
δ_{aux}	Auxiliary flap deflection, deg
δ_e	Elevator deflection, deg
δ_{sp}	Spoiler deflection, deg
δ_{t_2}	Engine inlet total pressure ratio
θ	Body pitch attitude, deg
θ_{am}	Total air temperature ratio

ABBREVIATIONS

BLC	Boundary layer control
DLC	Direct-lift control
MCT	Maximum continuous thrust
PLF	Power for level flight
SAS	Stability augmentation system

DESCRIPTION OF TEST AIRPLANE

The Boeing Model 367-80 (fig. 1) has been used as a developmental test bed for several company programs and for NASA research studies. Figure 2 presents a two-view drawing of the airplane with pertinent geometrical data. The following paragraphs describe the various systems which made up the test airplane.

Trailing Edge Flaps

The trailing edge flap system consisted of a main flap with blowing boundary layer control (BLC) and an aft auxiliary slotted-type flap for direct-lift control. Both the main and auxiliary flaps were simple-hinged assemblies that extended along 68 percent of the wing span. The flaps were modified for Phase III by removing that portion of the original

BLC flap aft of the flap rear spar (about 40 percent flap chord removal) and installing the auxiliary flap. A detailed description of the original BLC flap is given in ref. 6. Figure 3 shows a three-quarter rear view of the flap assembly.

BLC System

Boundary layer control was provided by blowing high-pressure engine bleed air through a spanwise slot in the wing over the upper surface of the main flap. The slot was part of an ejector system which allowed secondary underwing air to mix with the primary bleed air to increase the mass flow of air for blowing. The engine bleed air was ducted from the high-pressure compressor of each engine to the ejector. A series of modulating and shutoff valves in the supply duct system allowed the bleed air to be controlled from the cockpit. The BLC system is shown in fig. 4 and discussed in detail in ref. 6.

DLC Flap System

The auxiliary flap was divided into three spanwise segments per side, namely a 30-inch-chord inboard and center flap and a 22-inch-chord outboard flap. Each flap segment had a deflection range of 10° up and 30° down (40° total travel) with respect to a faired position with the main flap. For this program, the DLC-null deflection angle was 10° down from the faired position, thus allowing 20° of travel in either direction for lift control. (Note: All auxiliary flap deflection angles noted in this report are with respect to the faired position with the main flap, down flap being positive deflection.) Figure 5 shows a planform view of the DLC flaps; details of the flap are presented in fig. 6 and discussed in ref. 7.

Since the auxiliary flaps acted as primary control surfaces, they required high deflection rates. The flaps had an instantaneous (no load) surface deflection rate of 40° per second and a loaded rate of about 29° per second. Lower deflection rates, about 15° per second, were noted for the center auxiliary flap at high power due to the impingement of the inboard engine. Each flap segment was controlled through an external, dual tandem, electrohydraulic actuator mounted between the main and the auxiliary flap. The actuators were of the type used to power the elevators on the Boeing 727 airplanes. An underwing photograph of the actuators is shown in fig. 7.

DLC Spoiler System

The spoiler system for DLC consisted of five spoiler panels per side. Each panel had a deflection capability of 8° in either direction from the DLC-null setting of 8°. Thus, the spoilers were closed for full "airplane up" DLC and were raised 16° from the flush position for full "airplane down" DLC. Their deflection rates were about 55° per second. Spoiler

roll inputs could be applied to the outboard four panels simultaneously with the resultant spoiler deflection reflecting the algebraic sum of the roll and DLC inputs. The innermost panel was used for DLC only. A planform view of the DLC spoiler system is shown in fig. 5.

Powerplants

Four Pratt and Whitney JT3D-1 bypass turbofan engines were used to power the airplane. The inboard engines were situated so that engine exhaust air impinged on the trailing edge flaps, mainly the center auxiliary flap. Figure 8 shows a sketch of the inboard engine/flap relationship. Engine performance characteristics are noted in Appendix A.

Leading Edge Devices

Wing leading edge devices consisted of a cambered flap extending from the inboard engine strut halfway to the fuselage and a cambered slat extending outboard from the inboard engine strut to the wing tip. In addition, a cambered slat was installed on the horizontal tail leading edge for increased trim capability. All leading edge devices were in a fixed position.

Variable Stability System

The 367-80 airplane is capable of simulating other airplanes through its variable stability system, which consists of an on-board analog computer/interface system. The system was not used as such during this program; however, during the basic aerodynamic performance testing of the flap, the computer operator controlled both the desired fixed auxiliary flap deflections and the desired flap step inputs for dynamic evaluation. Fixed spoiler positions and spoiler steps were also controlled from the computer.

Instrumentation

Extensive instrumentation to measure aerodynamic and performance characteristics was installed on the airplane. Vanes were installed on a 17-foot nose boom to measure angles of attack and sideslip. Transducers were used to measure angles, rates, accelerations, pressures, control positions, and various electronic measurements.

Data were recorded by pulse duration modulation (PDM) and narrowband frequency modulation (NBFM) data recording systems on magnetic tape. The PDM system was used to record static and quasi-static data at a rate of 2.5 samples per second. The FM system was used to record dynamic data in frequency ranges up to 110 Hz. Data reduction was

accomplished at the Boeing-Wichita facilities using computer programs developed by Boeing-Seattle Flight Test. The computer runs were made in Wichita using an emulator to convert the computer program to the Wichita computer system.

In addition, static and dynamic data were recorded on two 50-channel oscillographs of the galvanometer type.

TEST PROCEDURES

The gross weight of the airplane during all test maneuvers ranged between 145,000 and 175,000 pounds. Center of gravity travel was about 30 (±1) percent of the mean aerodynamic chord. All airwork for the performance testing was conducted at altitude, in general, below 10,000 feet.

Direct-Lift Control Flaps

Steady-state testing.—Steady-state lift and drag characteristics of the DLC flap system were obtained from stall-type maneuvers. For these conditions, the main and auxiliary flaps and power were held fixed throughout each maneuver. The airplane was trimmed at several diminishing airspeeds in the desired flap/power/BLC configuration until stall buffet was reached. Ten to fifteen seconds of stabilized data were obtained at each trim speed. With the onset of buffet, airspeed was slowly reduced using elevator only until a 1-g stall occurred. At this point, the condition was terminated with normal stall recovery.

Steady-state data were obtained at auxiliary flap deflections of 30° (full-down DLC flap), 10° (DLC-null angle) and -10° (full-up DLC flap). Main flap angles were set at 30°, 40°, and 50°. Engine power settings ranged from idle to maximum continuous thrust (MCT) to note impingement effects. Both BLC on and off configurations were tested.

Dynamic testing.—Transient response characteristics of the airplane were obtained from step inputs to the auxiliary flaps. The airplane was trimmed in the desired configuration with the auxiliary flaps at their 10° null setting. After the flightpath had been established and stabilized by the pilot, the autopilot was engaged, and the desired incremental step deflection was made to the auxiliary flaps from the computer/interface. Aircraft motion and data were recorded for about 10 seconds following the step. No pilot inputs were made during this time.

Dynamic testing was conducted at main flap deflections of 30°, 40°, and 50°. Power settings ranged from idle to maximum continuous thrust. Both BLC on and off conditions were tested.

Direct-Lift Control Spoilers

Steady-state testing.—Steady-state lift and drag characteristics of the DLC spoiler system were obtained from stall maneuvers similar to the flap configuration stalls. Data were obtained at spoiler deflections of 0 (closed), 5^{o}, 10^{o}, and 15^{o} with the main/auxiliary flaps set at $40/10^{o}$ and the BLC on.

Dynamic testing.—Transient response characteristics of the DLC spoiler system were obtained from step inputs to the spoilers. The maneuvers were accomplished in the same manner as were the flap step maneuvers. Step inputs of 4^{o} and 8^{o} were made in both directions to the spoilers from their DLC-null setting of 8^{o} up from the flush position. A main/auxiliary flap configuration of $40/10^{o}$ was used with 90 percent N_2 power and the BLC on.

RESULTS AND DISCUSSION

Direct-Lift Control Flaps

Steady-state characteristics.—The results of the stall-type maneuvers in which steady trimmed data were obtained are presented in the form of lift curves and drag polars in Figures 10 through 22. Equations for the coefficients of lift and drag and measured values of momentum coefficient are shown in Appendix B. The lift curves may be used to determine the flap effectiveness for DLC by noting the lift change at constant angle of attack with auxiliary flap deflection. Incremental lift for full "airplane-up" DLC is the change in lift coefficient (ΔC_L) between the null-flap setting (10°) and full-down auxiliary flap (30°). Decremental lift for full "airplane-down" DLC is the ΔC_L between the null setting and full-up flap (-10°). Total DLC capability, as seen in the sketch in fig. 9, is the ΔC_L between full-down and full-up flap. The steady-state results will be discussed in terms of the total DLC capability. (Note' For this discussion, ΔC_L will be taken at constant angle of attack, although in actual use of DLC during a landing approach, the airplane most likely would not maneuver under constant α conditions.) The drag polars may be used to show the corresponding drag change with flap deflection.

Data were obtained at several engine power settings to note thrust impingement effects. Power settings will be referred to in this discussion in percentage terms of the approximate high-pressure compressor speed, N_2, where 100 percent N_2 = 9655 rpm. Idle power is about 57 percent N_2. Engine characteristics are given in Appendix A.

Figures 10 and 11 present data with 30^{o} main flaps and no BLC blowing. Power settings are at idle and power for level flight (PLF). (Note: All PLF configurations were set with level flight occurring at the initial trim speed with the auxiliary flaps at their

DLC-null angle of 10^{o}. As a result, approximately the same power setting was used for all auxiliary flap angles tested at a fixed main flap setting.) It may be noted at the lower α's commensurate with landing approach that a total ΔC_L of 0.36 is available for DLC at idle power. With power for level flight, the total ΔC_L is 0.40, an increase of about 18 percent over idle power. The increased DLC flap effectiveness arises from a higher magnitude of lift at the 30^{o} auxiliary flap setting with increased power due to impingement effects.

Figures 12 and 13 show data with 30^{o} main flaps and the BLC on. Power settings are 60 percent N_2 and PLF , respectively. (Note: A 60 percent N_2 setting was only a small percentage over idle power, but it was used to provide slightly more engine bleed air for blowing and better engine response. It may be termed a BLC idle setting.) The data show a total ΔC_L of 0.40 available for lift control at both power settings. The reason that PLF does not increase the total ΔC_L is that the increased impingement and blowing associated with the higher power increased the lift magnitude of both full-up and full-down flap by the same amount, so that the ΔC_L between the two remains the same. The higher power increases to a greater extent the lift acting on the 10^{o} null flap, so that the incremental lift for "airplane-up" DLC (ΔC_L between 10^{o} and 30^{o} flaps) is reduced and is increased for "airplane-down" DLC (ΔC_L between -10^{o} and 10^{o} flaps).

Figures 14 and 15 present data with 40^{o} main flaps and no BLC. Power settings are idle and PLF, respectively. It may be noted that DLC flap effectiveness at this main flap setting is less than at 30^{o} main flaps. The total ΔC_L is only 0.25 at idle power. With PLF, the total ΔC_L available rises to 0.28. Again, incremental lift for "airplane-up" DLC is reduced and is increased for "airplane down" DLC because of a more effective lift increase with power at 10^{o} null flap.

Figures 16 and 17 show data at 40^{o} main flaps with blowing BLC. Power settings of 60 percent N_2 and PLF show total ΔC_L's of 0.34 and 0.38, respectively. These figures represent an increase in total DLC capability of about 35 percent over the no-blowing 40^{o} main flap configuration at similar power settings. Since impingement effects should be about the same at similar power settings, the increase in DLC capability must be attributed to BLC.

Figures 18 and 19 present data with 50^{o} main flaps and no blowing at power settings of idle and PLF, respectively. Only "airplane-up" DLC capability is presented, since only 10^{o} and 30^{o} auxiliary flap data are shown. Time prevented testing at the -10^{o} angle. It may be seen that this "airplane-up" capability with idle power at this main flap setting is quite poor compared with that of 30^{o} and 40^{o} main flaps. With PLF, this capability increased to approach the "airplane-up" capability of the 40^{o} main flap with PLF configuration.

Figures 20, 21, and 22 present data at 50^{o} main flaps with BLC at power settings of 60 and 90 percent N_2 and maximum continuous thrust (MCT), respectively. With 60 percent N_2, the total ΔC_L is 0.30, whereas values of 0.40 and 0.34 are achieved for

30 and 40° main flaps, respectively. With MCT, which is approximately level flight power for 50° main flaps and nominal gross weight, the total ΔC_L rises to 0.42 because of increased blowing and power effects. This value compares favorably with the respective values of 0.40 and 0.38 for PLF configurations at 30° and 40° main flaps. It should be noted that the trailing edge flaps are situated more in the path of the engine exhaust stream at the 50° setting, which leads to increased impingement effects.

Figure 23 presents a bar chart of the incremental lift attained with full-flap deflection from the 10° null setting for the various configurations. Total ΔC_L's may be noted by the whole length of each bar.

$C_{L_{max}}$ was not obtained for all configurations, for several reasons. In most cases, heavy buffet occurred before peak maximum lift, making data measurement difficult and, as will be discussed later, some stall conditions were terminated early because of low altitude. The foregoing discussion on DLC flap effectiveness, therefore, was centered around the ΔC_L's at the lower angles of attack typical of landing approach. It may be noted for most of the configurations, however, that these incremental lift values remain nearly constant with angle of attack. The result of this is that maximum lift and, hence, stall speed, vary with auxiliary flap deflection at fixed power. This signifies that the safety margin for landing approach will change with use of the flaps for DLC.

Initial buffet generally occurred for all flap configurations at about 11° of angle of attack at a moderate level. The buffet intensity increased with α and was rather heavy at 14° to 15° α.

During the approach and landing evaluation phase of this program, the approach speeds were taken as 1.3 times the minimum speeds attained for a fixed main flap configuration with 10° DLC null flaps and power for a 3° approach. This safety margin was reduced somewhat with up-auxiliary-flap deflection. However, some of the margin was recovered in that up-flap deflection commanded "airplane-down" and, therefore, less than 1-g flight. In any event, the margin appeared adequate for normal operations.

Figures 10 through 22 also present drag polars for the various DLC flap configurations. The polars show decreased drag with up-auxiliary-flap deflection and increased drag with down-flap deflection. The changes in drag do not appear to be as dependent upon main flap angle, power setting, and BLC as the changes in lift. For the most part, ΔC_D values of about ±.04 at constant α are noted for full-flap deflections from the null setting in the normal operational area.

As noted above, the use of flaps for DLC results in an unfavorable speed/drag relationship in that an increase in lift (down-flap) simultaneously results in an increase in drag, and vice versa. The effect of this is to increase or decrease the lift/drag ratio when exactly the opposite is desired. For example, for an airplane below the glide slope, the pilot would command an "up-airplane" (down-flap) signal. The immediate increase

in lift from the flap would initially cause the desired action. However, the increase in drag with time would cause a long-term effect of an undesired steeper flightpath unless power was added. Thus, an autothrottle system to reduce pilot workload would be beneficial, if not essential, to such a DLC system.

It will be noted that some scatter exists in the drag data, especially at lower power settings. This was due primarily to the method of steady-state testing. The test procedure at low engine power was to initially trim the airplane at 10,000 feet altitude and obtain data for a series of airspeeds during descent. With low power, i.e., high rates of descent, data were recorded during short intervals of time at each airspeed so that the given configuration could be completed during a single pass in order to conserve time. However, with high descent rates, turbulent air conditions, and inadvertent pilot inputs, this sometimes produced unrealistic dh/dt values for drag computation because of the tapeline method of fitting altitude change with time. Since the dh/dt term in the drag equation is a greater proportion of the total drag with low power and high descent, small offsets in dh/dt can produce corresponding offsets in drag. At higher power settings where rate of descent was closer to zero, data were recorded during longer intervals of time so that more accurate dh/dt values were produced. This plus the fact that the dh/dt term was now a lesser proportion of the total drag resulted in less scatter at these power settings. In all cases, the drag polars have been smoothly faired rather than connected point by point.

This method of testing also affected maximum lift in some cases. The stall point for some configurations occurred at low altitude and, for obvious reasons, the airplane was taken close to but not completely through stall.

No quantitative pitching moment data were obtained. However, a discussion on pitching moments with auxiliary flap deflection is provided in a later section.

Dynamic characteristics.—Figures 24 through 41 show airplane response to $\pm 10^{\circ}$ and $\pm 20^{\circ}$ auxiliary flap step inputs. The data are presented in the form of time history plots that show pitch attitude, elevator deflection, equivalent airspeed, and normal acceleration. The step inputs were made to main flap/power configurations similar to those tested during the stall maneuvers.

The elevator deflection was due to a pitch axis stability augmentation system (SAS) in the autopilot mode that was mechanized to improve the airplane's handling qualities during the landing approaches. The SAS essentially held pitch attitude constant through the primary longitudinal controls, i.e., the elevators, using pitch angle and pitch rate as feedback. This system was used during the dynamic testing. It may be noted from the time histories that usually some small change in pitch attitude did occur, mainly because of feedback gain limitations inherent in this type of SAS. In general, the system overcompensated so that a small airplane nose-up attitude change occurred with a down-flap step and a nose-down attitude change occurred with an up-flap step.

As noted earlier, no pitching moment data were obtained during the stall maneuvers. However, pitching moment changes with auxiliary flap deflection are small. The elevator traces show that 4^{o} to 5^{o} of elevator are sufficient to balance the moments with 20^{o} full-flap steps, which is well within the capability of the elevator system. Elevator requirements for constant pitch attitude are even less than shown on the elevator traces because of the overcompensation of the SAS (nose-up pitch accompanies down-flap step).

It may be noted that with a down-flap input, i.e., a lift increase, airspeed was reduced. Conversely, airspeed increased with an up-flap step. In general, speed changes of 3 to 4 knots may be seen with full-flap steps for most configurations 5 seconds after the step.

Normal acceleration data in terms of g units are shown for the airplane center of gravity. The data show airplane response occurring almost instantaneously with the flap step. In general, peak increments of about +0.10 (down-flap) and -0.13 g (up-flap) may be noted with full-flap steps for most conditions regardless of main flap or power settings. Down-flap data may have been penalized slightly at the higher power settings because of reduced deflection rates on the center auxiliary flap from engine impingement.

The variation in the normal acceleration trace reflects the change in lift as a result of the flap step. An approximation of the lift change is given by the equation

$$\Delta C_L = \Delta N_{CG} \times C_{L_{trim}}$$

where ΔN is the incremental normal acceleration from 1-g flight. It may be noted that the ΔC_L's from the flap steps as obtained by the above equation are slightly lower in magnitude than the ΔC_L's from the static maneuvers for similar configurations. This trend may be seen in figs. 42 and 43, which show the incremental lift from both the static and dynamic maneuvers for the conditions of 30^{o} main flap, idle power, and BLC off. The static ΔC_L's on these two plots represent the increment in lift at constant α between the DLC null flap and full-down or full-up flap from fig. 10, whereas the dynamic ΔC_L's are the result of $\pm 20^{o}$ flap steps. For this particular configuration, the dynamic ΔC_L for the down-flap step was 80 percent of the static value. For the up-flap step, the dynamic ΔC_L was 90 percent of the static value.

As discussed in detail in Reference 4, several factors contribute to this difference. The normal acceleration increment due to the flap step results in a vertical velocity and hence an angle-of-attack change. Since the flap requires a finite time to reach its commanded deflection, some angle-of-attack change will have occurred in a direction to reduce the peak lift increment. Additionally, uncommanded pitch attitude changes and the opposing lift due to the elevator deflection required for flap pitching moment compensation contributed to the loss of lift. Wing bending, accelerometer characteristics, and other second order effects probably account for the remainder of the decrement in maximum acceleration.

Altitude response.—The primary function of DLC in a landing approach is flightpath control, i.e., control of height during approach. In conjunction with the flap steps of figs. 24 through 41, time histories of altitude response to the steps are presented in figs. 44 through 61. These plots show indicated pressure altitude with time before and after the steps. (Note: The arrow denoting the time of the flap step has been moved one second to the right to account for lag in the barometric system.) The dashed line on each plot represents the initial flightpath, i.e., the rate of descent before the step input, so that the change in height due to the step can be noted. In general, height changes of about 40 to 50 feet were attained 5 seconds after full 20° steps; fig. 54 shows the largest height change. However, examination of its corresponding time history (fig. 34) shows substantial elevator activity and a nose-up pitch change occurring before the step. In all probability, the airplane was in an untrimmed state prior to engagement of the autopilot mode.

It may be noted from the altitude time histories that changes to the flightpath occurred almost instantaneously with the steps. This response to the flap inputs makes the DLC system highly effective for touchdown control during flare and for arrestment of high descent rates.

Direct-Lift Control Spoilers

Steady-state characteristics.—DLC characteristics using spoilers are presented in figs. 62 and 63 with 85 and 95 percent N_2 power settings, respectively. These engine ratings give approximately 3° descent and level flight power, respectively, with $40/10^{\circ}$ flaps (main/auxiliary) and BLC on. Lift and drag characteristics are shown for spoiler deflections of 0°, 5°, 10°, and 15°. The lift data show a total ΔC_L capability of 0.52 at 85 percent N_2 and of 0.60 at 95 percent N_2 with the major portion of the lift change taking place in the first 10° of spoiler travel from the flush position. Figure 64 presents a bar chart of the lift changes with spoiler deflections from the spoiler-closed position.

Maximum lift characteristics with spoilers are slightly different from those with the flaps. It may be remembered that the ΔC_L due to flap deflection remained nearly invariant with angle of attack through the stall. The data for the spoilers, however, show that the lift change with spoiler deflection varies with α, becoming less as the stall is approached.

The drag characteristics from the polars show decreased drag (at constant α) with up-spoiler deflection. This trend results from an induced drag reduction. The data show total ΔC_D's at constant α of about 0.06 to 0.08 occurring in the operating region. The use of spoilers for DLC at constant speed results in a favorable speed/drag relationship in that an increase in lift (down spoiler) simultaneously gives a decrease in drag and vice-versa.

Dynamic characteristics.—Figures 65 and 66 present time histories to $\pm 4^{\circ}$ spoiler steps. Figures 67 and 68 present time histories to $\pm 8^{\circ}$ steps. All steps were made from a spoiler null setting of 8° up from the closed position. It may be noted that airspeed decreased with down spoilers and increased with up spoilers. The data show little

airspeed change with the 4° steps for a 5-second interval after the step. With full-spoiler steps, however, airspeed changes of 3 knots are shown. The autopilot SAS overcompensated with the down-spoiler steps, so that a 2° nose-up attitude change occurred. The system, however, worked well with the up-spoiler steps with no resultant pitch change after the step.

Peak normal acceleration increments of +0.17 and -0.08 g may be seen with the 4° steps. With full-spoiler steps, increments of +0.23 and -0.10 g are shown. It may be remembered that the variation in normal acceleration reflects the change in lift as a result of the step. Figures 69 and 70 show that the incremental lift from the full-spoiler steps is about 55 percent of the incremental lift from the steady-state tests. (Since the static maneuvers were not conducted at the 8° spoiler null setting and the 16° full-up position, interpolation and extrapolation were used to obtain the estimated ΔC_L's for these two settings. The steady-state data are shown for 85 and 95 percent N_2 test conditions. The spoiler steps were conducted with 90 percent N_2.) As discussed earlier, the angle-of-attack change due to the normal acceleration increment and other effects probably contribute to the reduced dynamic lift. In addition, spoiler activity may change the ejector flow and, hence, BLC characteristics.

Altitude response.—In conjunction with figs. 65 through 68, time history plots of altitude response to the spoiler steps are presented in figs. 71 through 74. Again the arrow denoting the time of the step has been moved 1 second to the right to account for barometric system lag. With full ±8° spoiler steps, height changes of +75 and -50 feet are attained after a 5-second interval. It may be noted that flightpath change occurs almost instantaneously with the step.

CONCLUSIONS

The following conclusions were drawn from the results of this investigation:

- In general, steady-state total ΔC_L levels of about 0.30 to 0.40 (at constant α) were noted with full auxiliary flap travel (40°) for the majority of configurations tested. The ΔC_L levels ranged from 0.25 (40° main flap and idle power) to 0.42 (50° main flap and maximum continuous power with BLC). The ΔC_L levels generally decreased with higher main-flap deflection at fixed power settings.

- Thrust impingement from both the inboard engines and BLC tended to increase the steady-state ΔC_L capability by as much as 10 and 38 percent, respectively.

- Incremental normal acceleration capability on the order of 0.22 g total (+0.10 and -0.12 g from the DLC null flap) was obtained with ± 20° auxiliary flap steps during dynamic maneuvers. Slow actuation on the center auxiliary flap due to impingement may have reduced the acceleration capability of the down-flap steps at high power settings.

- Changes in lift due to the flap steps were lower by 10-20 percent for the 20^{o} step cases than their corresponding steady-state ΔC_L's. The reduced peak acceleration is believed to result from angle-of-attack variation and unsteady aerodynamic effects.

- Steady-state ΔC_L levels of about 0.52 to 0.60 were obtained with 15^{o} of spoiler DLC at various power settings and $40/10^{o}$ main/auxiliary flaps.

- Incremental normal acceleration capability of about 0.32 g total (+0.22 and -0.10 g from the DLC-null spoiler) was attained with $\pm 8^{o}$ spoiler steps.

- Changes in lift due to the spoiler steps were lower by 45 percent for the 8^{o} spoiler step cases than their corresponding steady-state ΔC_L's. The reduced peak acceleration is believed to result from angle-of-attack variation and unsteady aerodynamic effects, as well as possible variable blowing system characteristics due to spoiler activity.

- Airplane flight path response closely followed both flap and spoiler inputs.

A final conclusion may be drawn from the above. The auxiliary flaps as tested were feasible as control surfaces for DLC. The flaps did not show as much DLC capability in terms of static ΔC_L and incremental normal acceleration as did the spoilers. It must be pointed out, however, that the flap system was designed within the "existing hardware" on the airplane and possibly was not fully optimized for DLC. A flap designed from the outset for DLC would likely show more capability, although the design of such a flap could penalize the maximum lift capability.

The Boeing Company,
Seattle, Washington,
February 1969.

FIGURE 1.–BOEING 367-80 AIRPLANE DURING TAKEOFF

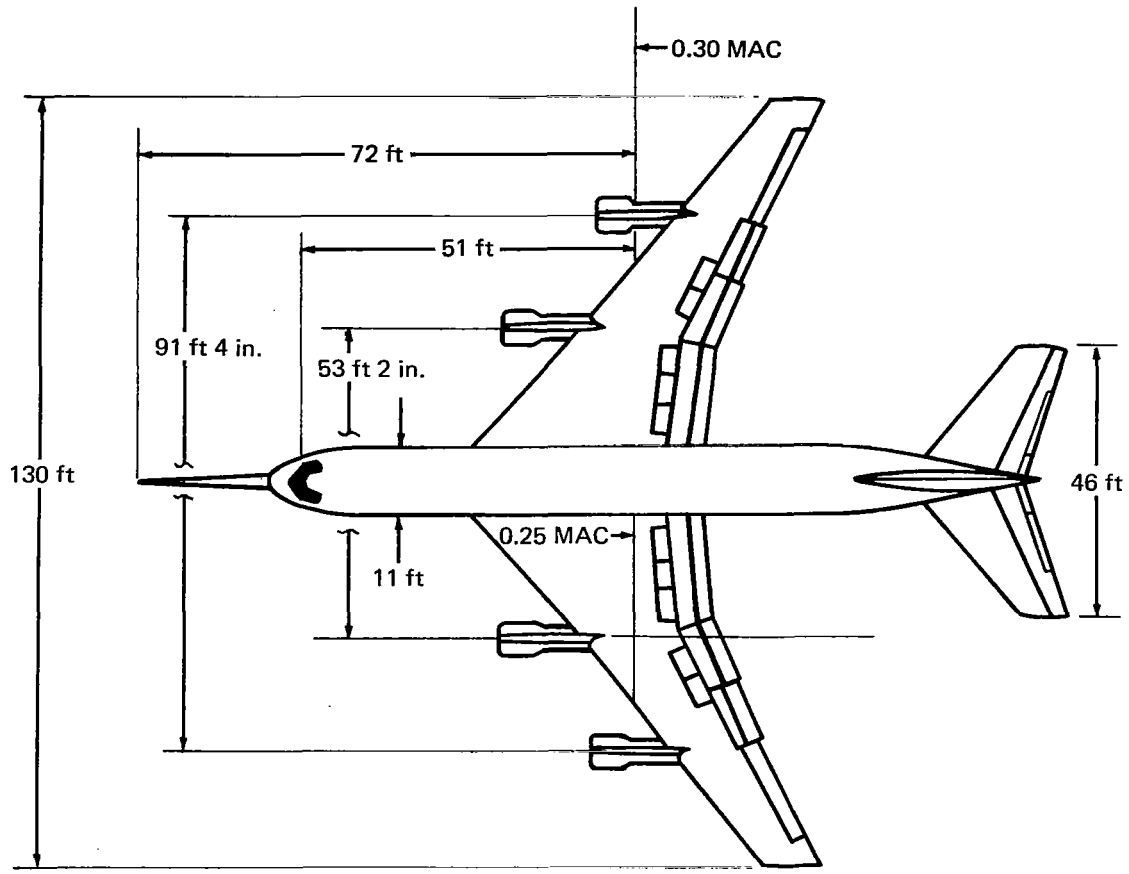

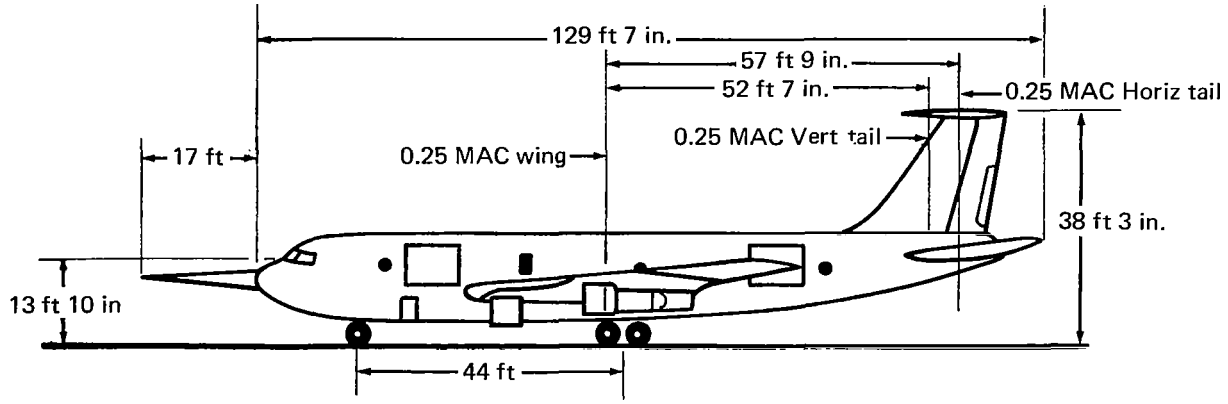

	Wing	Horizontal tail	Vertical tail
Area	2821 ft^2	625 ft^2	312 ft^2
Aspect ratio	6.0	3.37	1.46
Sweep (0.25c)	35°	35°	31°

Maximum takeoff weight	178 000 lb
Operating weight empty	135 000 lb

FIGURE 2.–GENERAL ARRANGEMENT OF 367-80 AIRPLANE

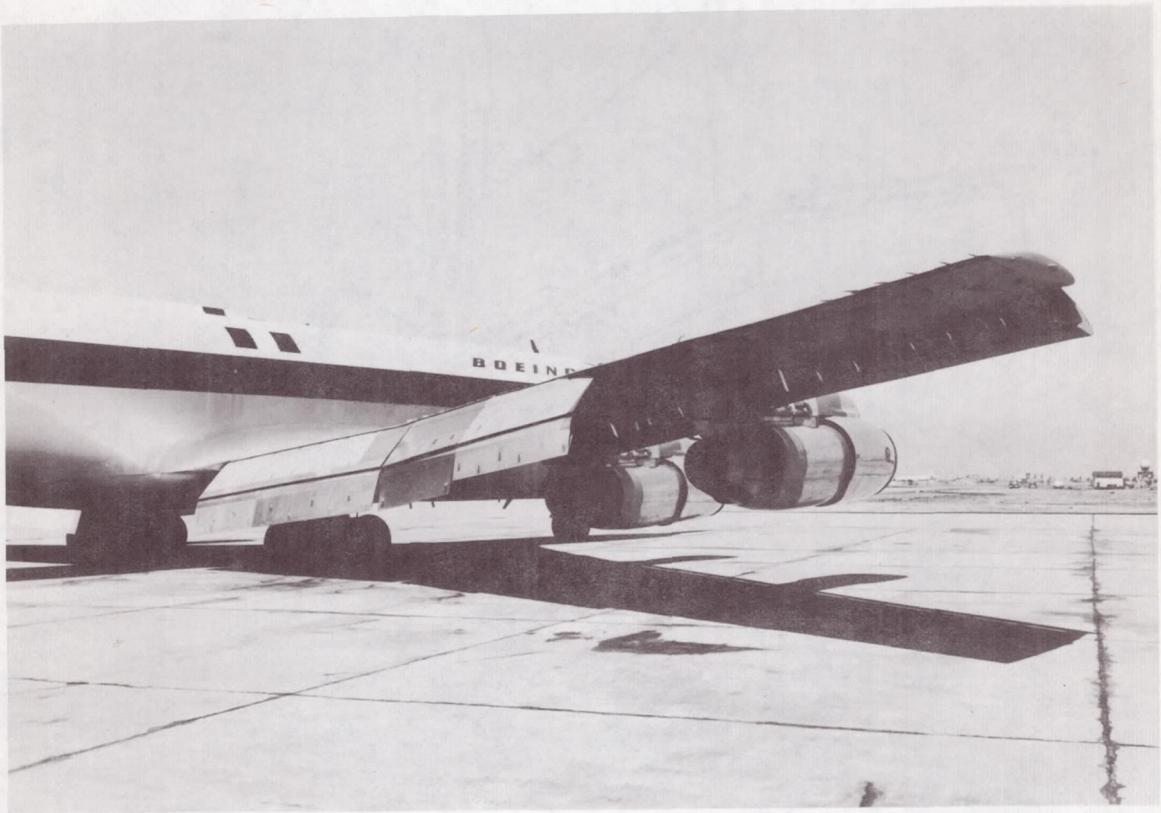

FIGURE 3.–367-80 AIRPLANE WITH DLC FLAPS

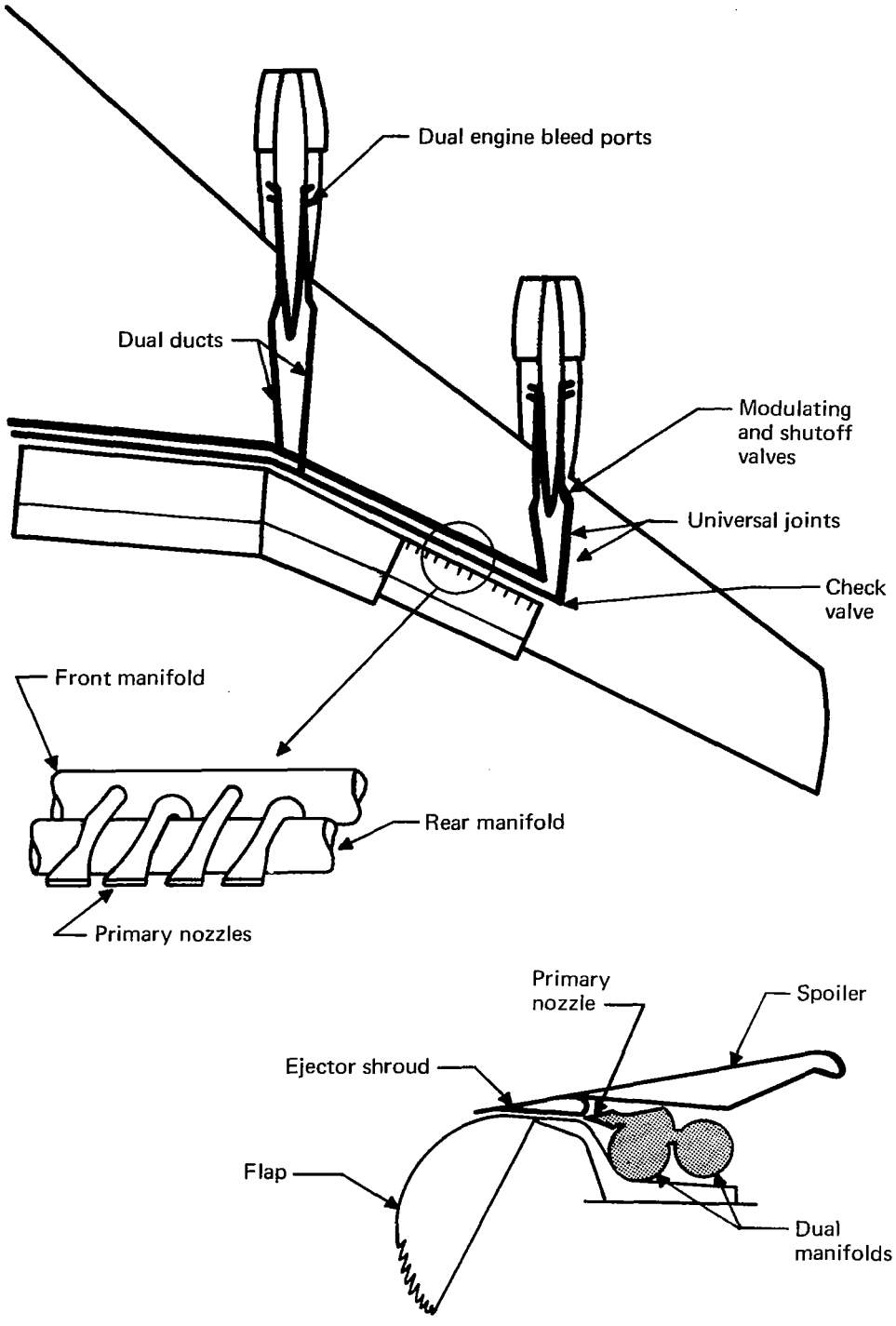

FIGURE 4.–367-80 BOUNDARY LAYER CONTROL SYSTEM

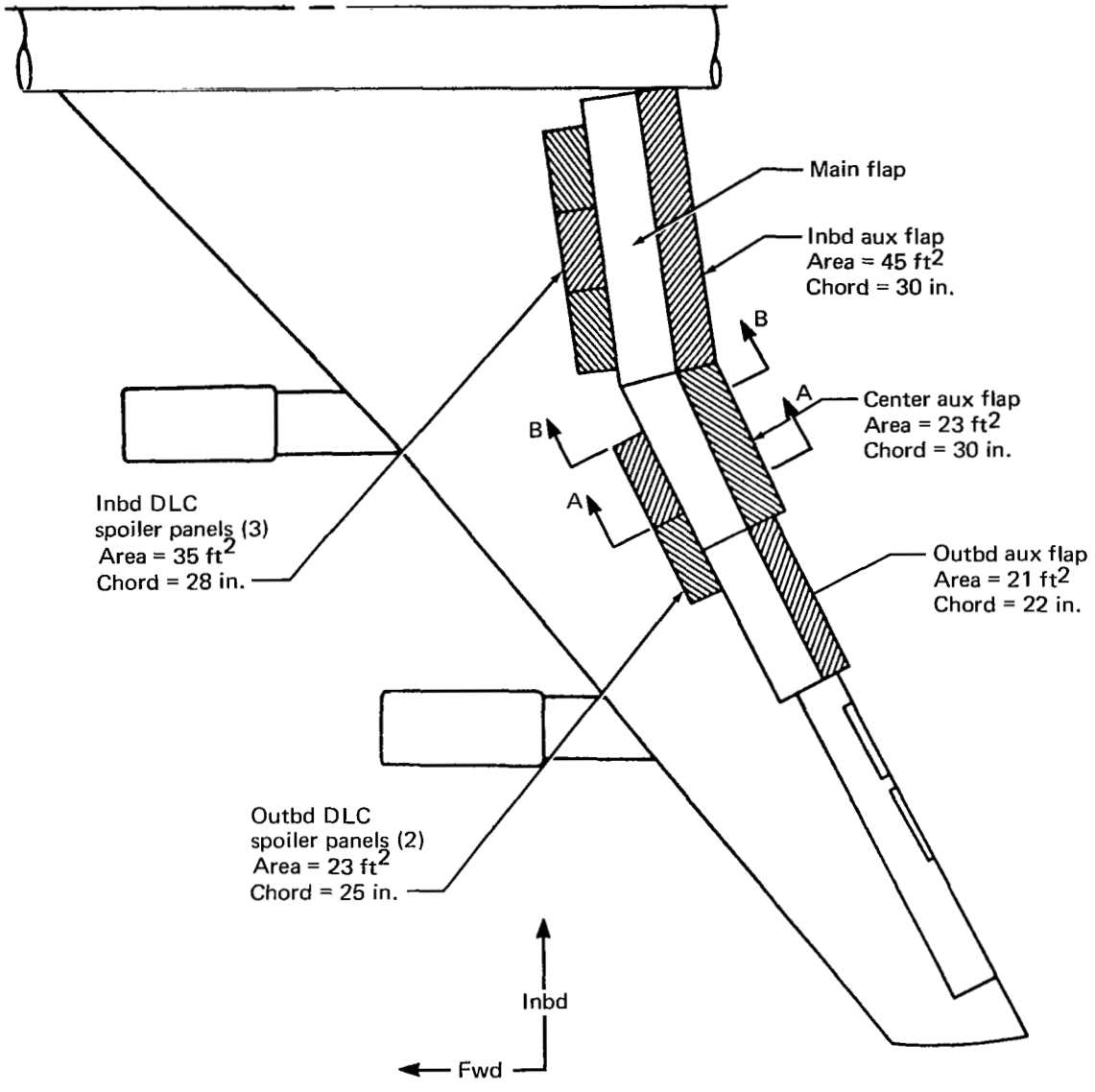

FIGURE 5.–PLANFORM VIEW OF DLC FLAPS AND SPOILERS

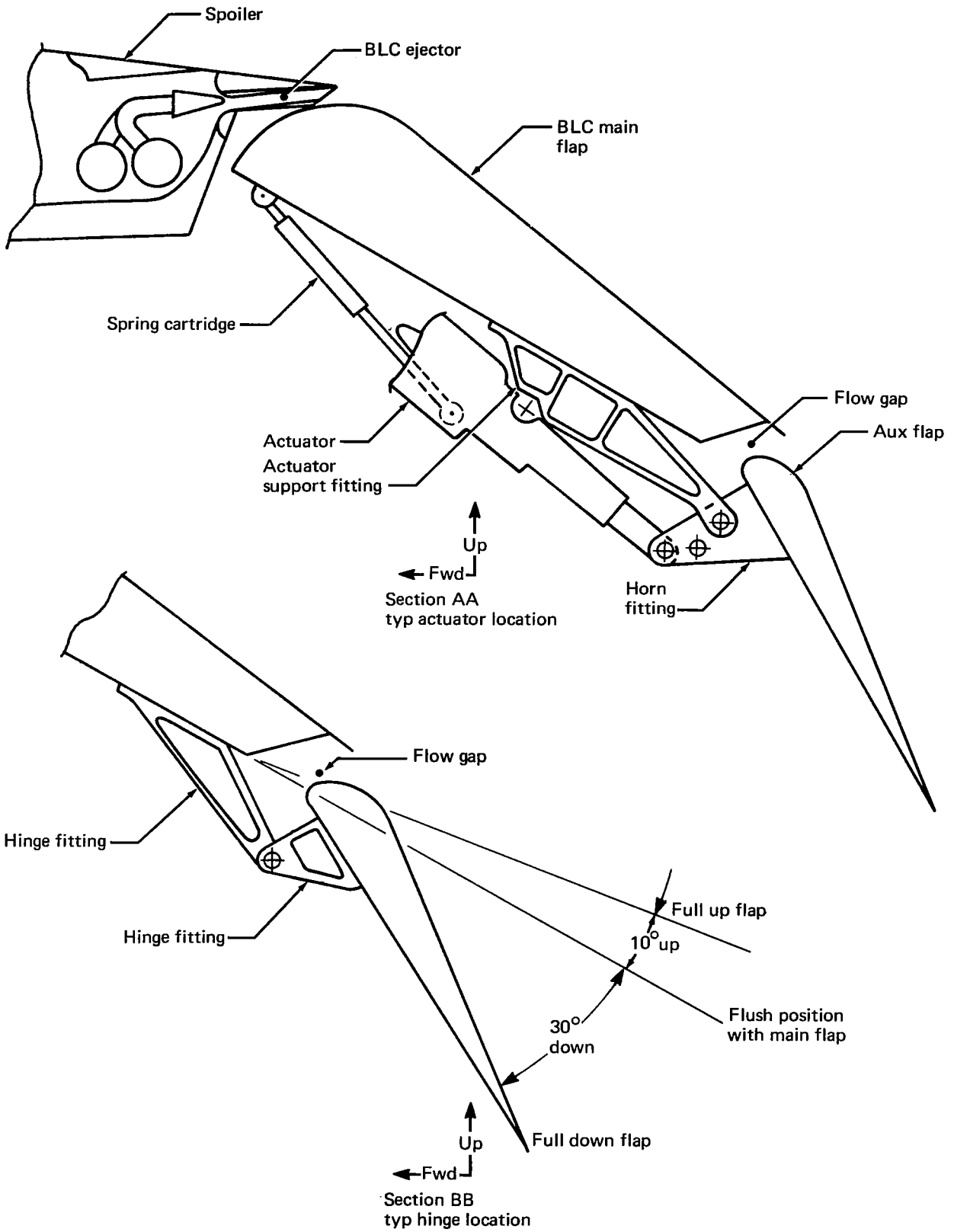

FIGURE 6.–DETAILS OF DLC FLAP SYSTEM

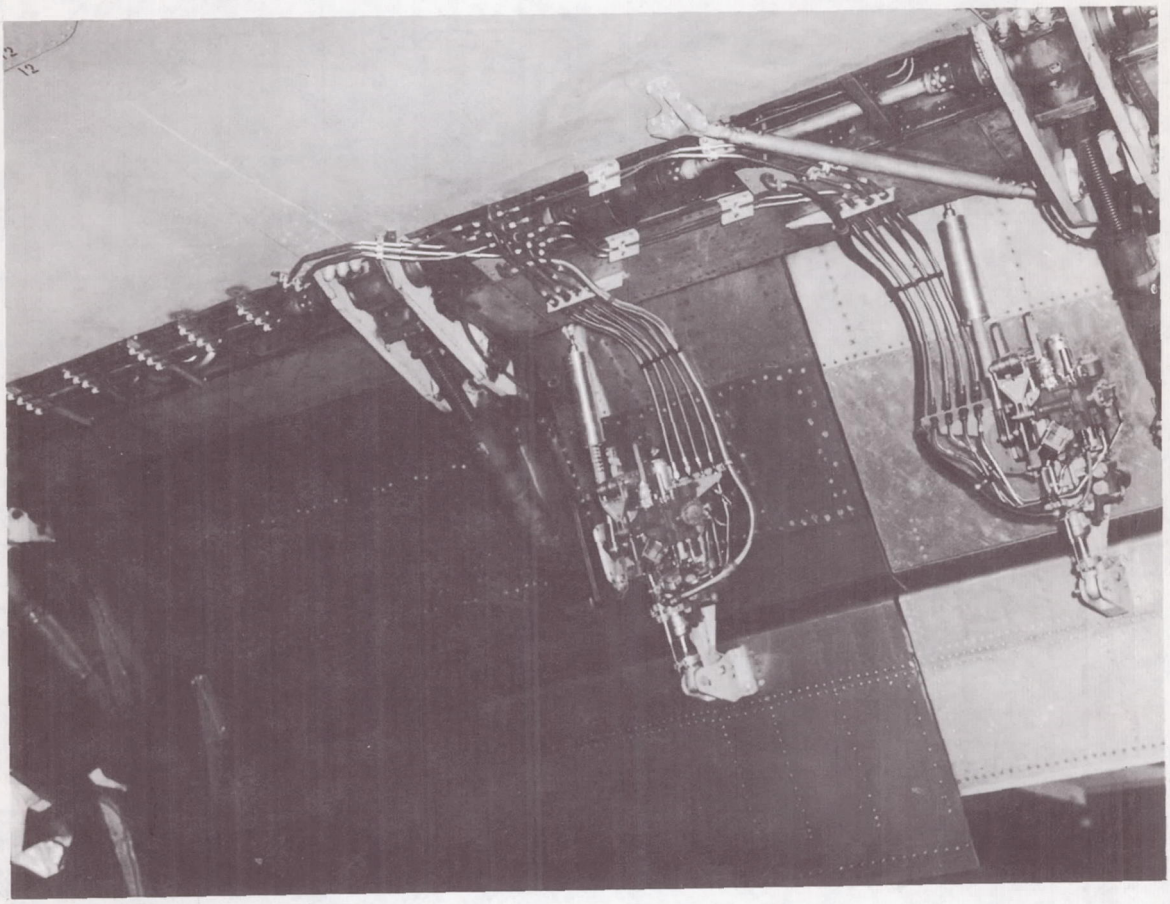

FIGURE 7.–DLC FLAP ACTUATORS

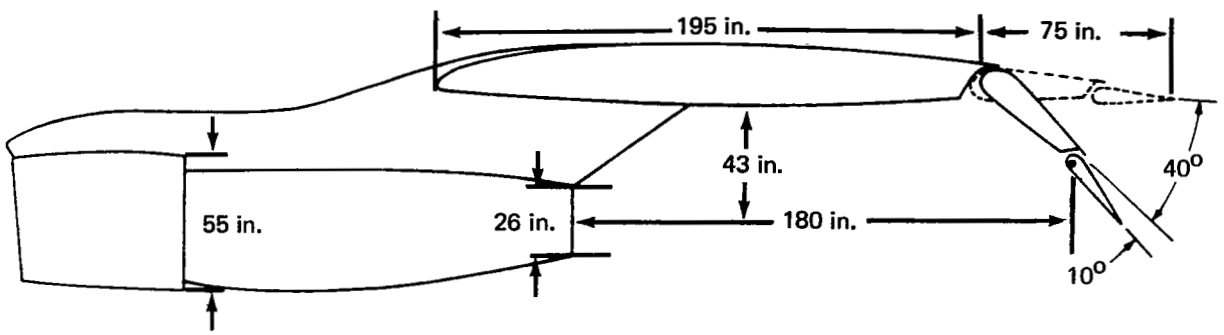

FIGURE 8.–ARRANGEMENT OF INBOARD ENGINE AND TRAILING EDGE FLAPS WITH 40° MAIN AND 10° AUXILIARY FLAP

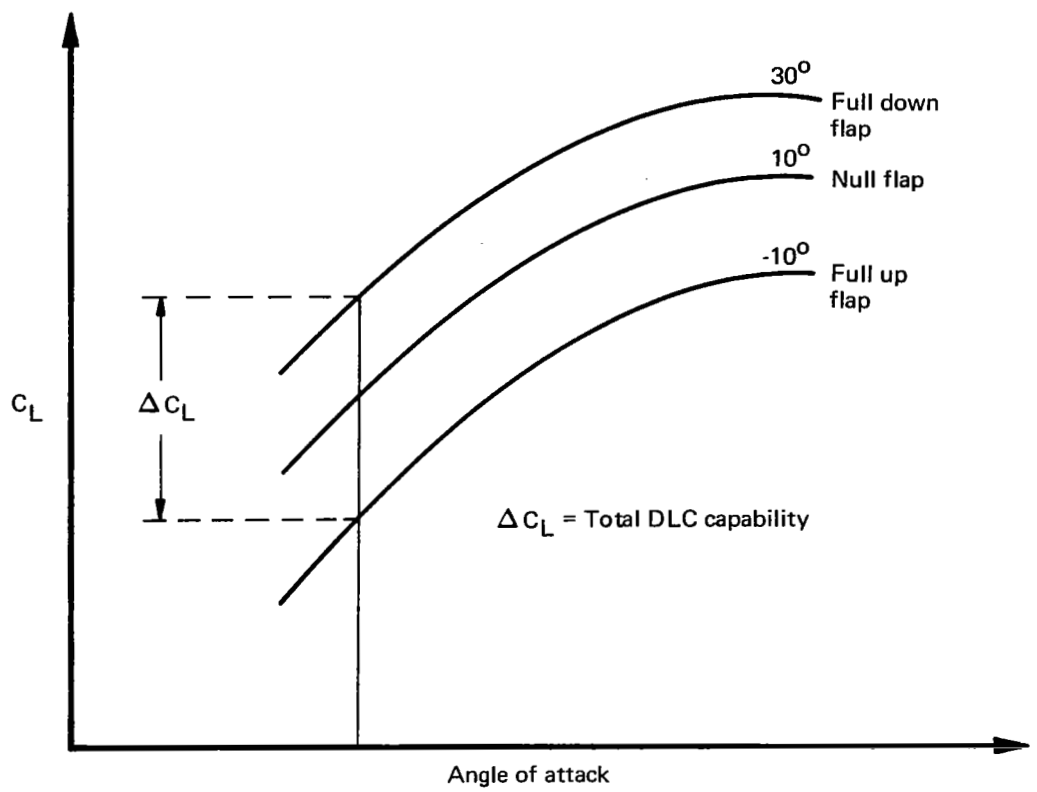

FIGURE 9.–ILLUSTRATION OF DLC FLAP EFFECTIVENESS

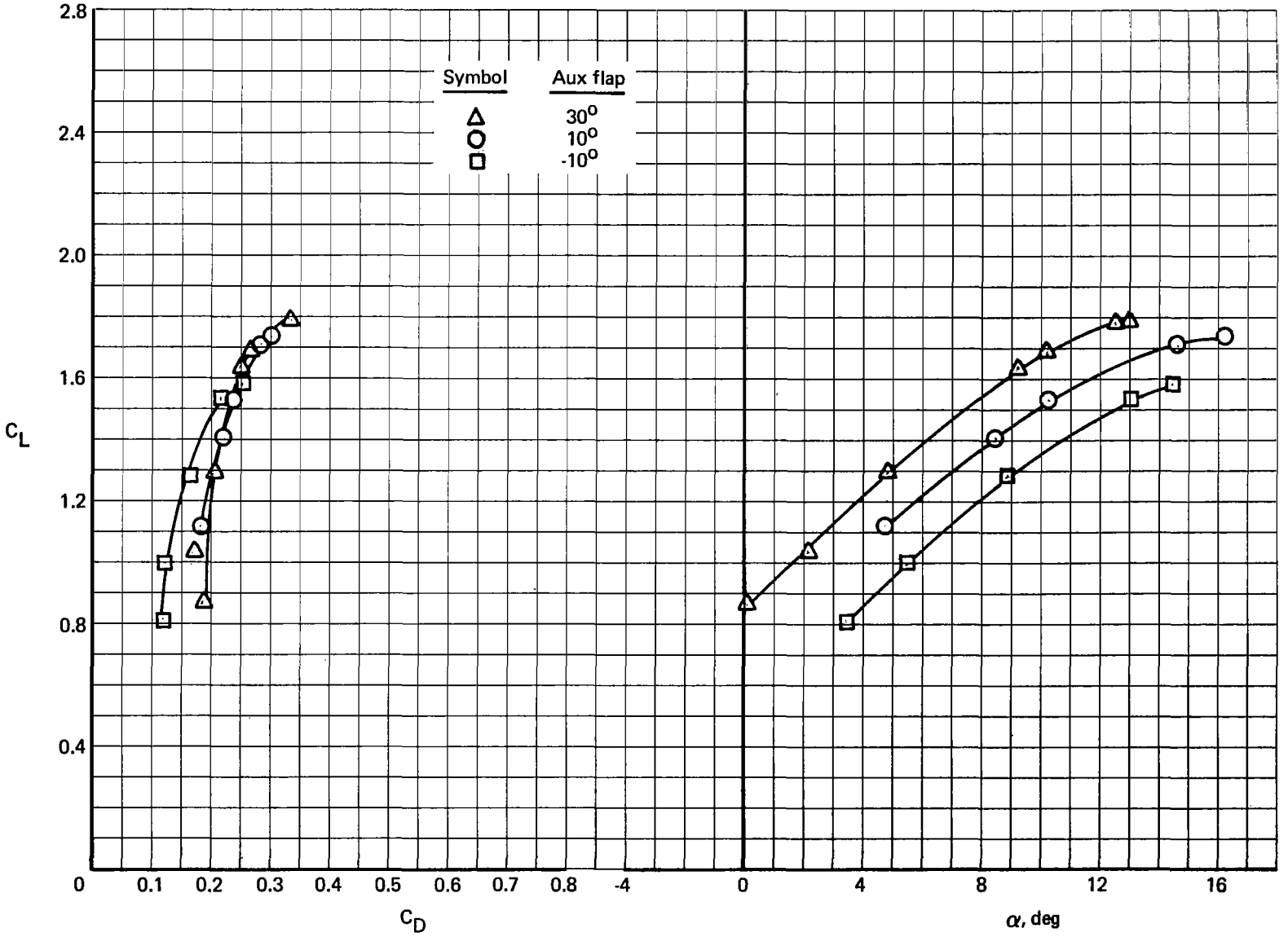

FIGURE 10.–DLC FLAP CHARACTERISTICS–30° MAIN FLAP AND IDLE POWER; BLC OFF

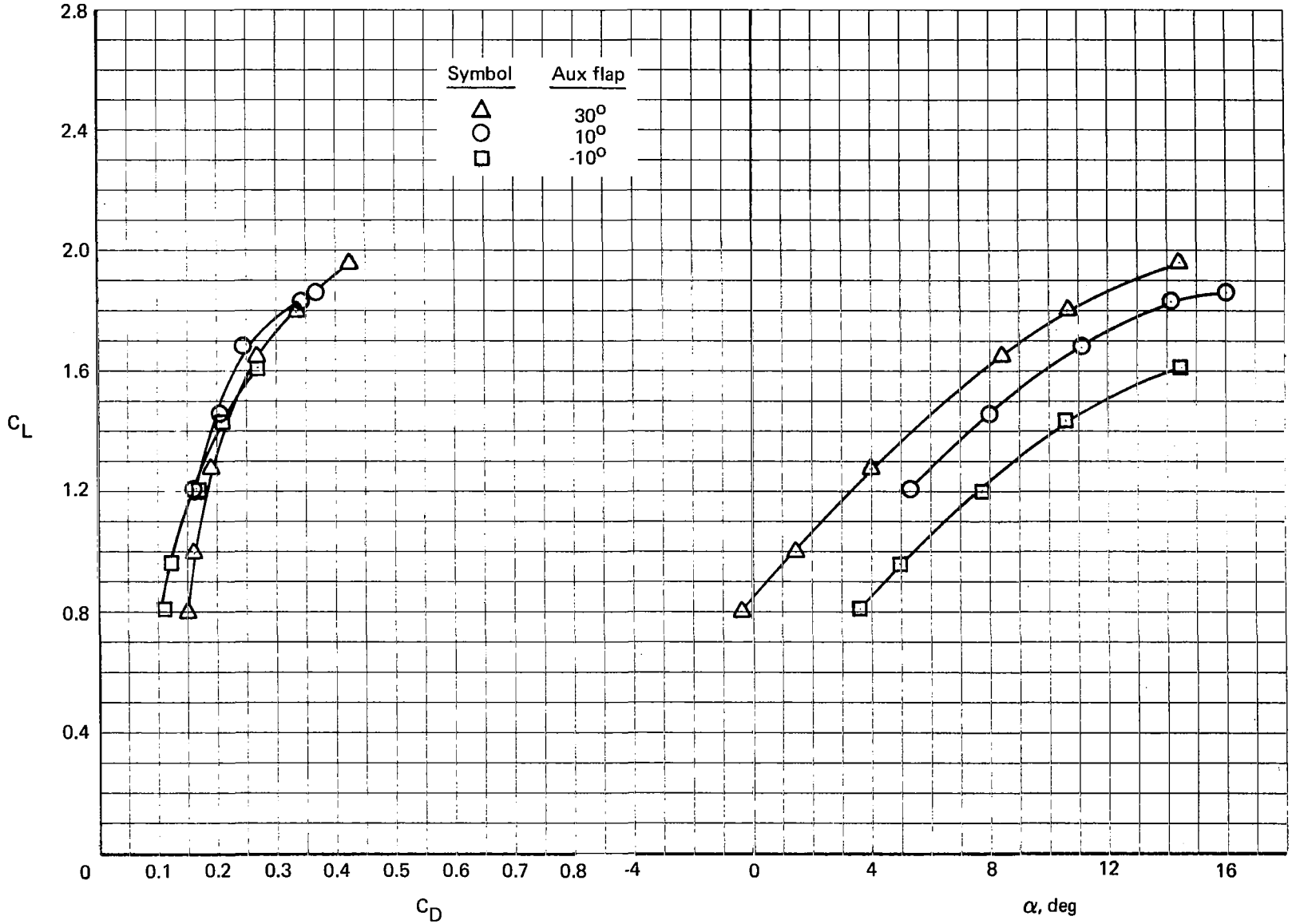

FIGURE 11.–DLC FLAP CHARACTERISTICS–30° MAIN FLAP AND POWER FOR LEVEL FLIGHT; BLC OFF

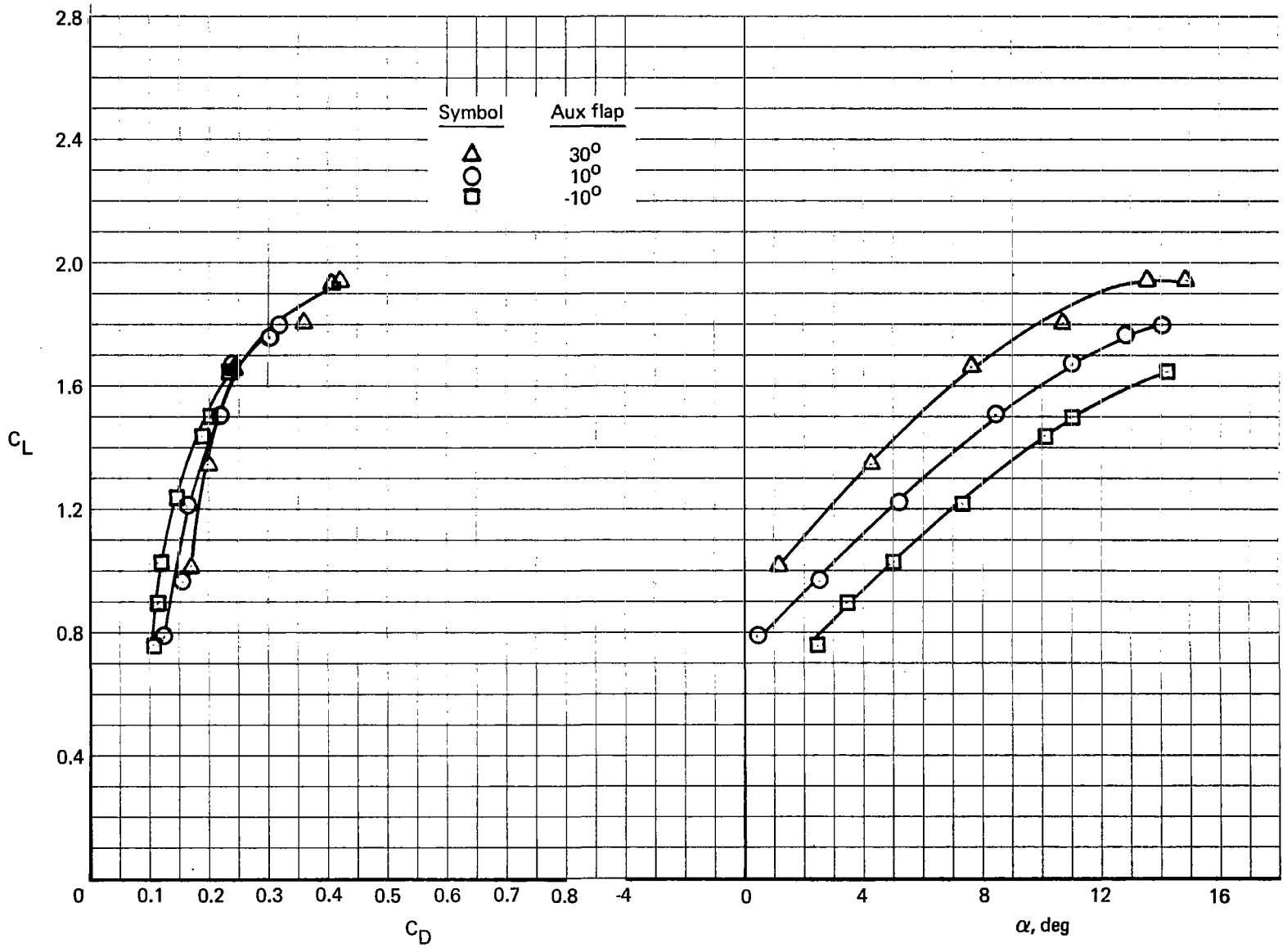

FIGURE 12.–DLC FLAP CHARACTERISTICS–30° MAIN FLAP AND 60% N_2 POWER; BLC ON

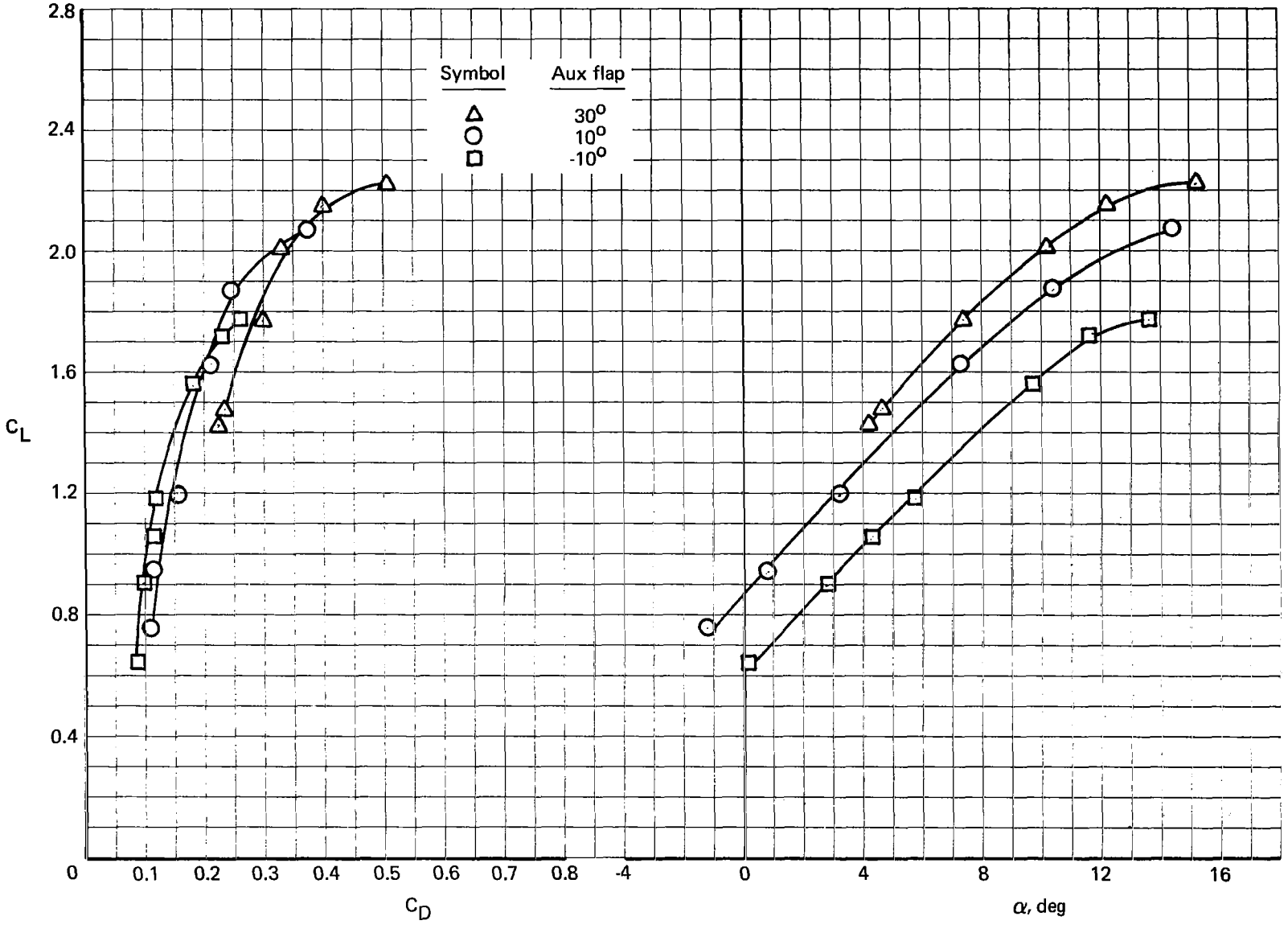

FIGURE 13.–DLC FLAP CHARACTERISTICS–30° MAIN FLAP AND POWER FOR LEVEL FLIGHT; BLC ON

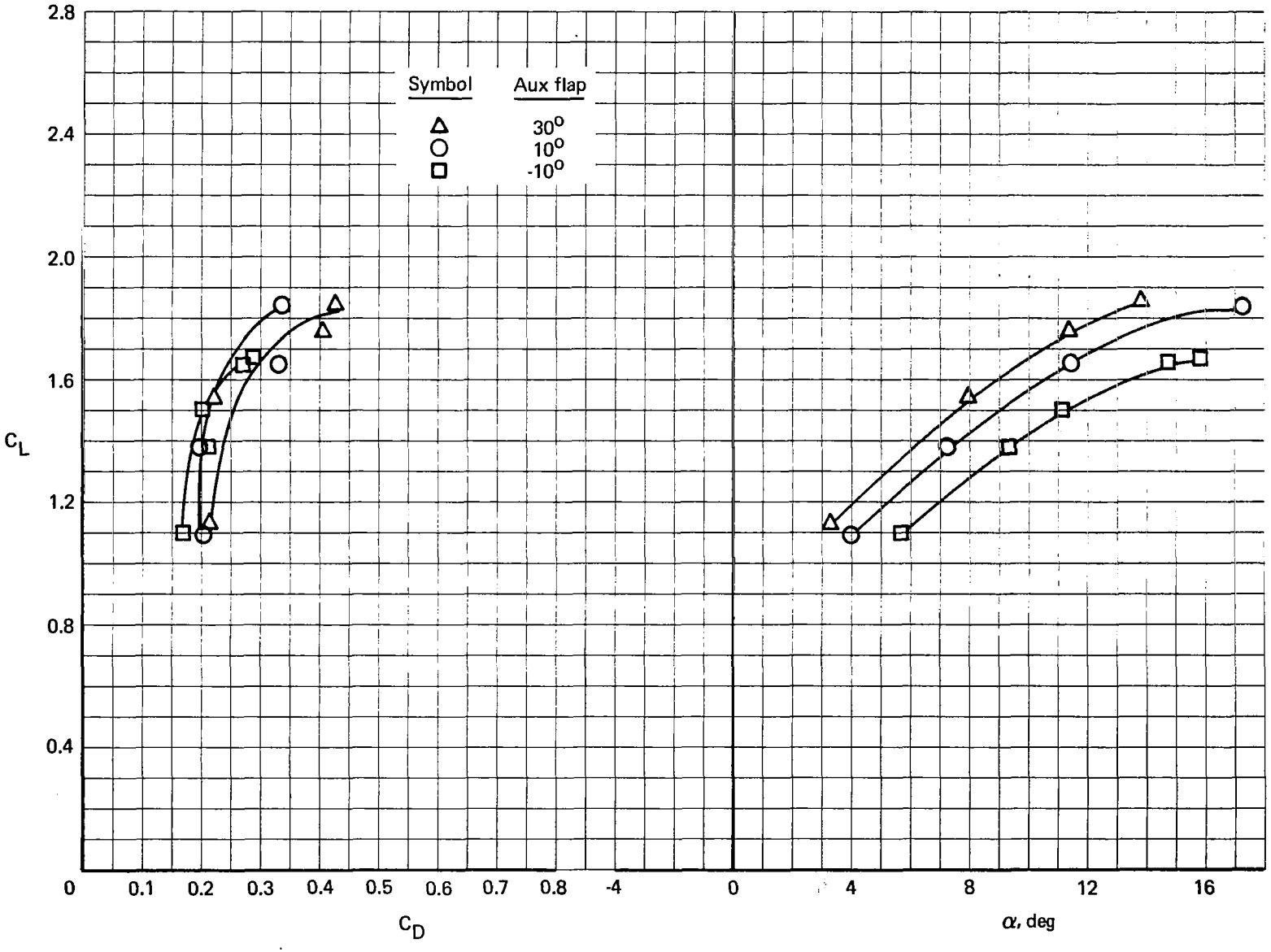

FIGURE 14.–DLC FLAP CHARACTERISTICS–40° MAIN FLAP AND IDLE POWER; BLC OFF

FIGURE 15.–DLC FLAP CHARACTERISTICS–40° MAIN FLAP AND POWER FOR LEVEL FLIGHT; BLC OFF

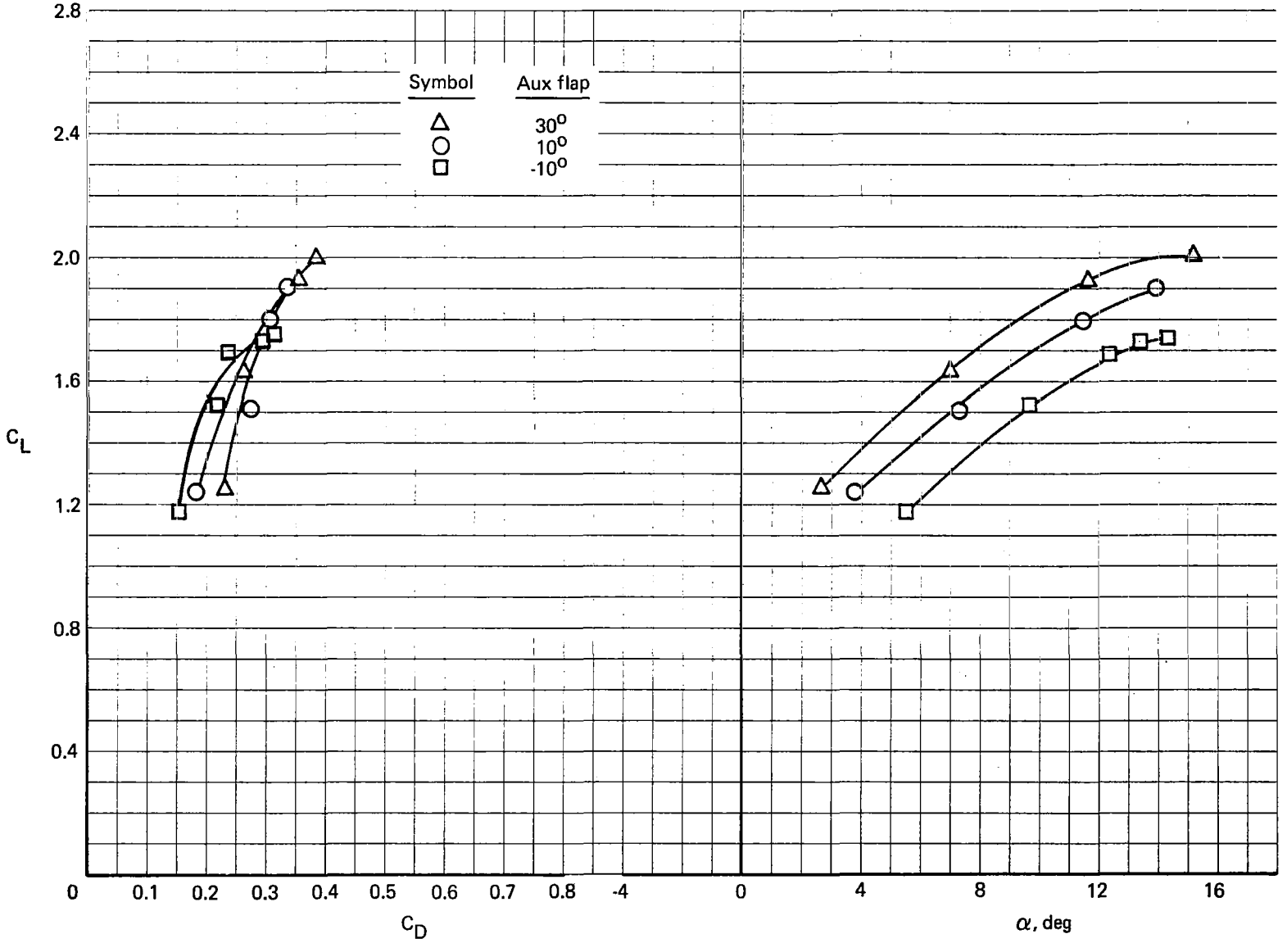

FIGURE 16.–DLC FLAP CHARACTERISTICS–40° MAIN FLAP AND 60% N_2 POWER; BLC ON

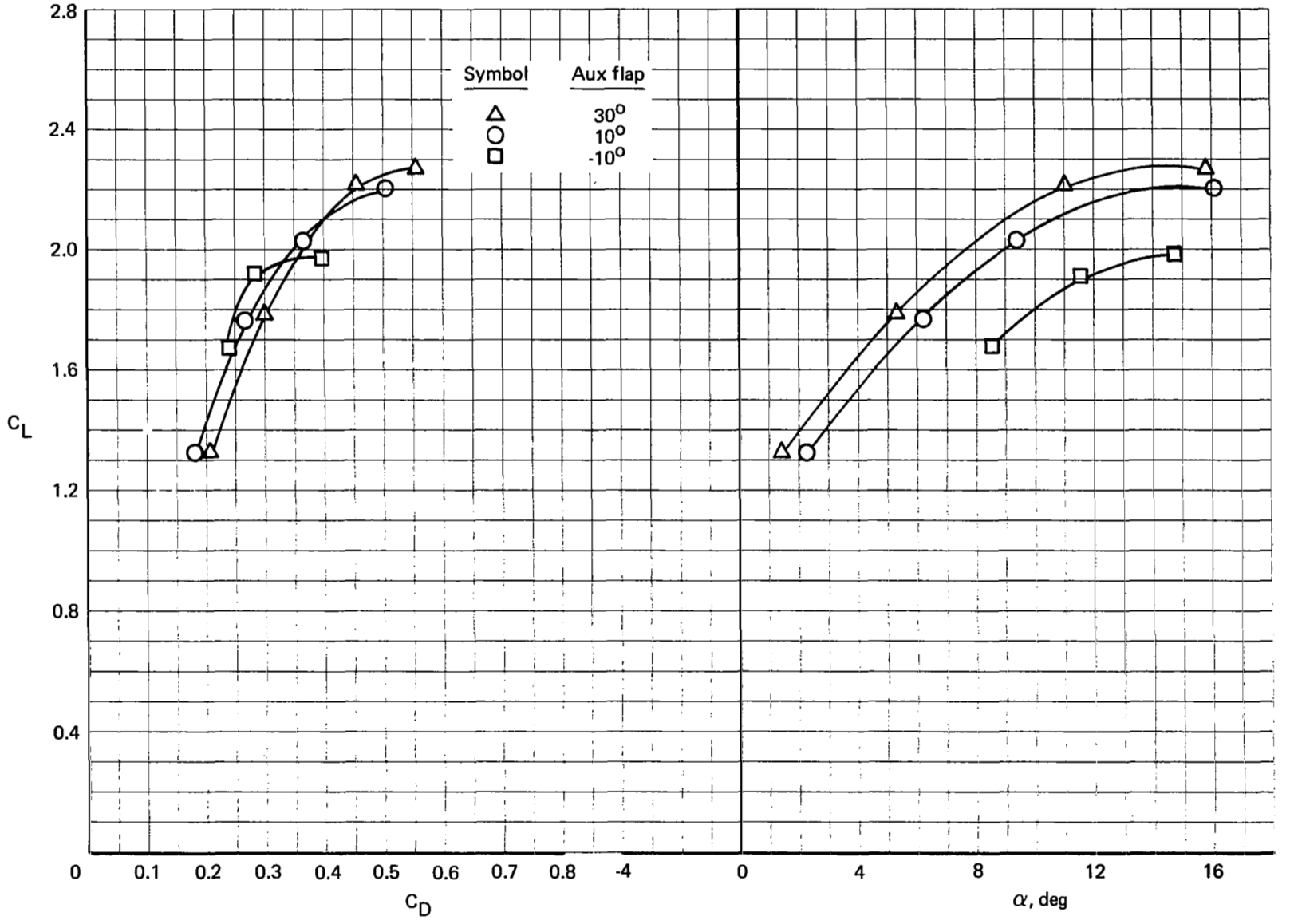

FIGURE 17.–DLC FLAP CHARACTERISTICS–40° MAIN FLAP AND POWER FOR LEVEL FLIGHT; BLC ON

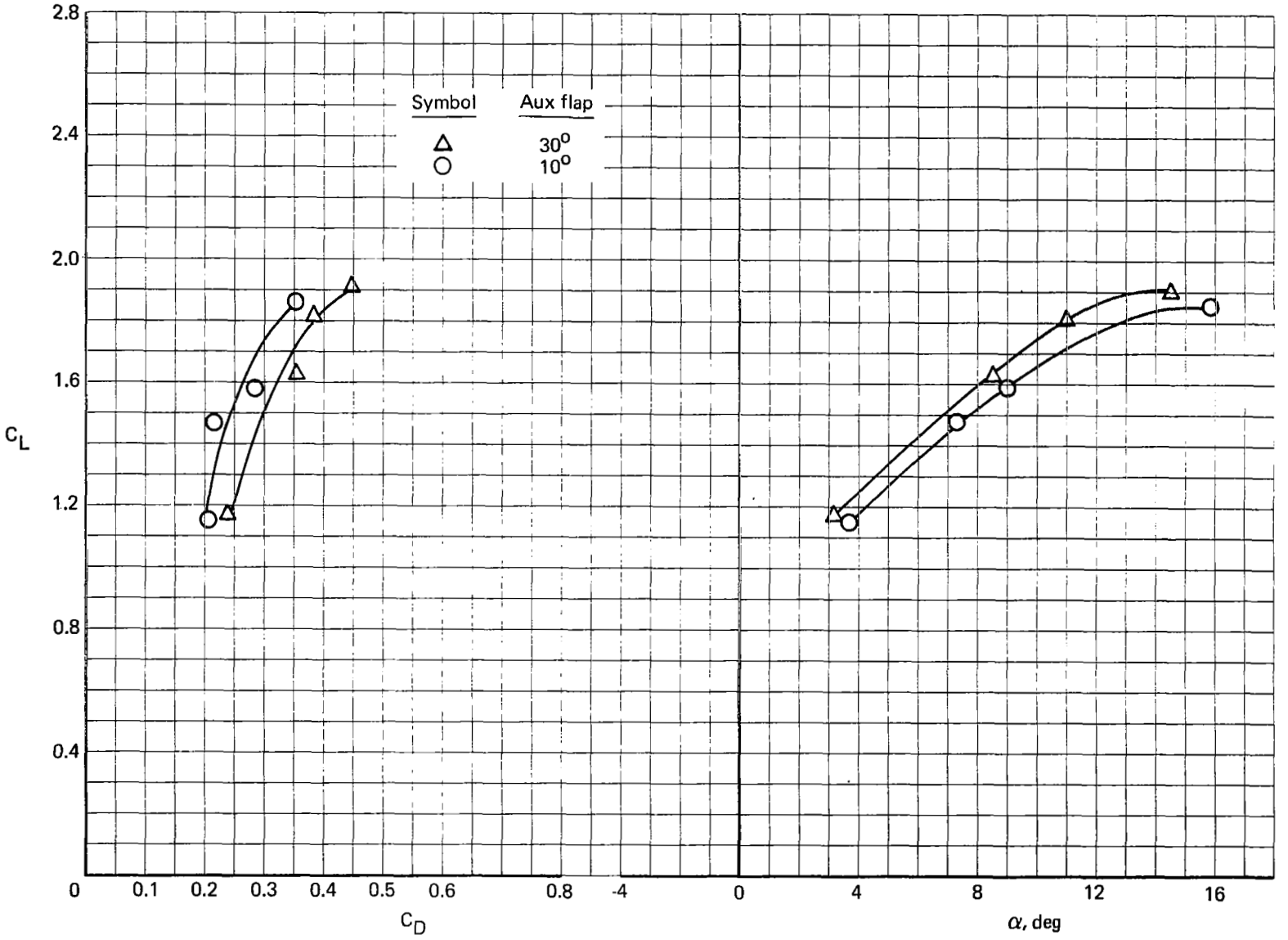

FIGURE 18.–DLC FLAP CHARACTERISTICS–50° MAIN FLAP AND IDLE POWER; BLC OFF

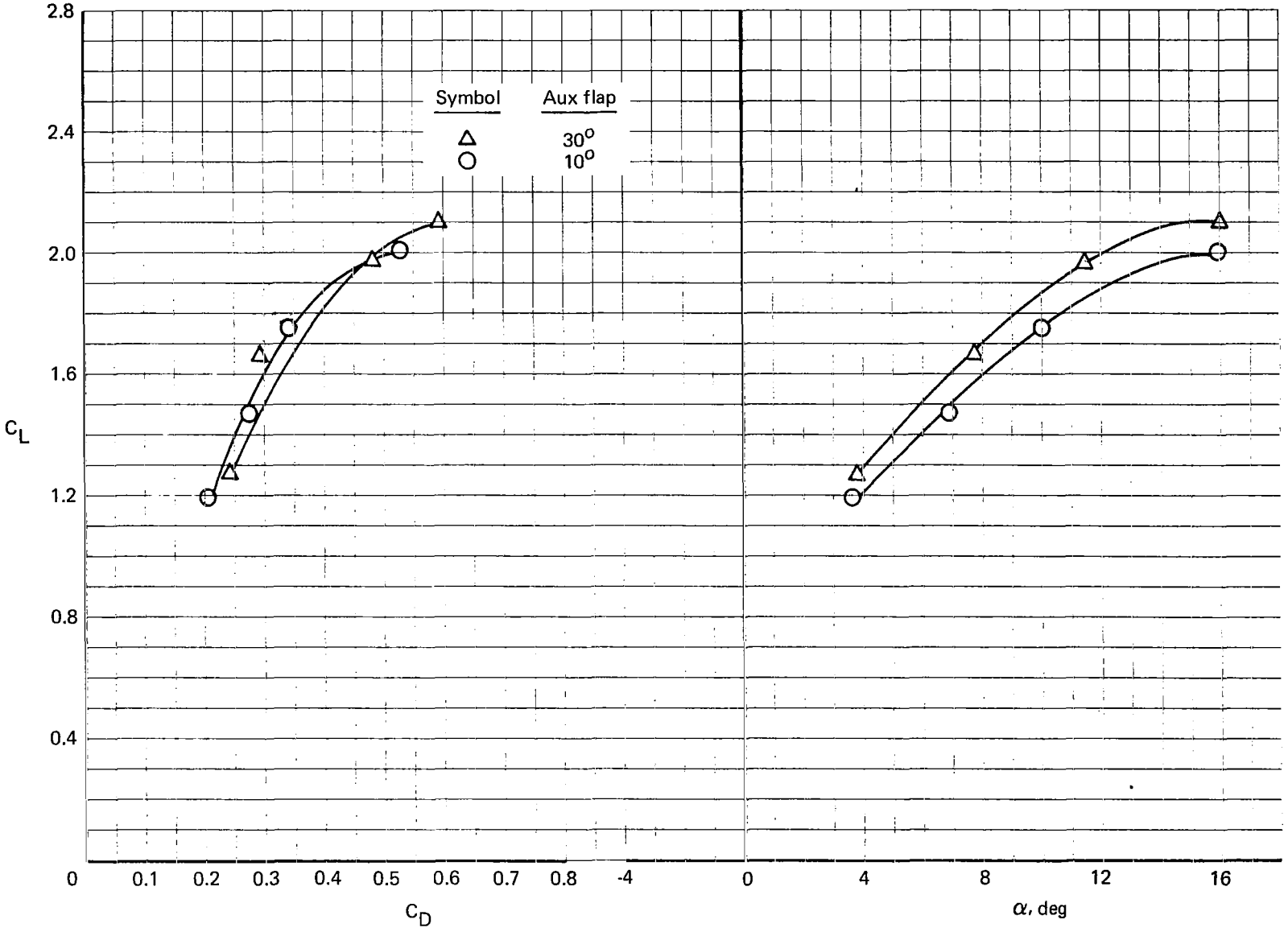

FIGURE 19.–DLC FLAP CHARACTERISTICS–50° MAIN FLAP AND POWER FOR LEVEL FLIGHT; BLC OFF

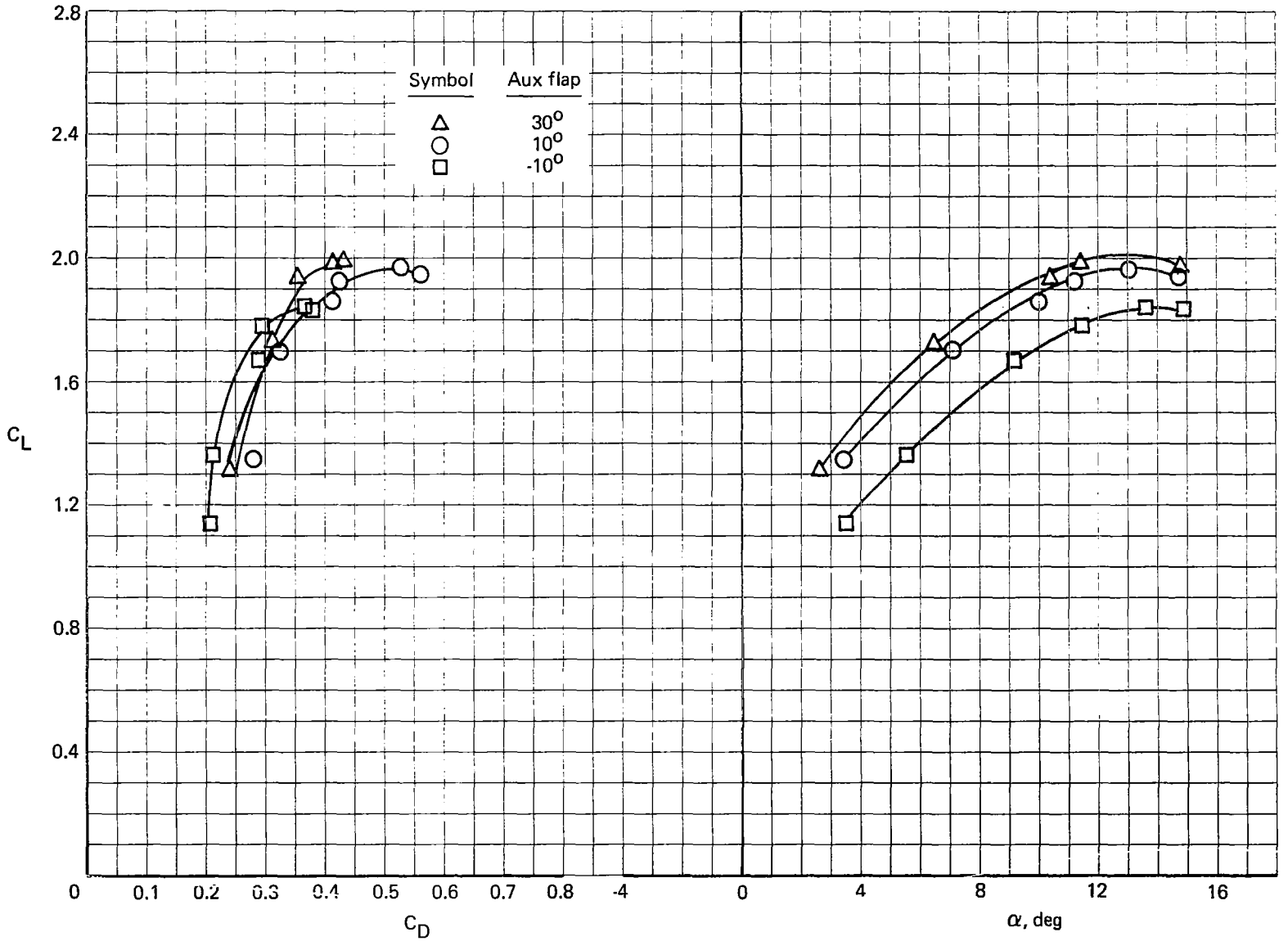

FIGURE 20.–DLC FLAP CHARACTERISTICS–50° MAIN FLAP AND 60% N_2 POWER; BLC ON

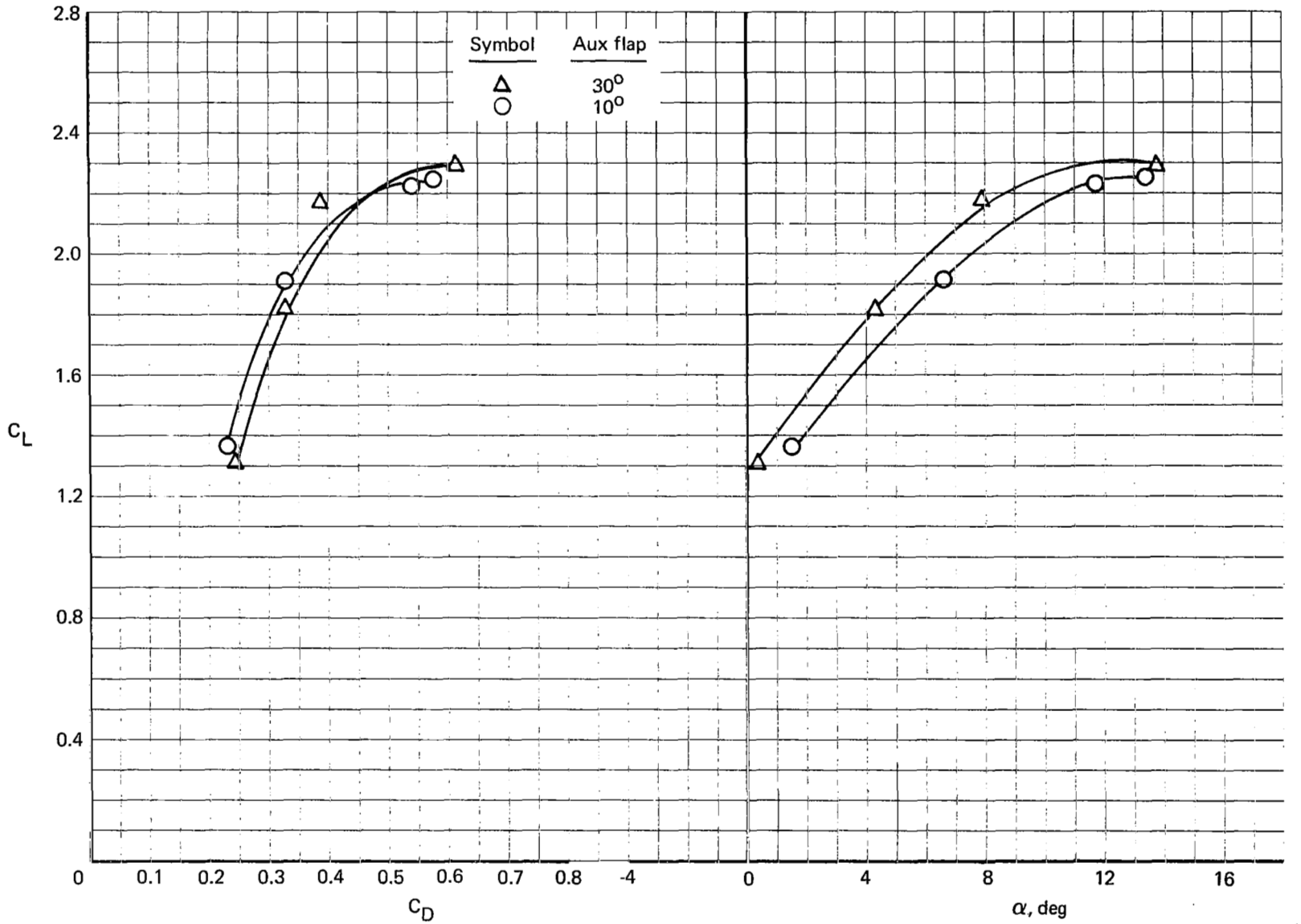

FIGURE 21.–DLC FLAP CHARACTERISTICS–50° MAIN FLAP AND 90% N_2 POWER; BLC ON

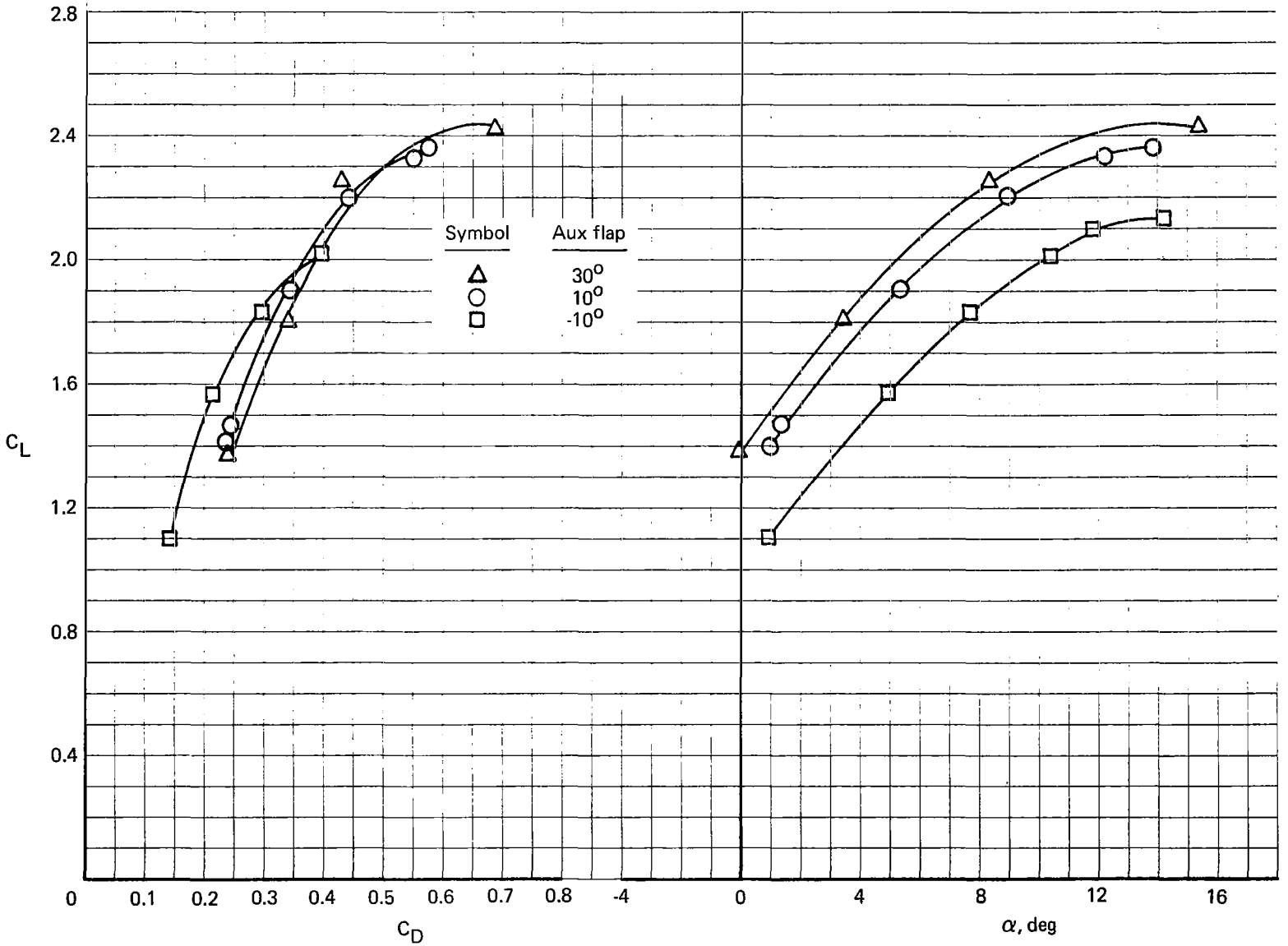

FIGURE 22.–DLC FLAP CHARACTERISTICS–50° MAIN FLAP AND MAXIMUM CONTINUOUS POWER; BLC ON

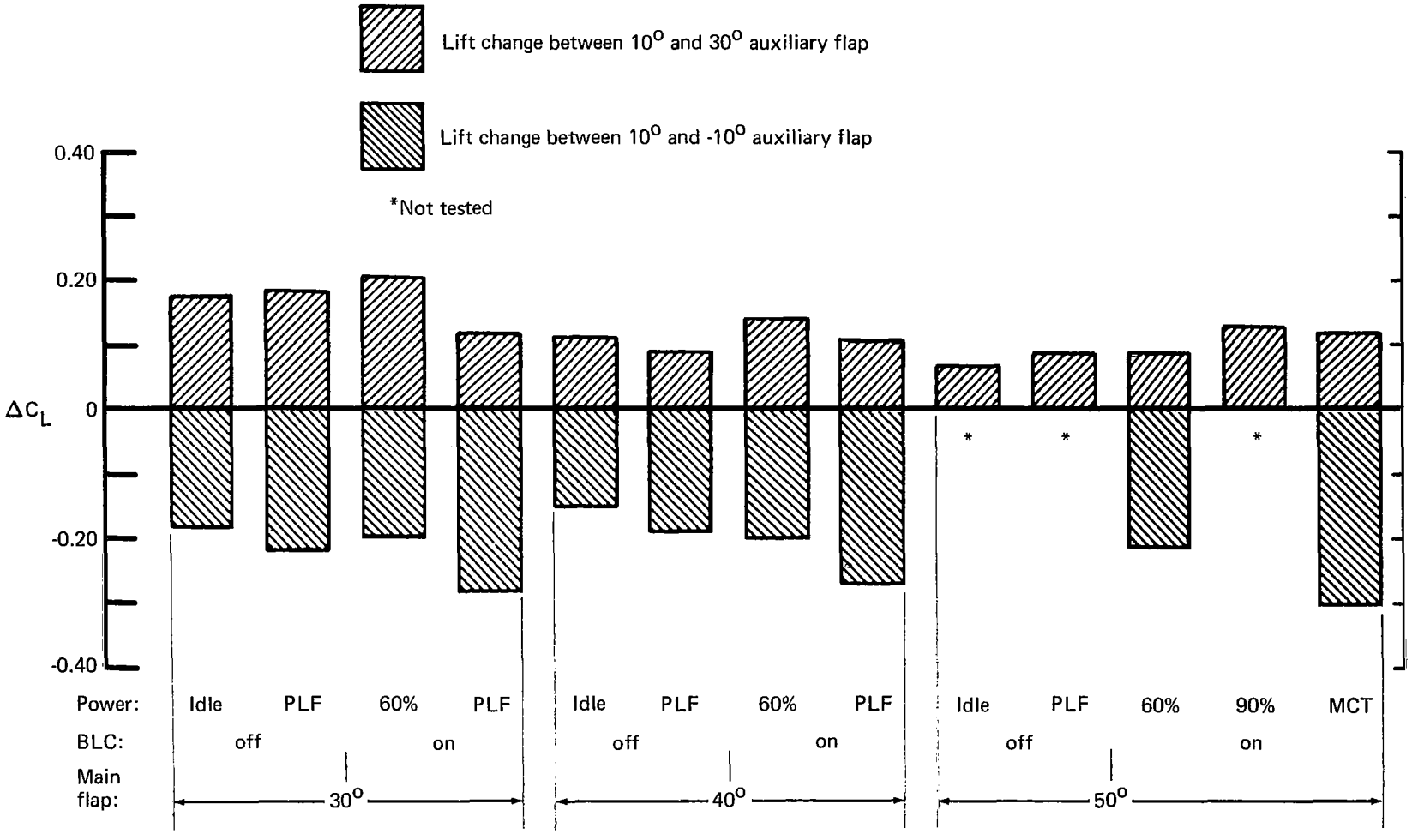

FIGURE 23.–STEADY-STATE DLC FLAP LIFT CAPABILITY AT CONSTANT ANGLES OF ATTACK FOR APPROACH

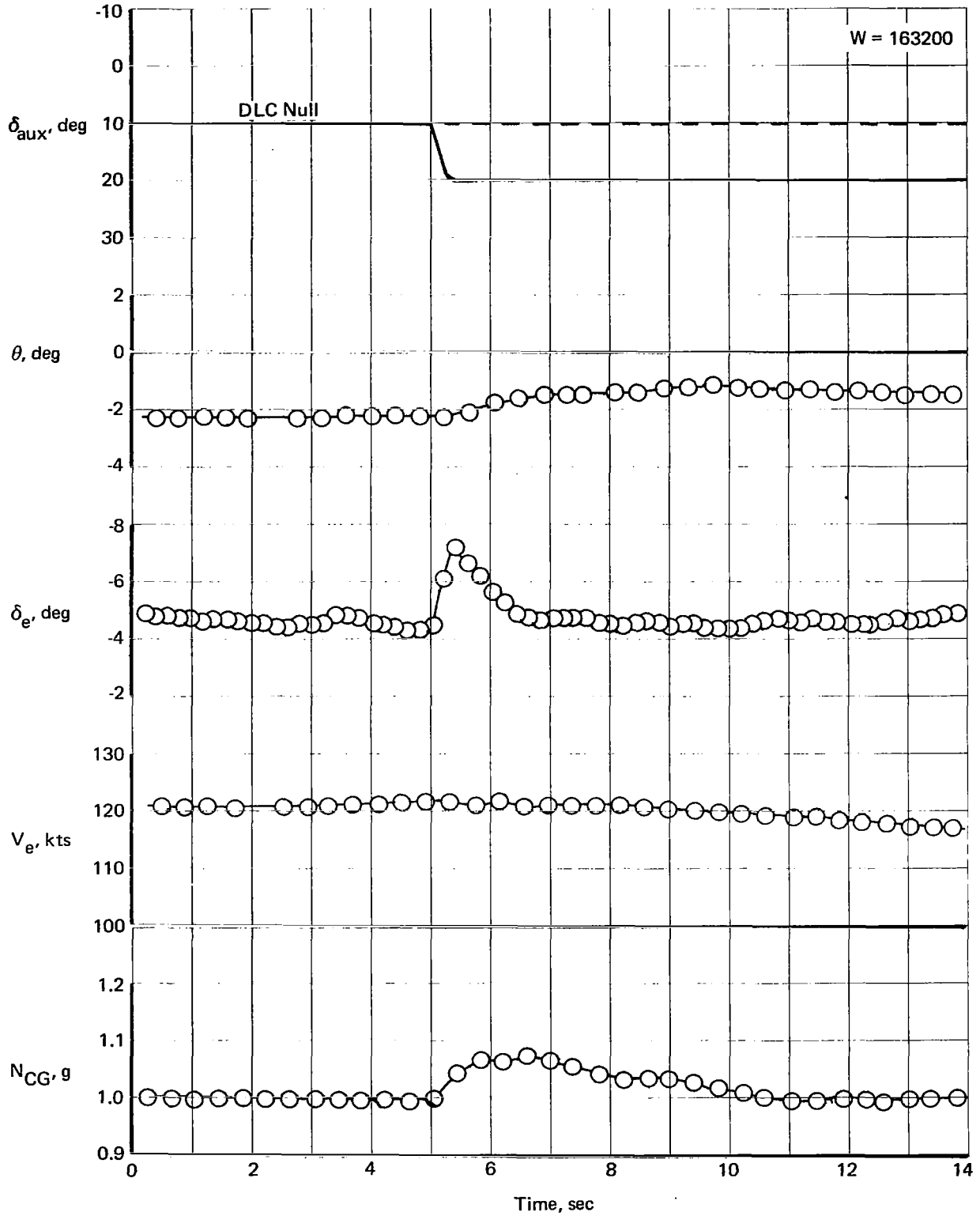

FIGURE 24.–AIRPLANE RESPONSE TO A 10° DOWN AUXILIARY FLAP STEP–30° MAIN FLAP AND IDLE POWER; BLC OFF

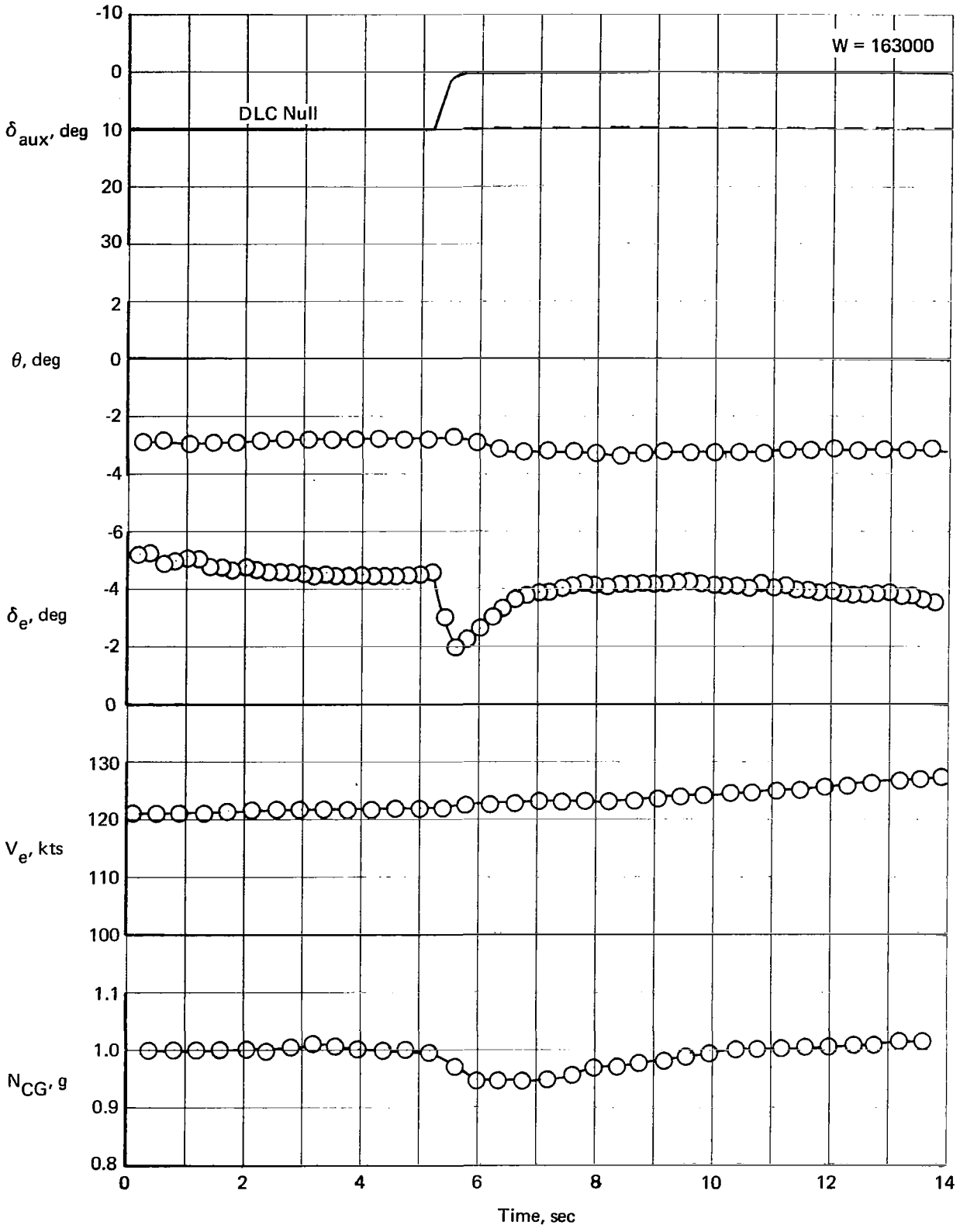

FIGURE 25.–AIRPLANE RESPONSE TO A 10^{O} UP AUXILIARY FLAP STEP–30^{O} MAIN FLAP AND IDLE POWER; BLC OFF

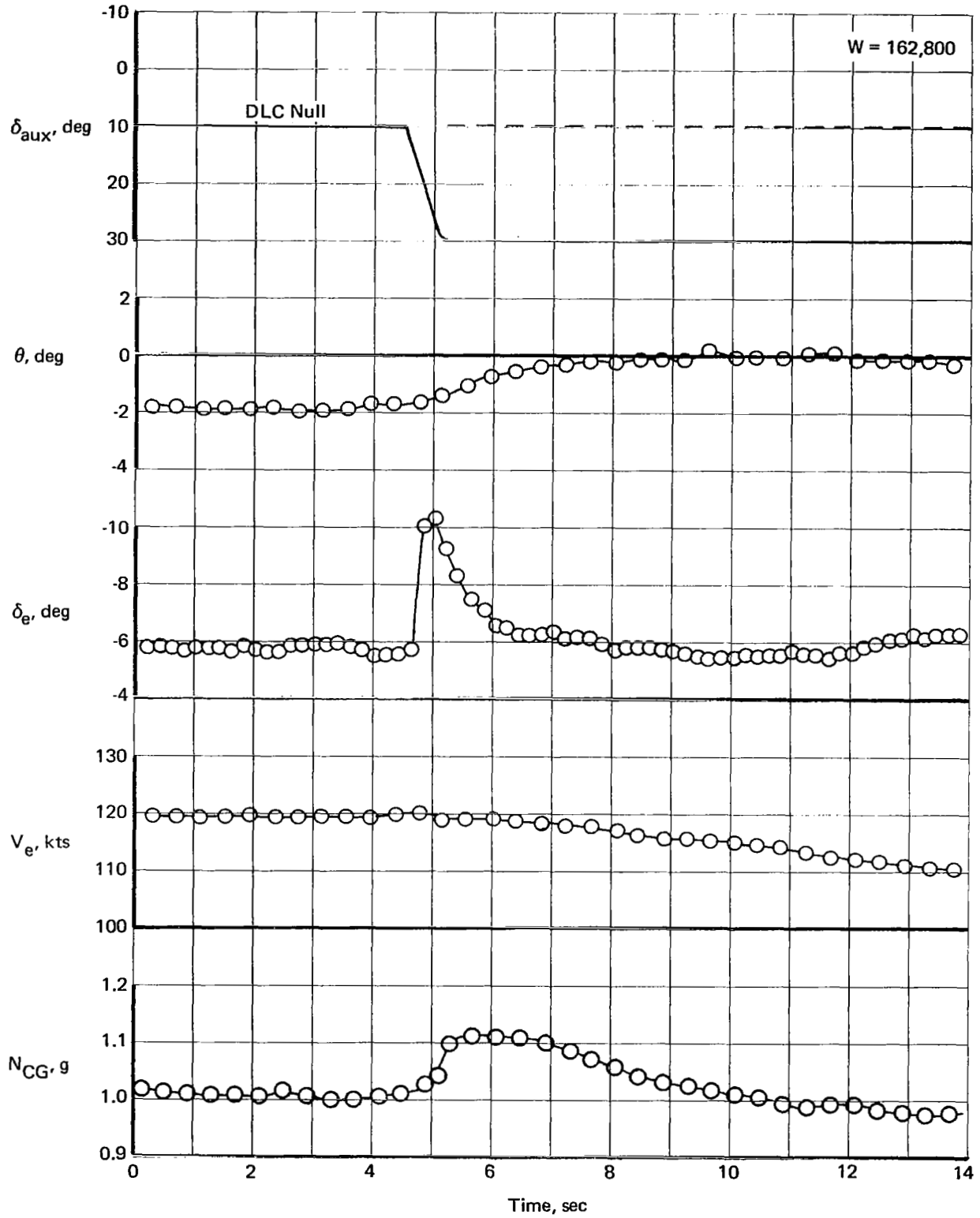

FIGURE 26.–AIRPLANE RESPONSE TO A 20° DOWN AUXILIARY FLAP STEP–30° MAIN FLAP AND IDLE POWER; BLC OFF

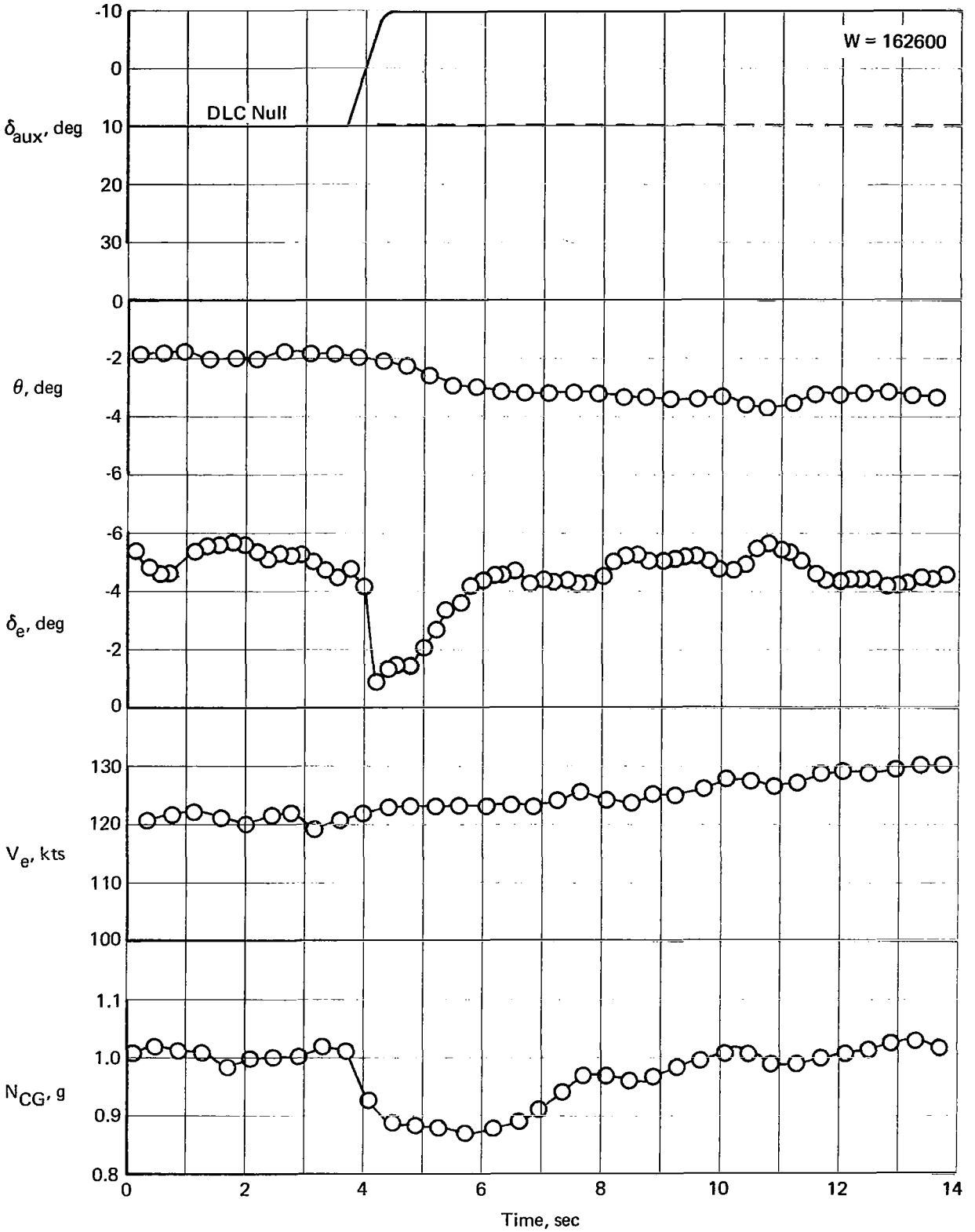

FIGURE 27.–AIRPLANE RESPONSE TO A 20° UP AUXILIARY FLAP STEP–30° MAIN FLAP AND IDLE POWER; BLC OFF

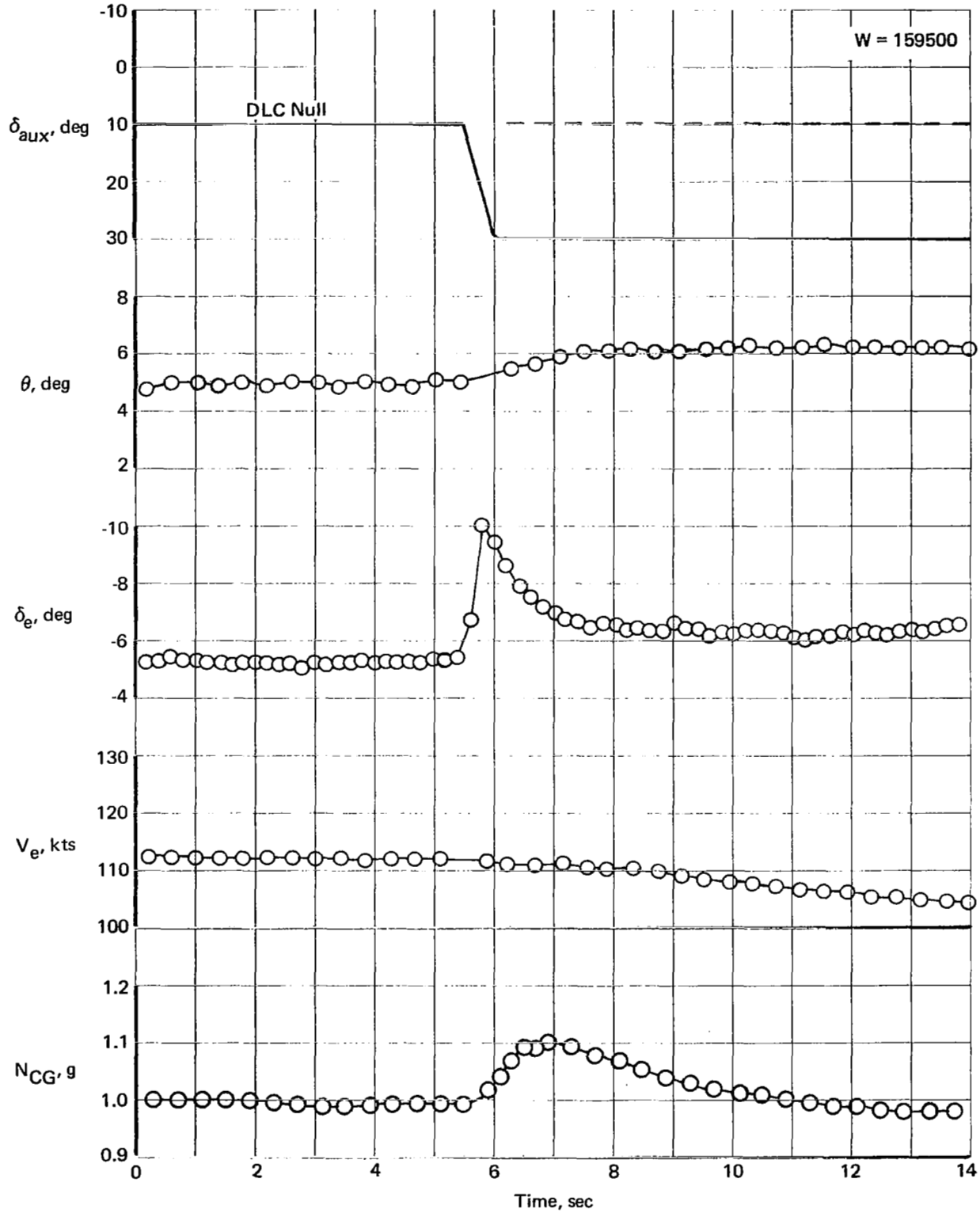

FIGURE 28.–AIRPLANE RESPONSE TO A 20^{O} DOWN AUXILIARY FLAP STEP–30^{O} MAIN FLAP AND POWER FOR LEVEL FLIGHT; BLC OFF

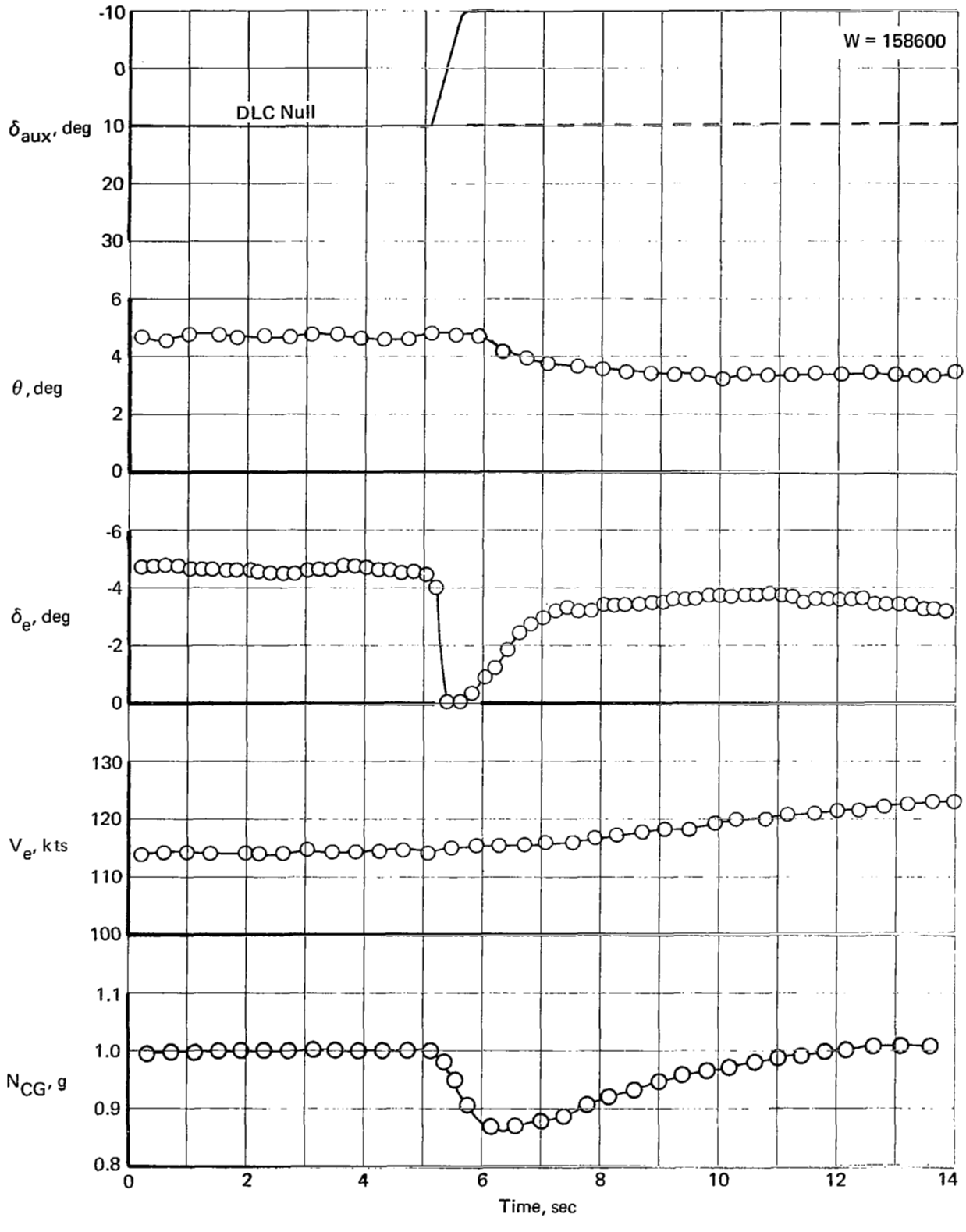

FIGURE 29.–AIRPLANE RESPONSE TO A 20° UP AUXILIARY FLAP STEP–30° MAIN FLAP AND POWER FOR LEVEL FLIGHT; BLC OFF

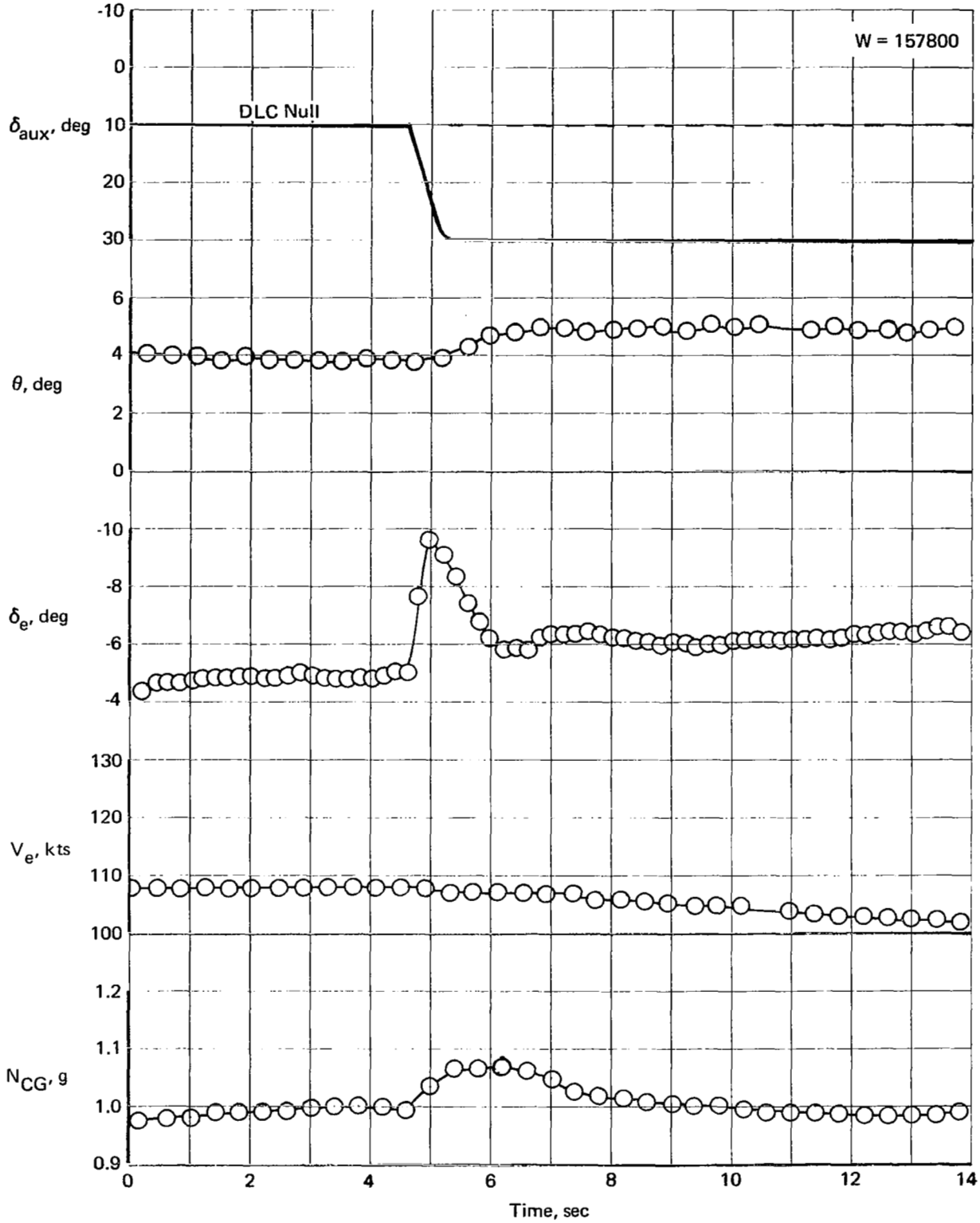

FIGURE 30.–AIRPLANE RESPONSE TO A 20° DOWN AUXILIARY FLAP STEP–30° MAIN FLAP AND POWER FOR LEVEL FLIGHT; BLC ON

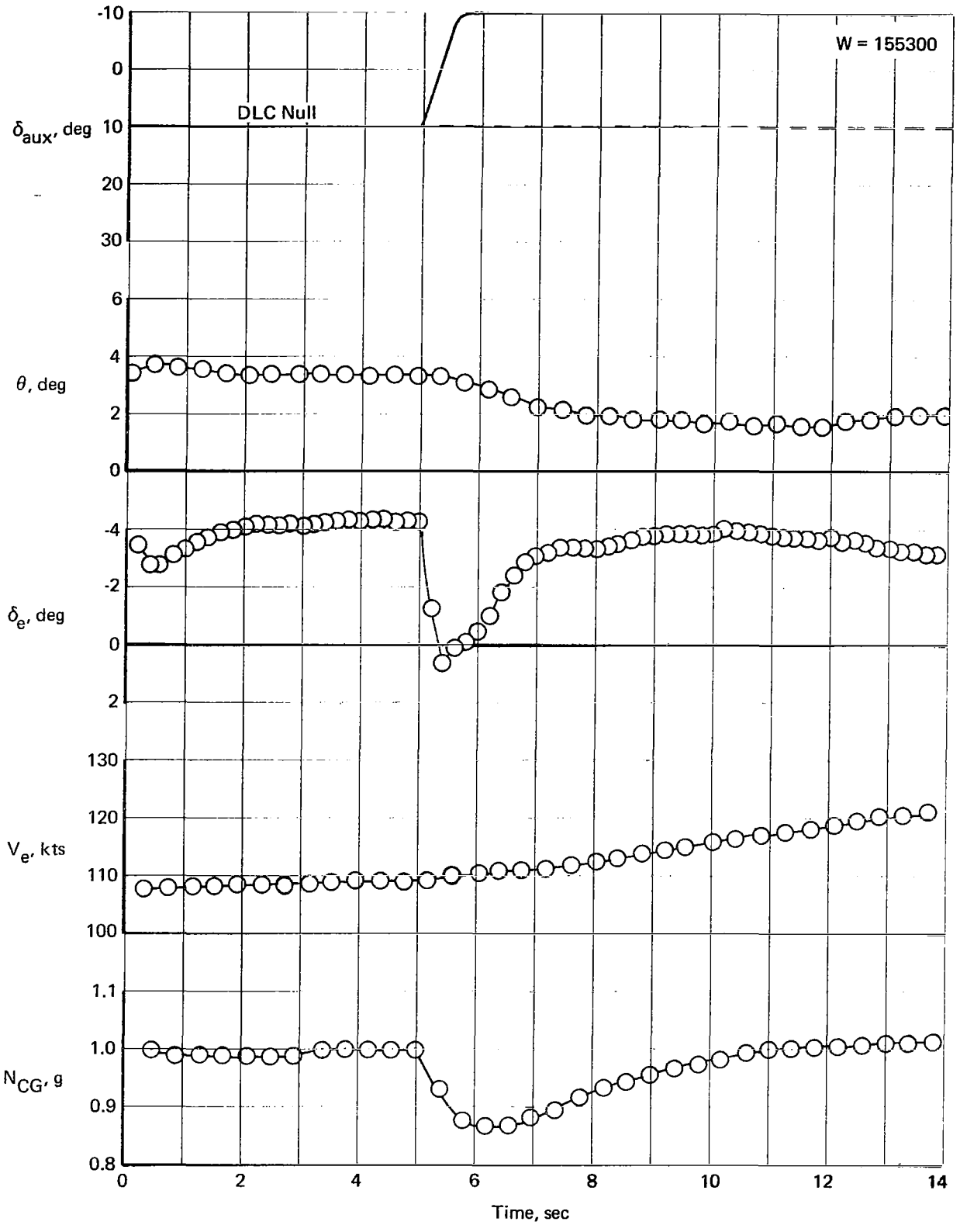

FIGURE 31.–AIRPLANE RESPONSE TO A 20° UP AUXILIARY FLAP STEP–30° MAIN FLAP AND POWER FOR LEVEL FLIGHT; BLC ON

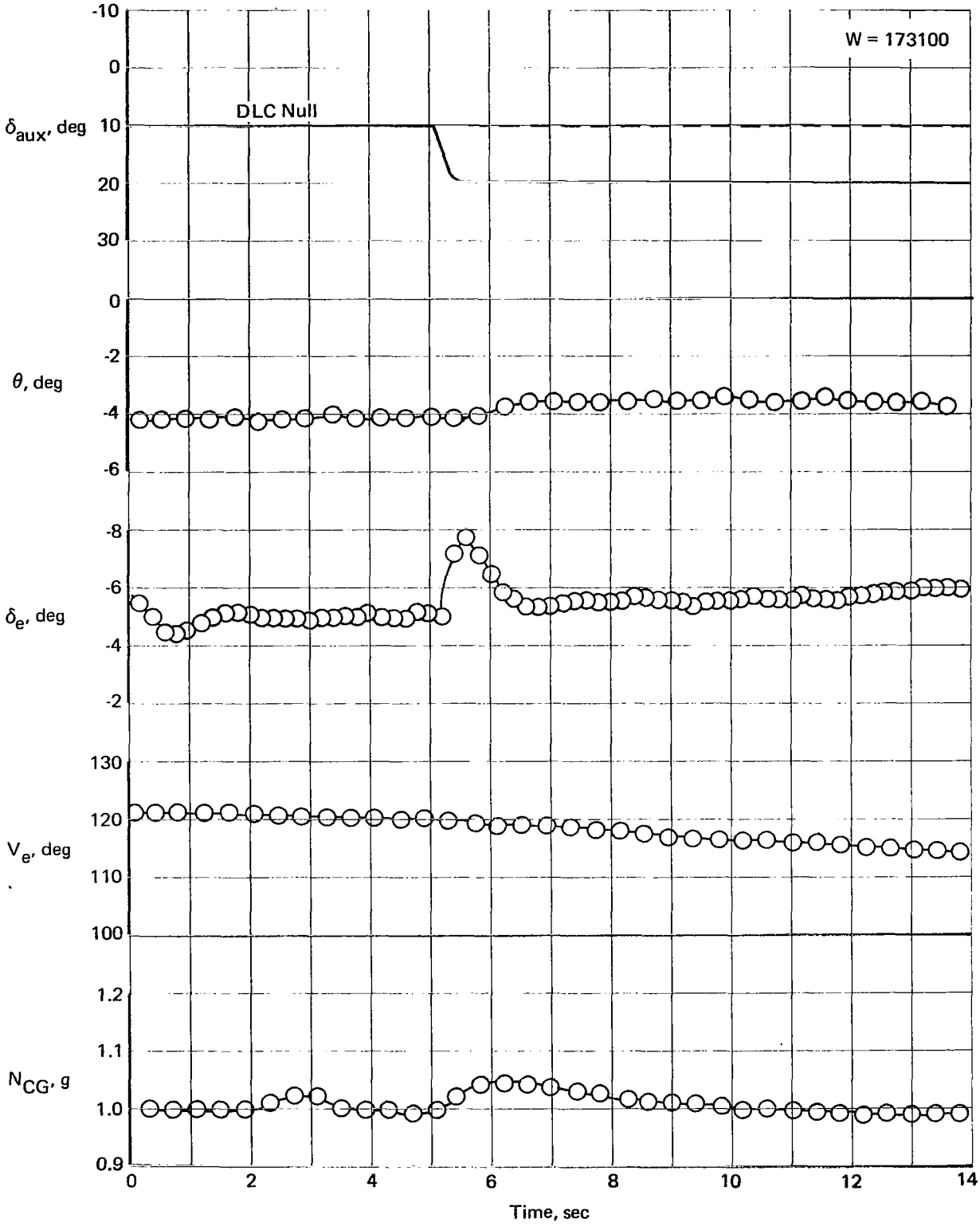

FIGURE 32.–AIRPLANE RESPONSE TO A 10° DOWN AUXILIARY FLAP STEP–40° MAIN FLAP AND 60% N_2 POWER; BLC ON

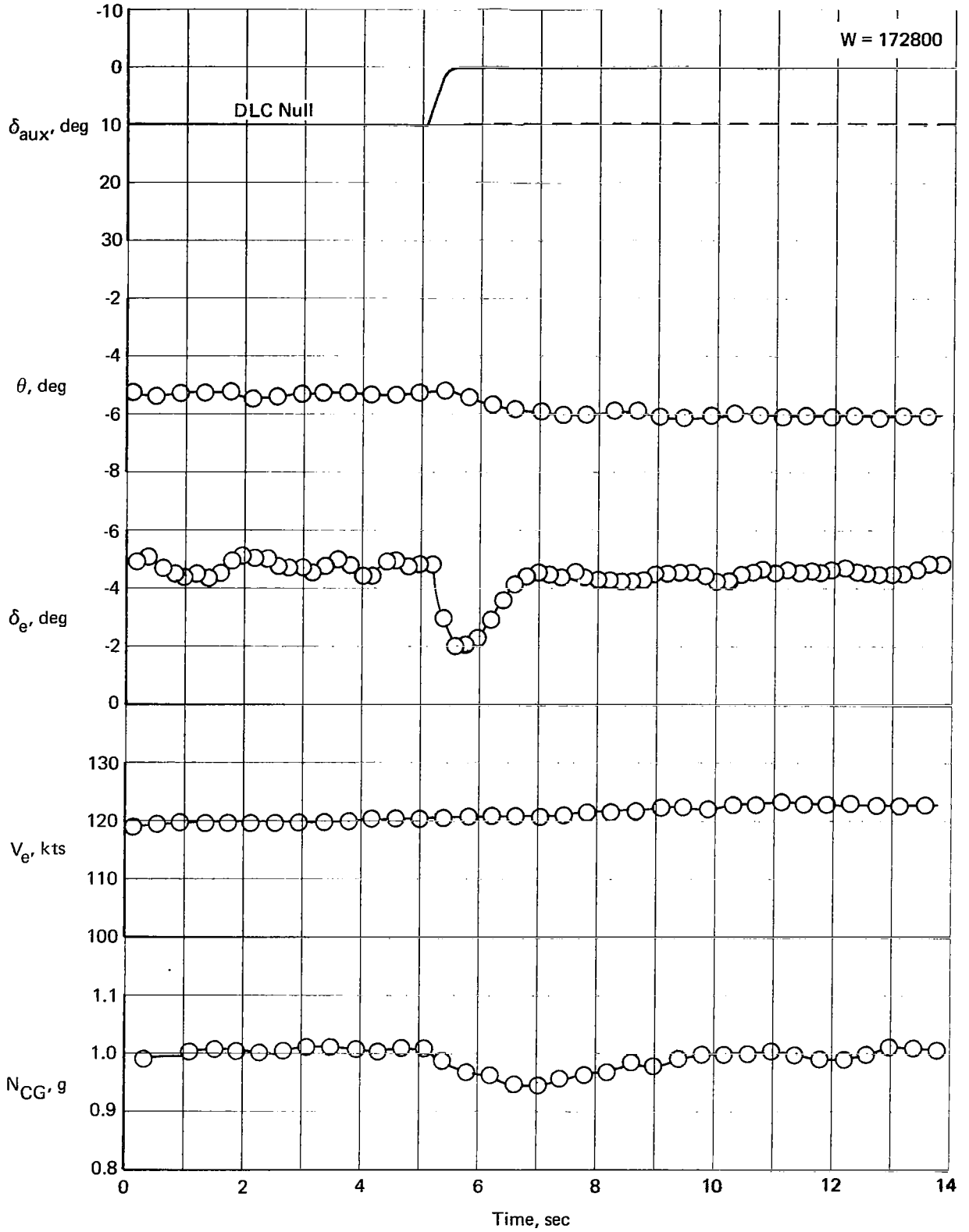

FIGURE 33.–AIRPLANE RESPONSE TO A 10° UP AUXILIARY FLAP STEP–40° MAIN FLAP AND 60% N_2 POWER; BLC ON

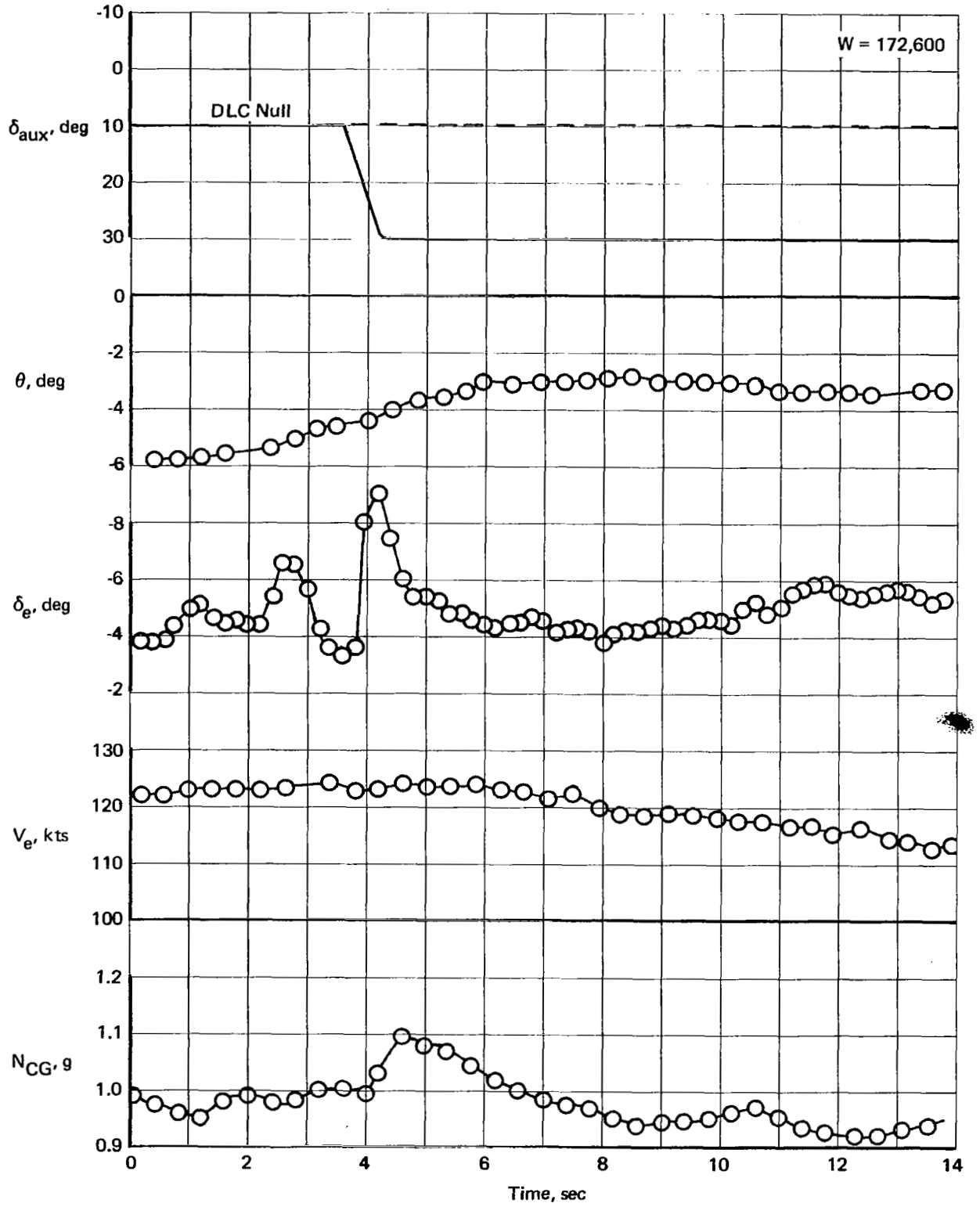

FIGURE 34.–AIRPLANE RESPONSE TO A 20° DOWN AUXILIARY FLAP STEP–40° MAIN FLAP AND 60% N_2 POWER; BLC ON

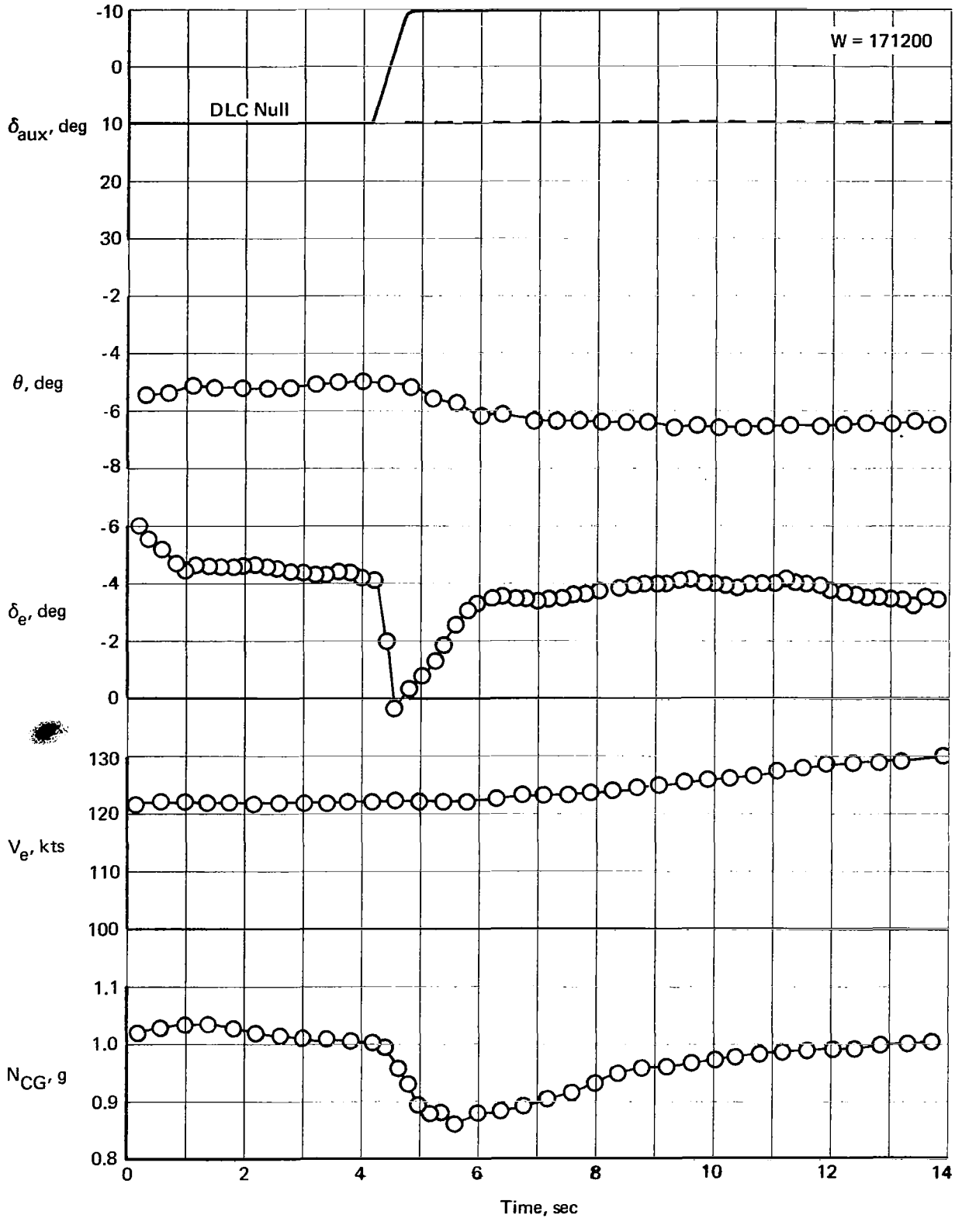

FIGURE 35.–AIRPLANE RESPONSE TO A 20° UP AUXILIARY FLAP STEP–40° MAIN FLAP AND 60% N_2 POWER; BLC ON

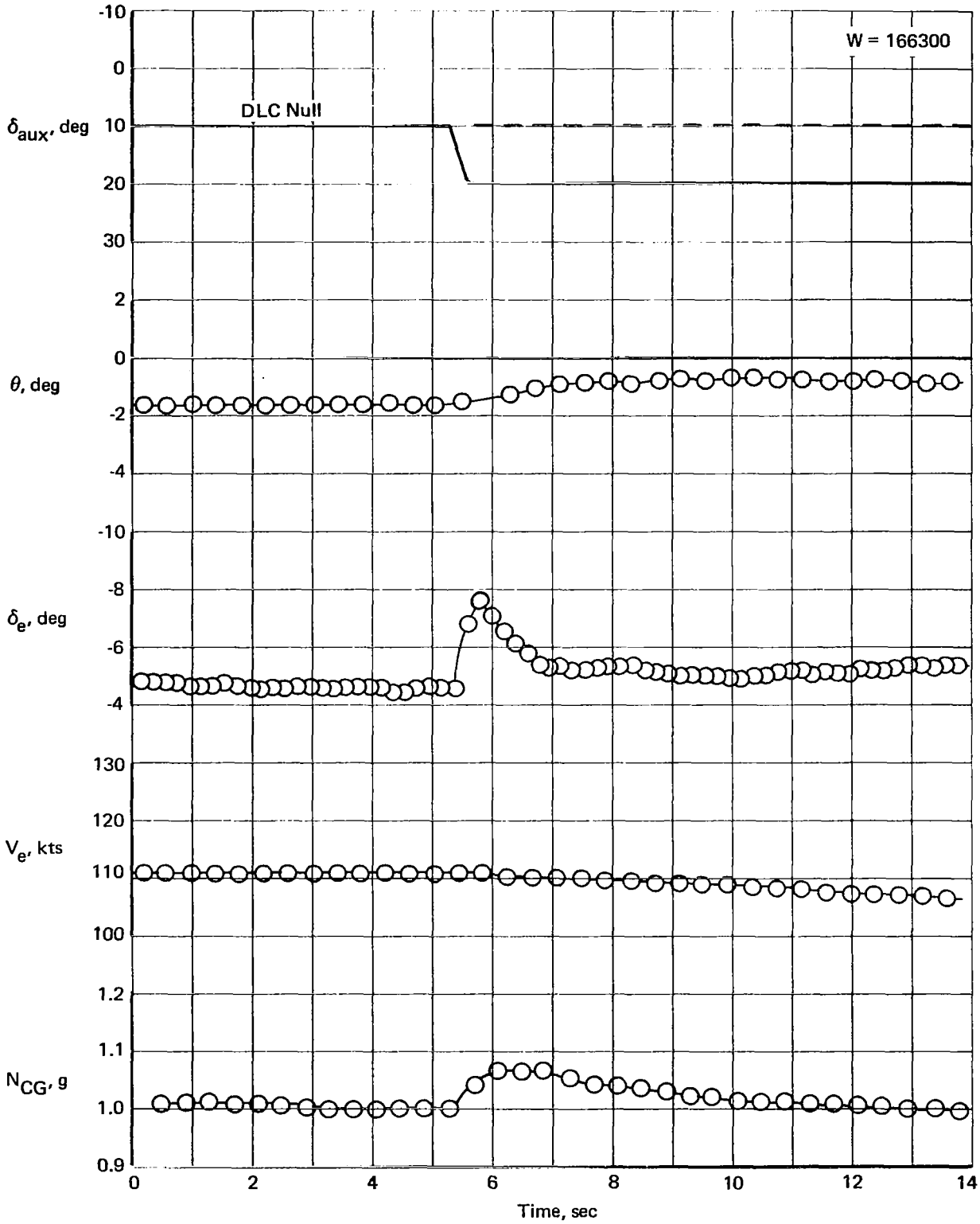

FIGURE 36.–AIRPLANE RESPONSE TO A 10° DOWN AUXILIARY FLAP STEP–40° MAIN FLAP AND 90%N_2 POWER; BLC ON

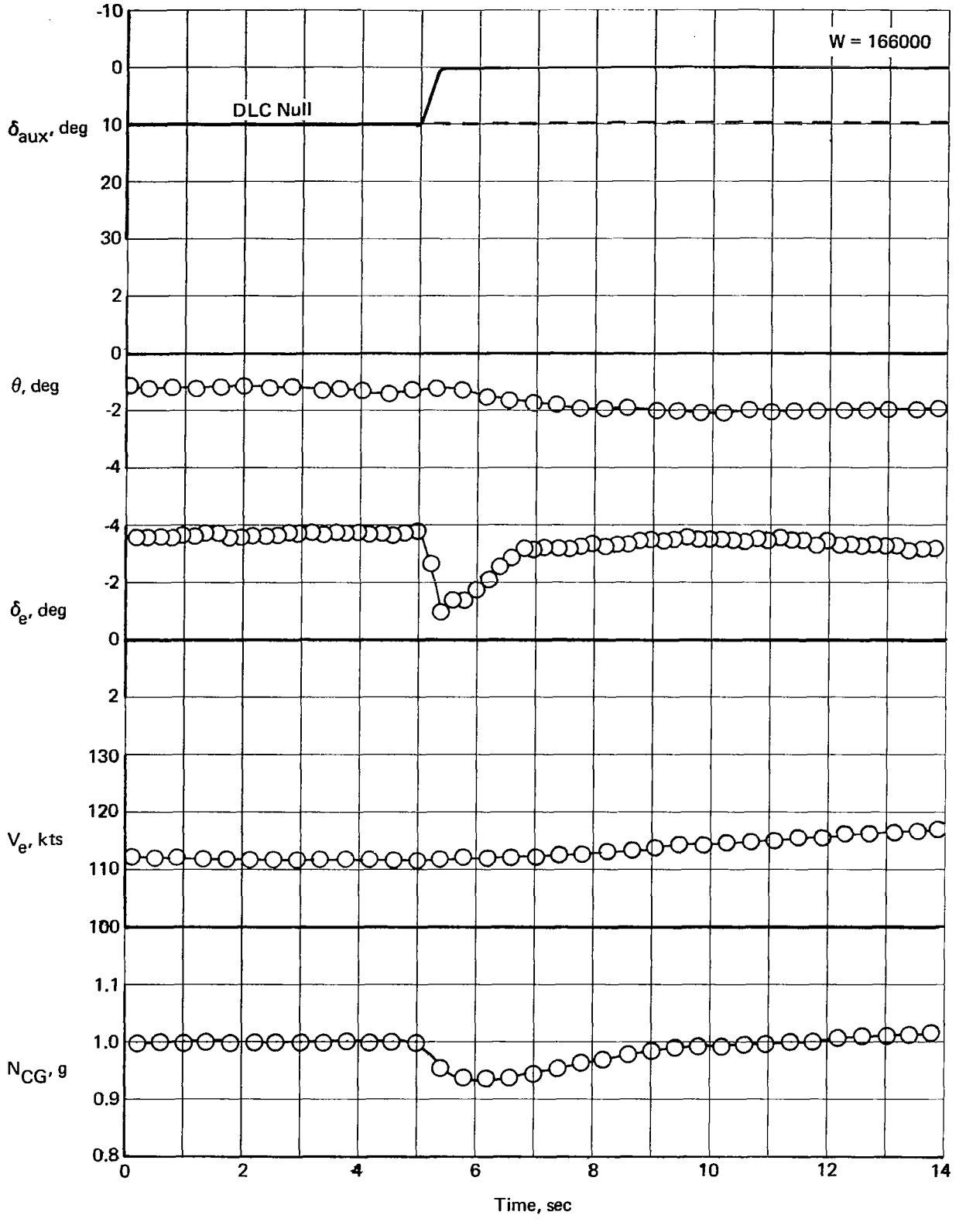

FIGURE 37.–AIRPLANE RESPONSE TO A 10° UP AUXILIARY FLAP STEP–40° MAIN FLAP AND 90% N_2 POWER; BLC ON

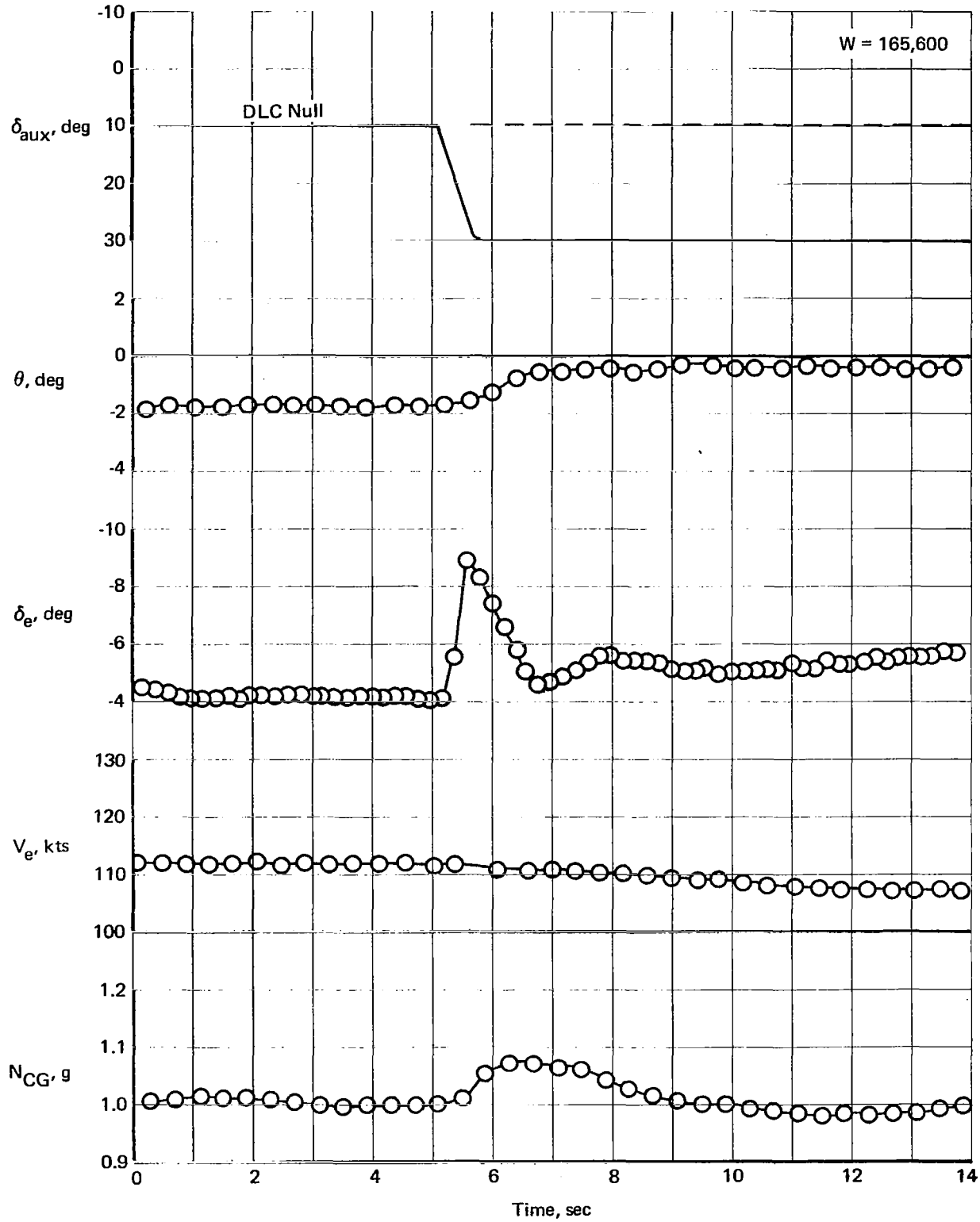

FIGURE 38.–AIRPLANE RESPONSE TO A 20° DOWN AUXILIARY FLAP STEP–40° MAIN FLAP AND 90% N_2 POWER; BLC ON

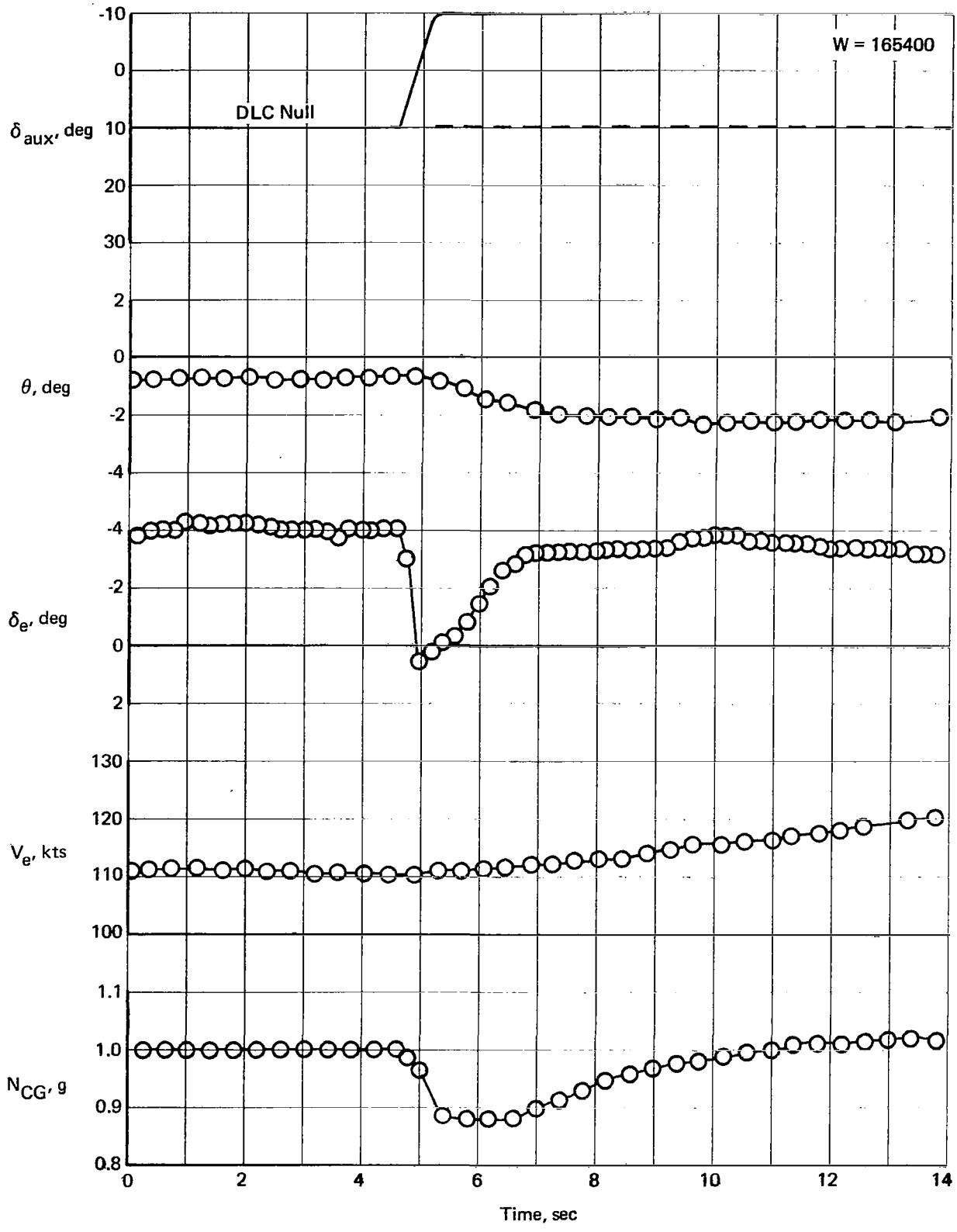

FIGURE 39.–AIRPLANE RESPONSE TO A 20° UP AUXILIARY FLAP STEP–40° MAIN FLAP AND 90% N_2 POWER; BLC ON

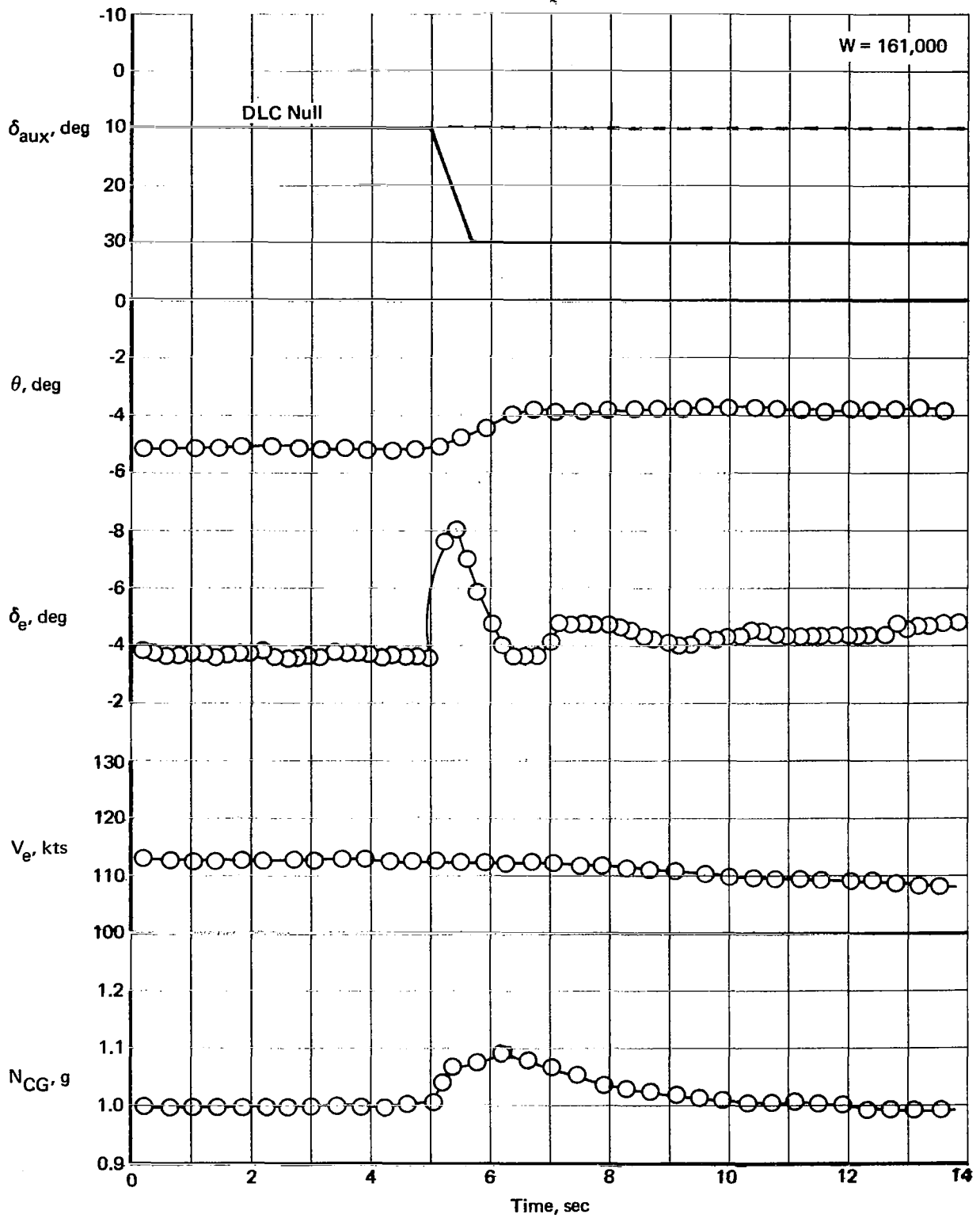

FIGURE 40.–AIRPLANE RESPONSE TO A 20° DOWN AUXILIARY FLAP STEP–50° MAIN FLAP AND 90% N_2 POWER; BLC ON

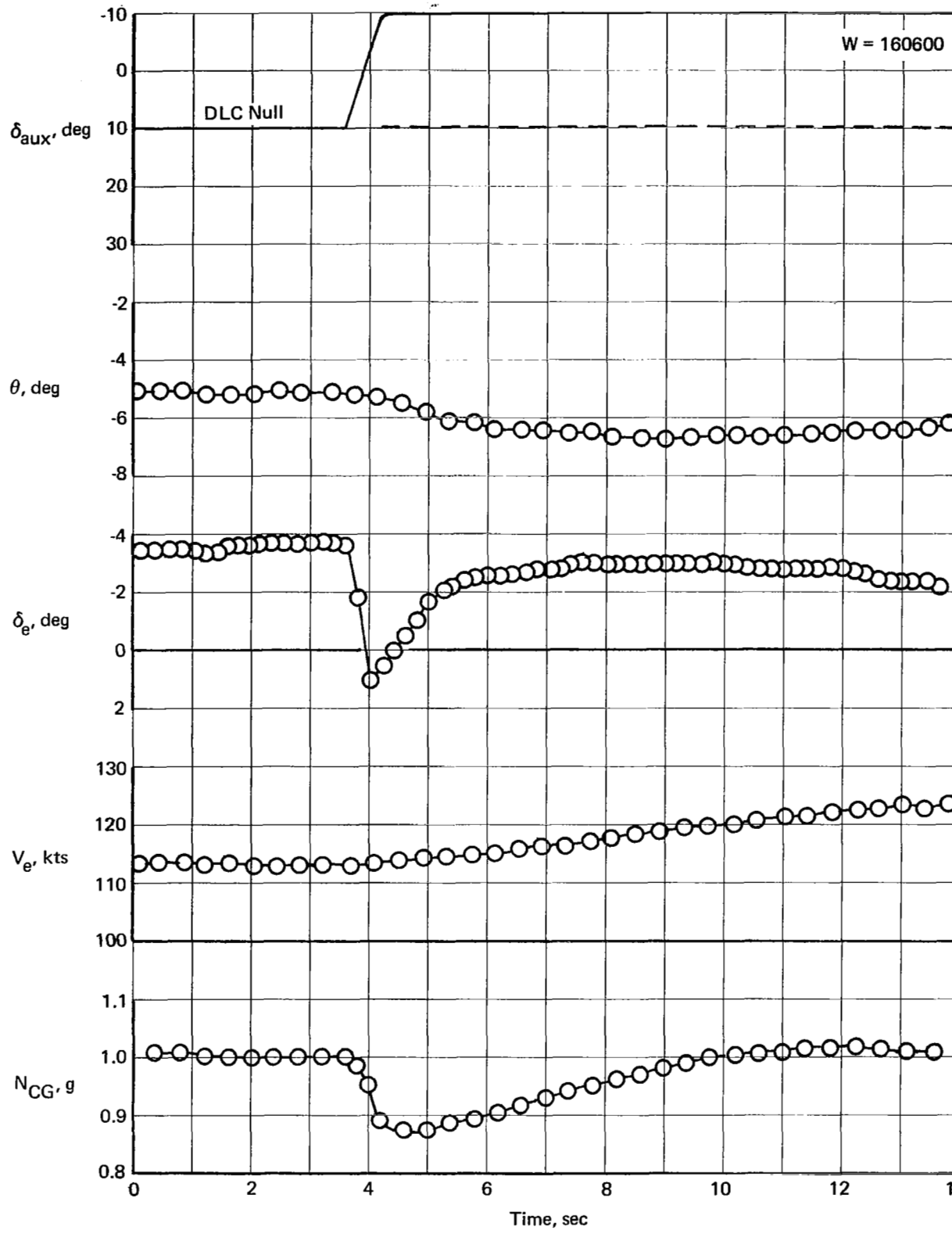

FIGURE 41.–AIRPLANE RESPONSE TO A 20° UP AUXILIARY FLAP STEP–50° MAIN FLAP AND 90% N_2 POWER; BLC ON

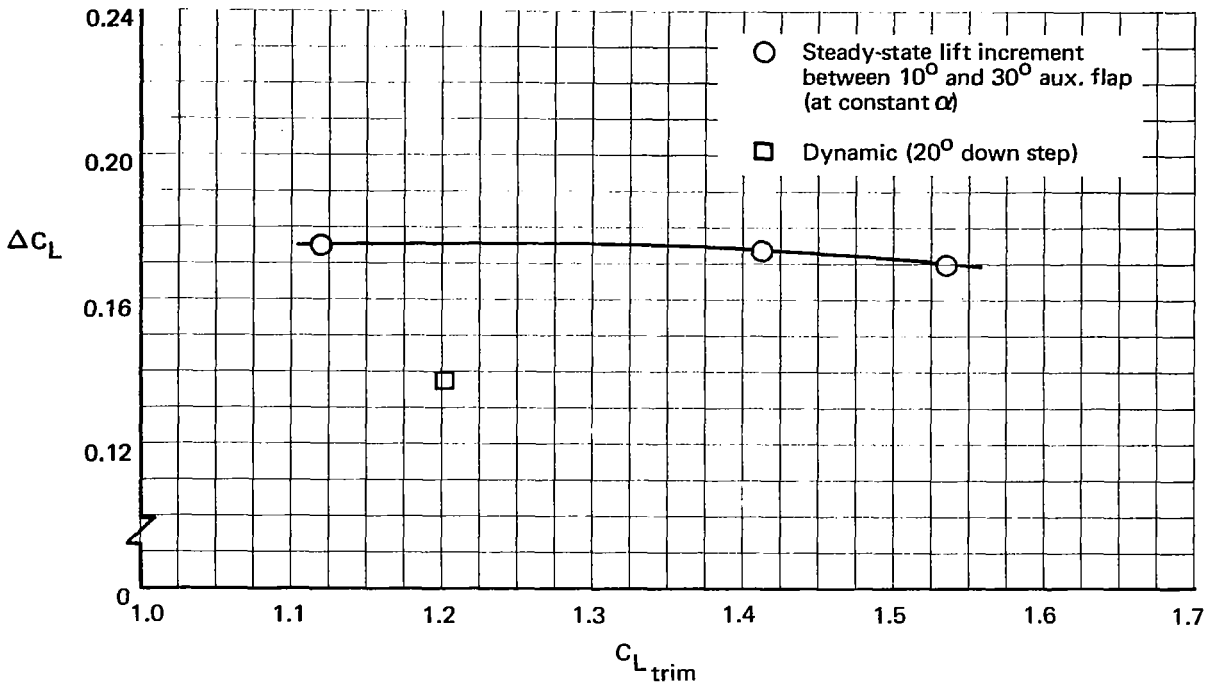

FIGURE 42.–COMPARISON OF DYNAMIC AND STEADY-STATE LIFT CHANGE WITH DOWN-AUXILIARY-FLAP DEFLECTION–30° MAIN FLAP AND IDLE POWER; BLC OFF

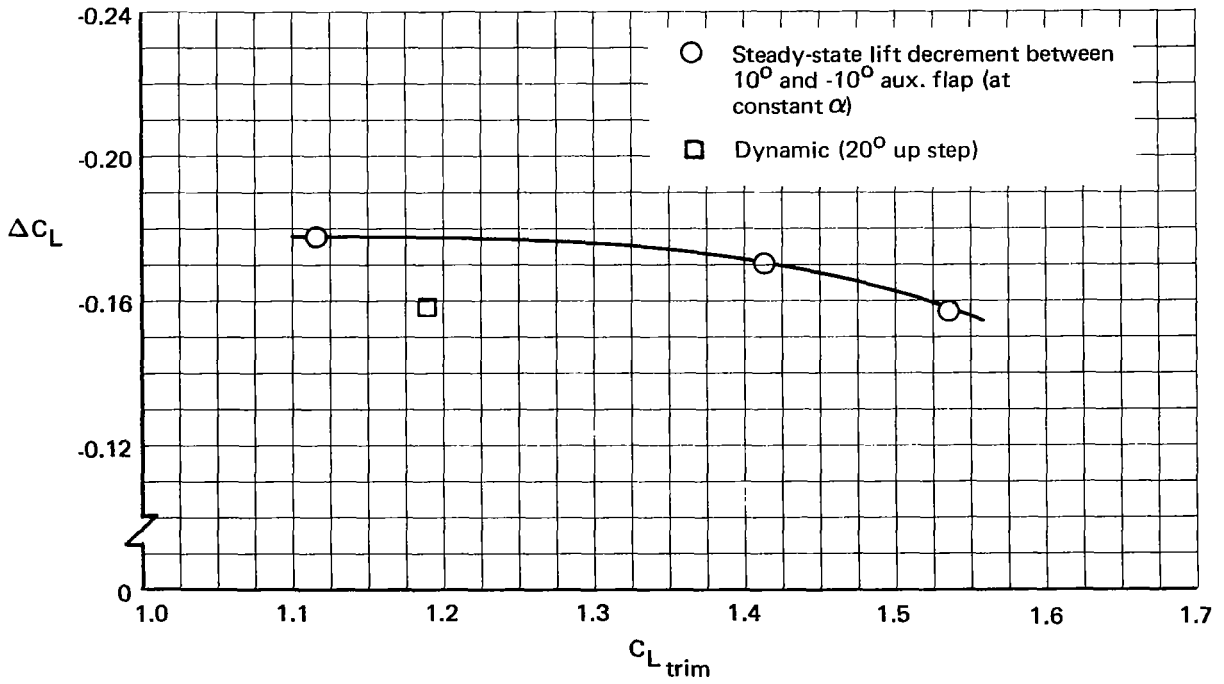

FIGURE 43.–COMPARISON OF DYNAMIC AND STEADY-STATE LIFT CHANGE WITH UP-AUXILIARY-FLAP DEFLECTION–30° MAIN FLAP AND IDLE POWER; BLC OFF

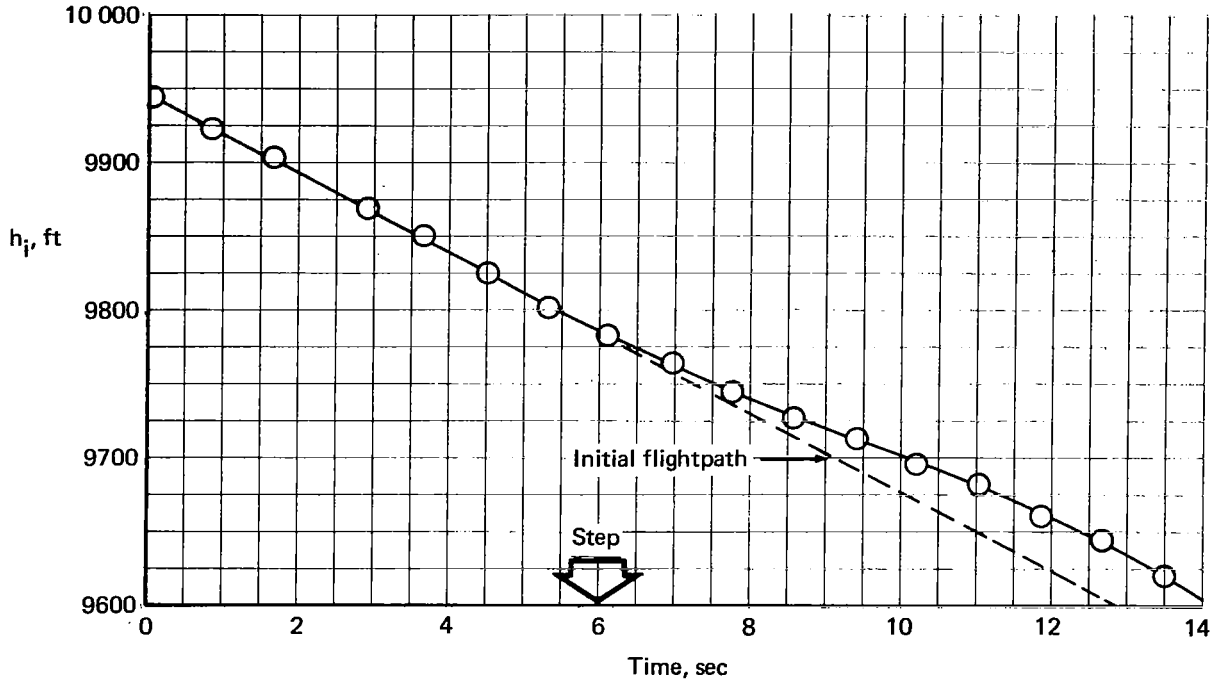

FIGURE 44.–ALTITUDE RESPONSE TO A 10° DOWN AUXILIARY FLAP STEP–30° MAIN FLAP AND IDLE POWER; BLC OFF

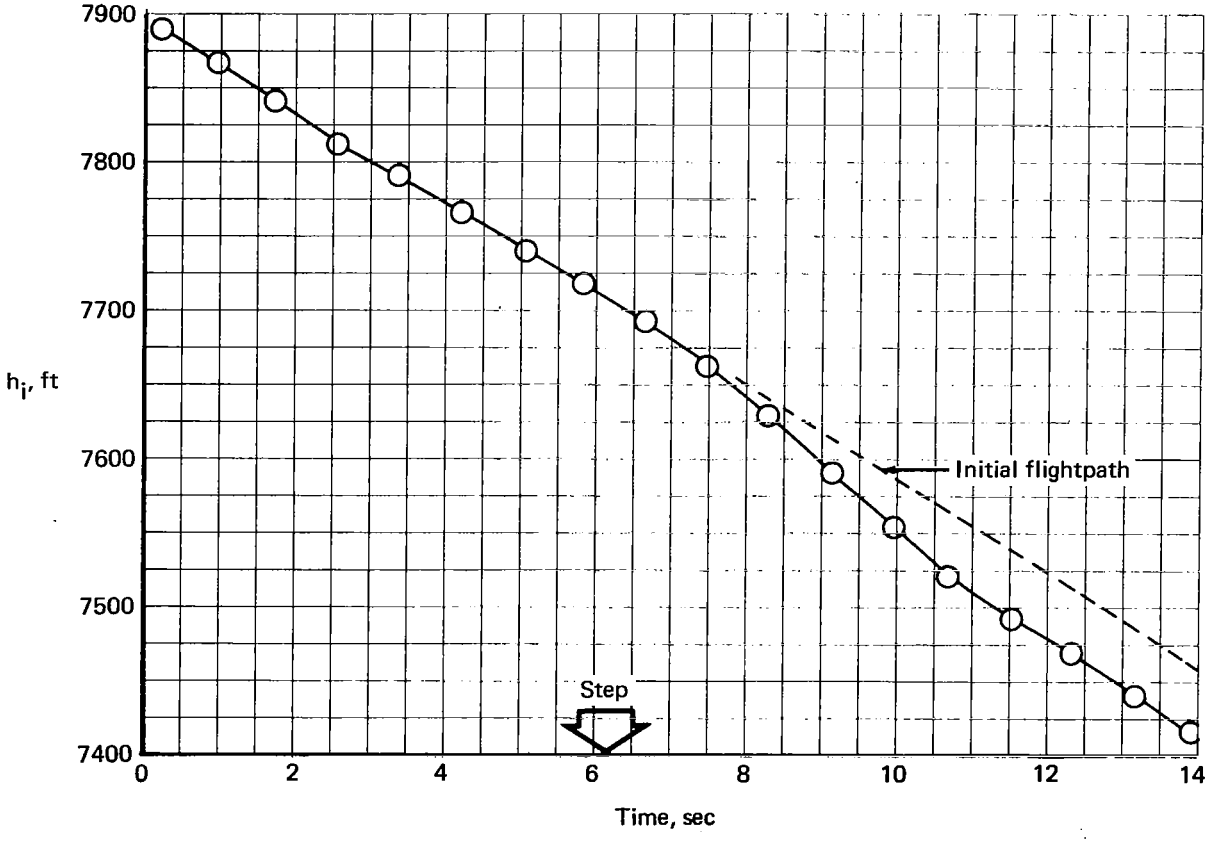

FIGURE 45.–ALTITUDE RESPONSE TO A 10° UP AUXILIARY FLAP STEP–30° MAIN FLAP AND IDLE POWER; BLC OFF

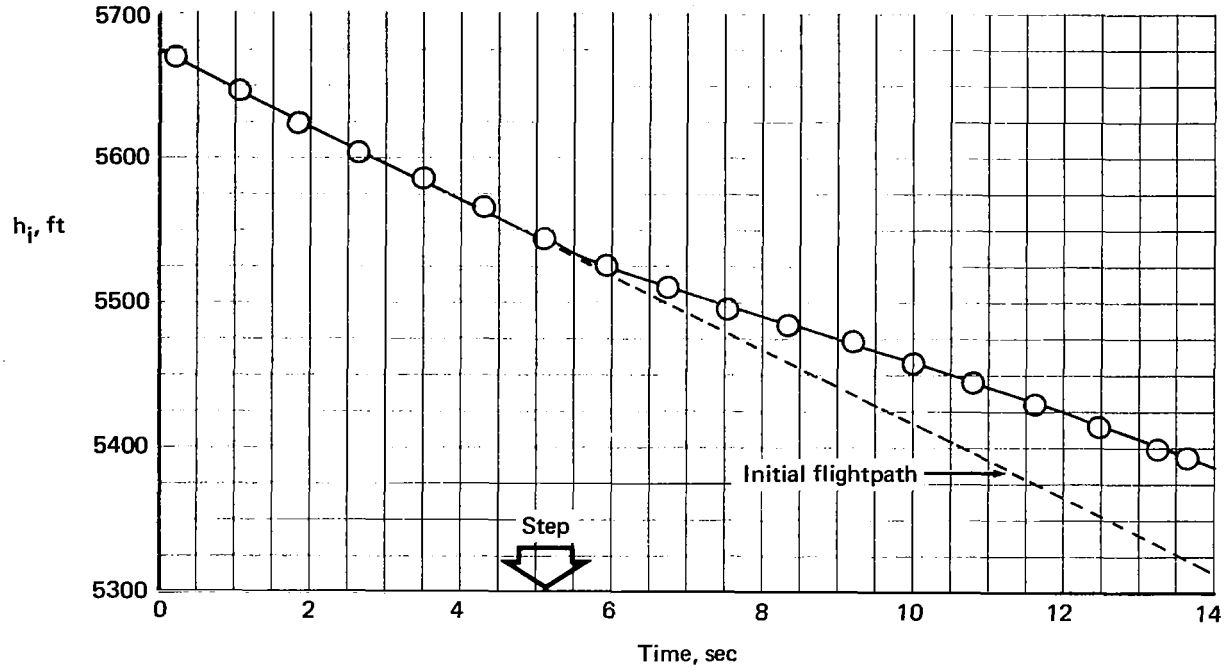

FIGURE 46.–ALTITUDE RESPONSE TO A 20° DOWN AUXILIARY FLAP STEP–30° MAIN FLAP AND IDLE POWER; BLC OFF

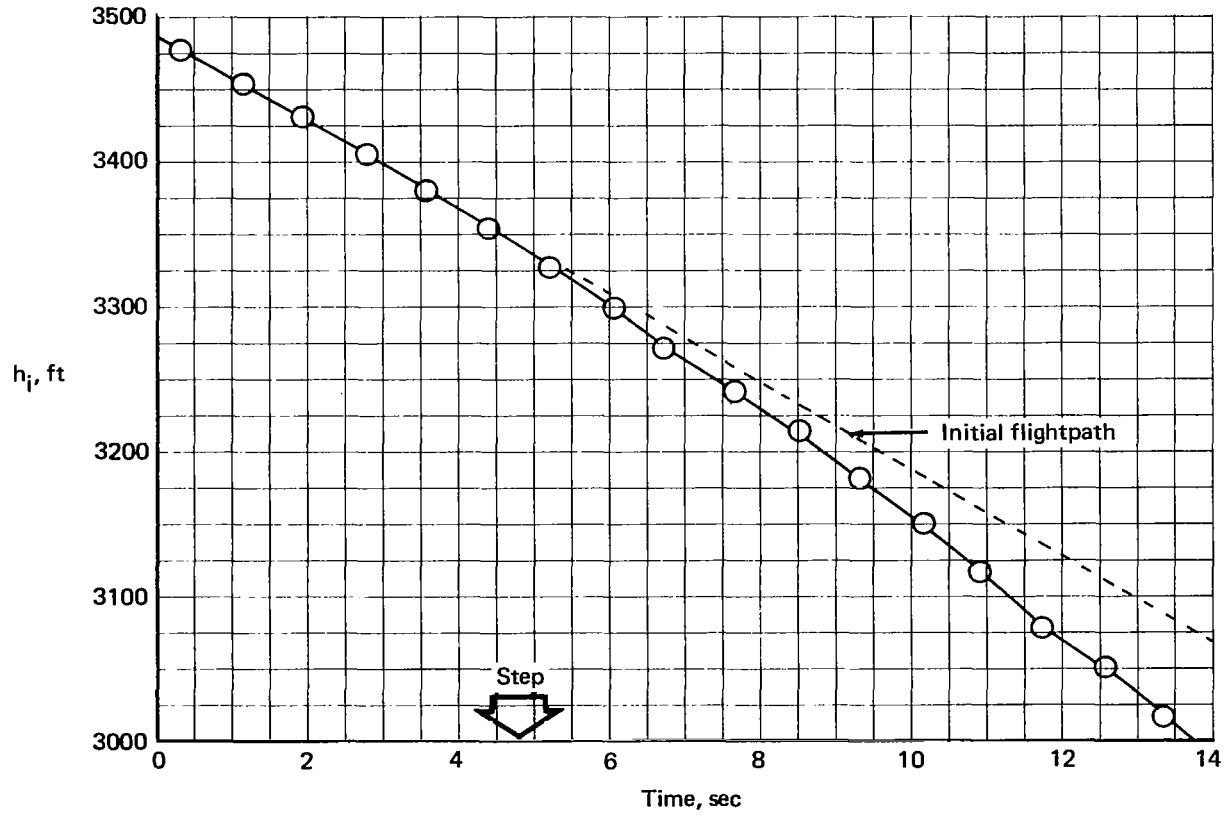

FIGURE 47.–ALTITUDE RESPONSE TO A 20° UP AUXILIARY FLAP STEP–30° MAIN FLAP AND IDLE POWER; BLC OFF

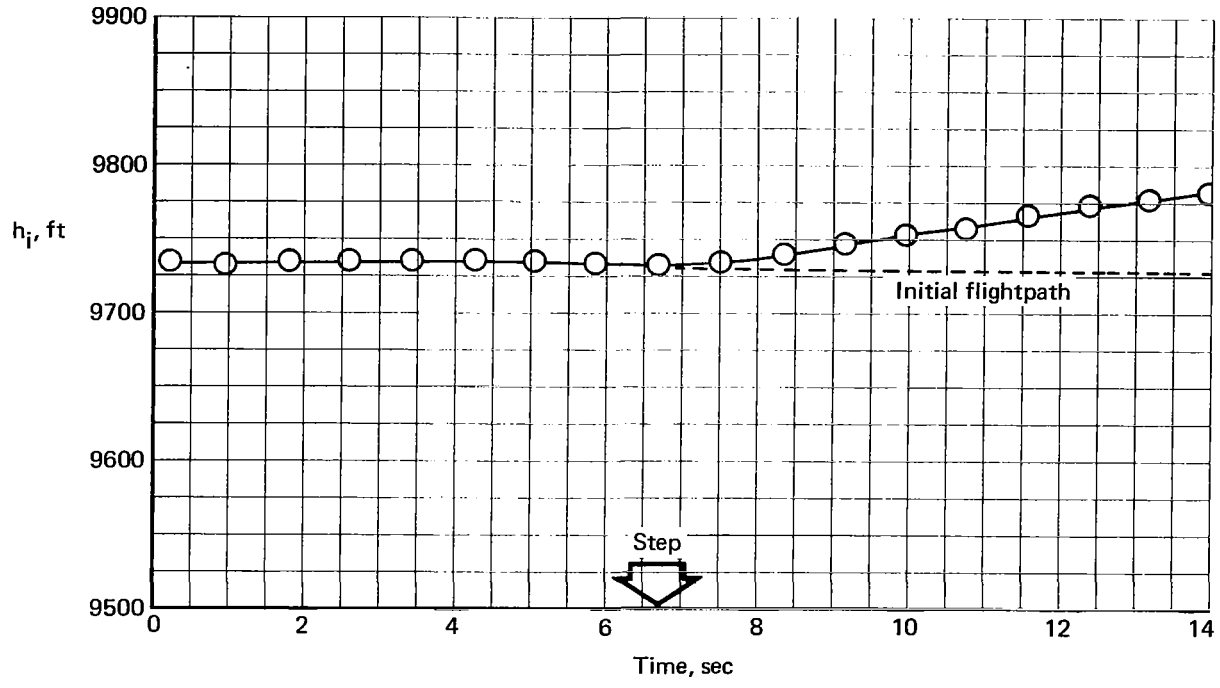

FIGURE 48.–ALTITUDE RESPONSE TO A 20° DOWN AUXILIARY FLAP STEP–30° MAIN FLAP AND POWER FOR LEVEL FLIGHT; BLC OFF

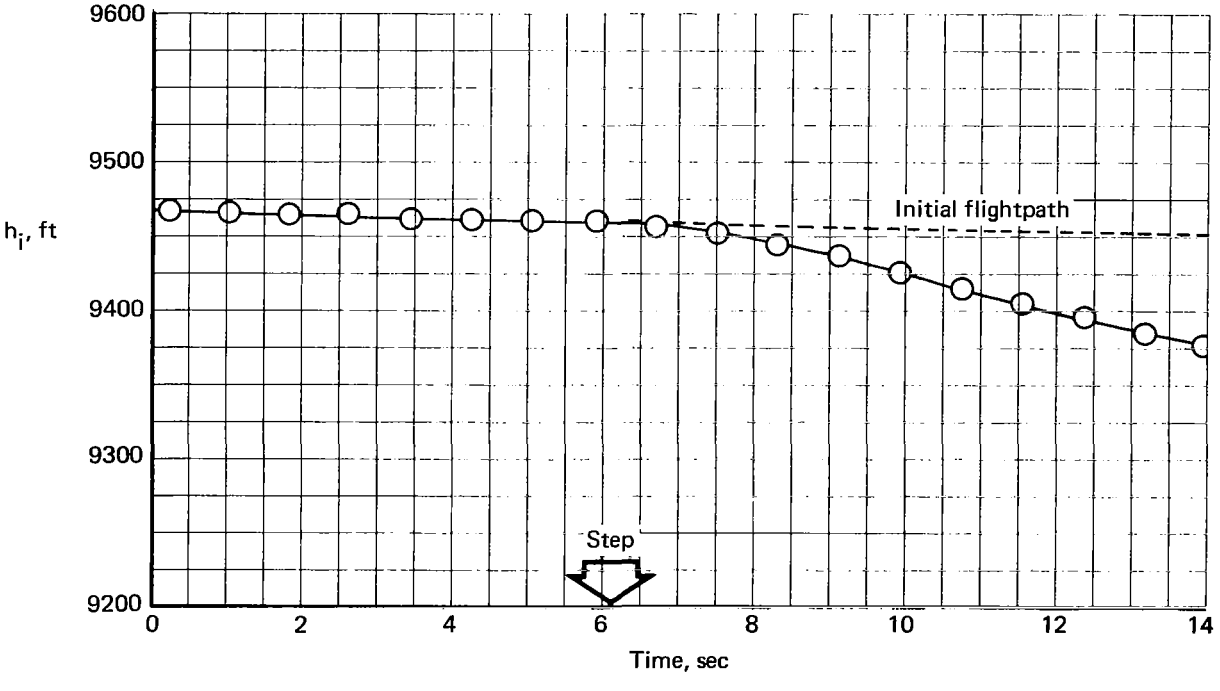

FIGURE 49.–ALTITUDE RESPONSE TO A 20° UP AUXILIARY FLAP STEP–30° MAIN FLAP AND POWER FOR LEVEL FLIGHT; BLC OFF

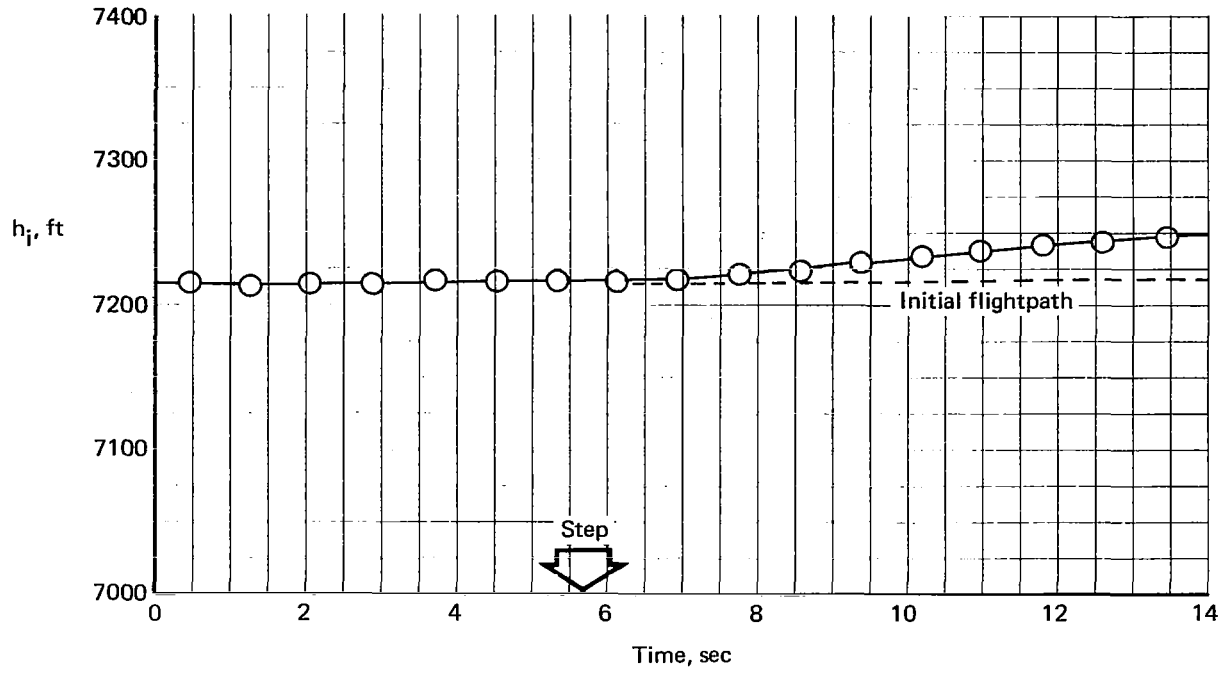

FIGURE 50.–ALTITUDE RESPONSE TO A 20° DOWN AUXILIARY FLAP STEP–30° MAIN FLAP AND POWER FOR LEVEL FLIGHT; BLC ON

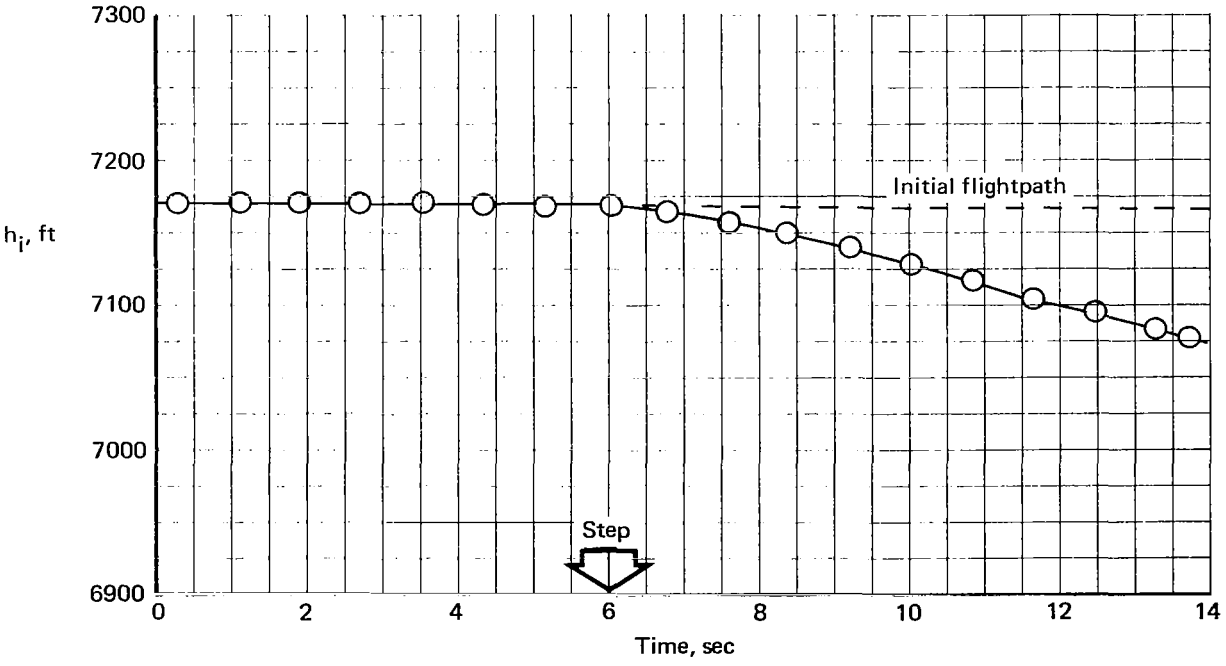

FIGURE 51.–ALTITUDE RESPONSE TO A 20° UP AUXILIARY FLAP STEP–30° MAIN FLAP AND POWER FOR LEVEL FLIGHT; BLC ON

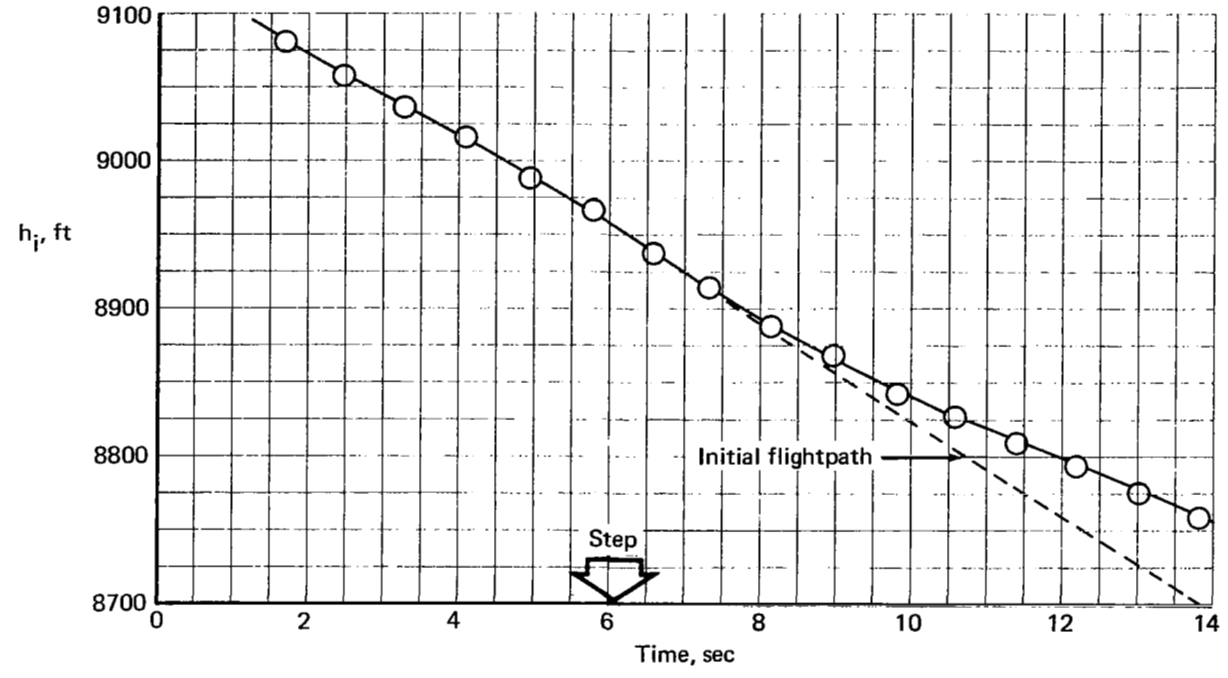

FIGURE 52.–ALTITUDE RESPONSE TO A 10° DOWN AUXILIARY FLAP STEP–40° MAIN FLAP AND 60% N_2 POWER; BLC ON

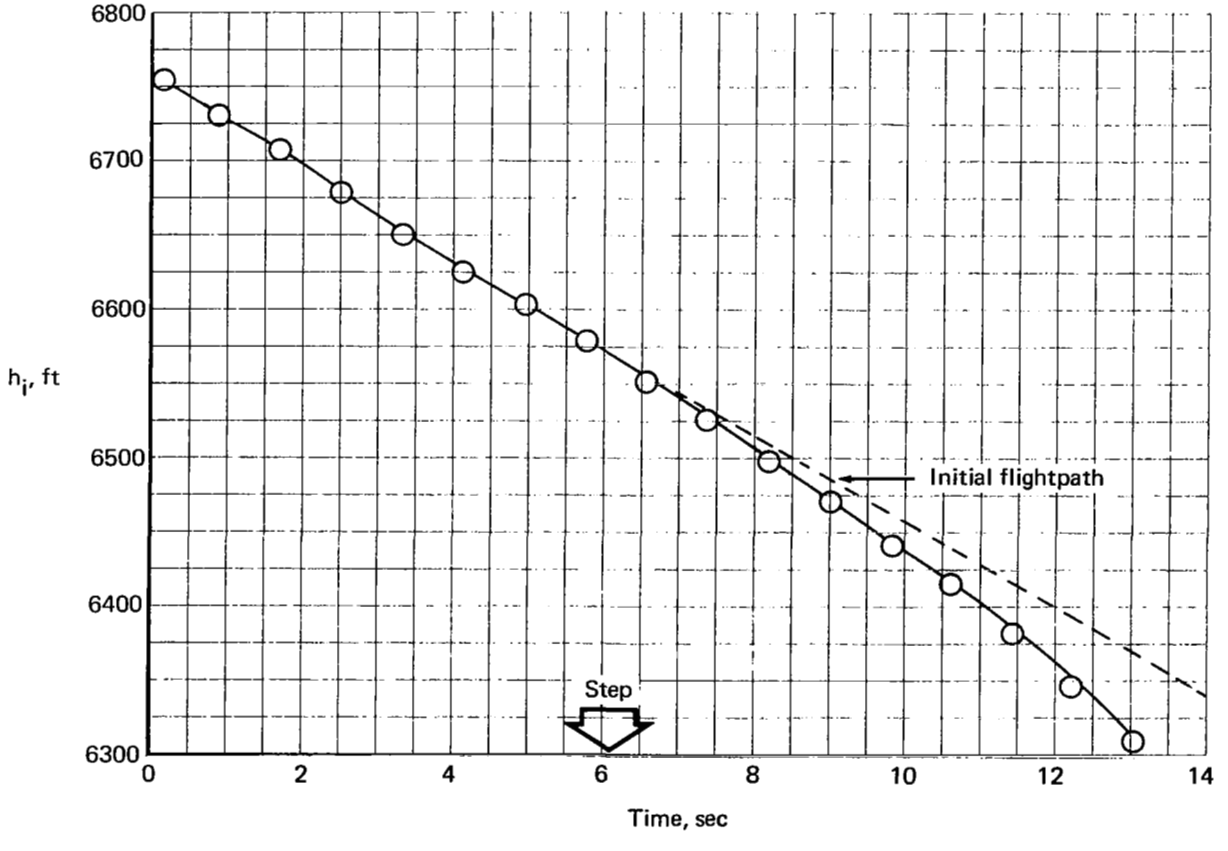

FIGURE 53.–ALTITUDE RESPONSE TO A 10° UP AUXILIARY FLAP STEP–40° MAIN FLAP AND 60% N_2 POWER; BLC ON

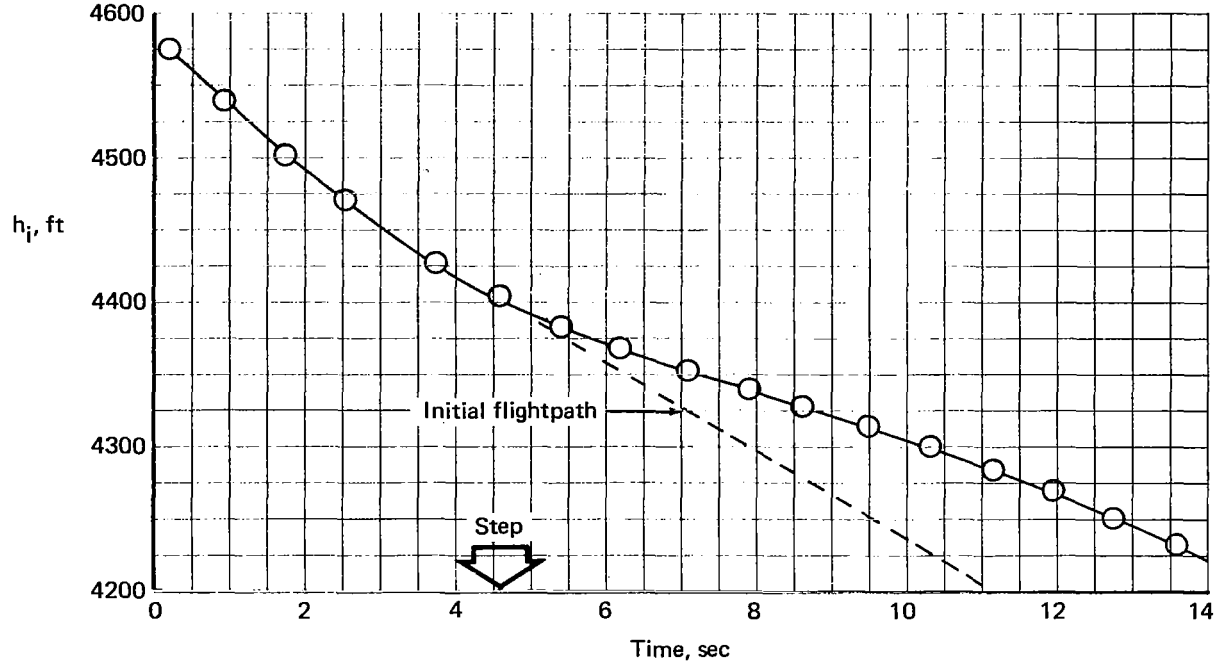

FIGURE 54.–ALTITUDE RESPONSE TO A 20° DOWN AUXILIARY FLAP STEP–40° MAIN FLAP AND 60% N_2 POWER; BLC ON

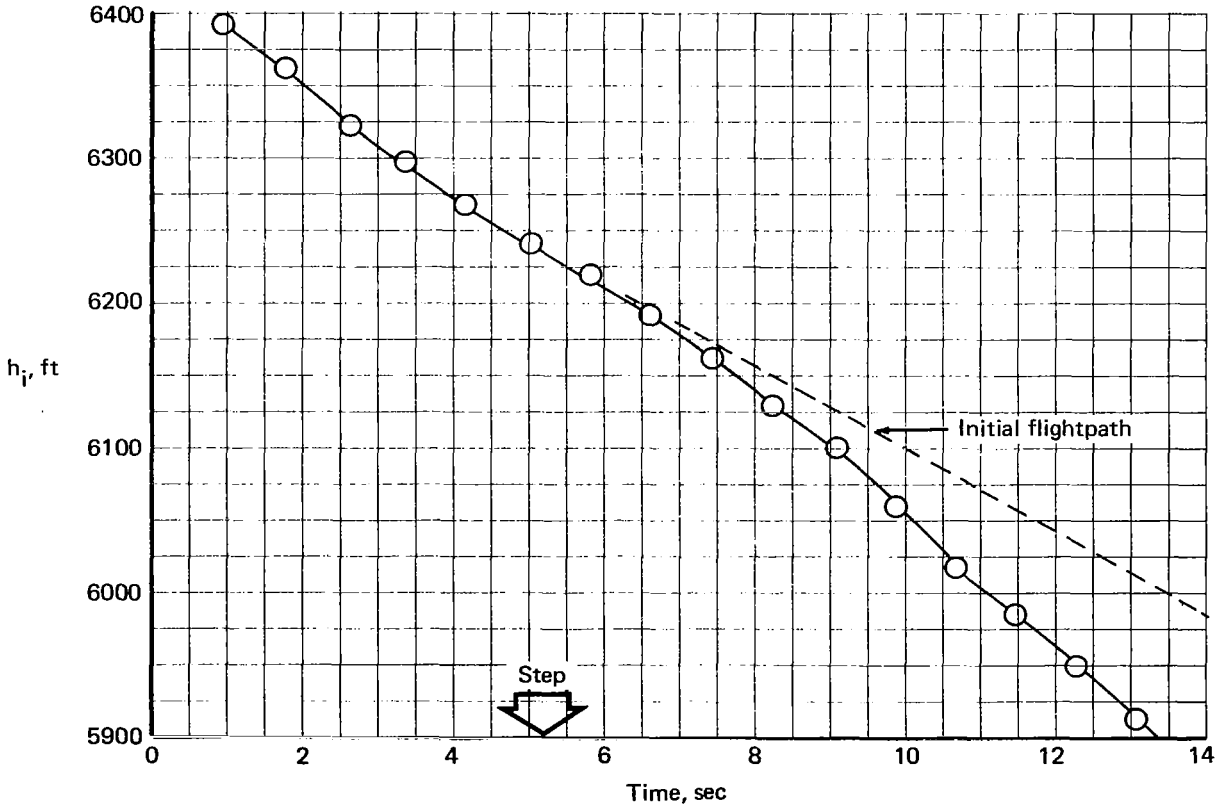

FIGURE 55.–ALTITUDE RESPONSE TO A 20° UP AUXILIARY FLAP STEP–40° MAIN FLAP AND 60% N_2 POWER; BLC ON

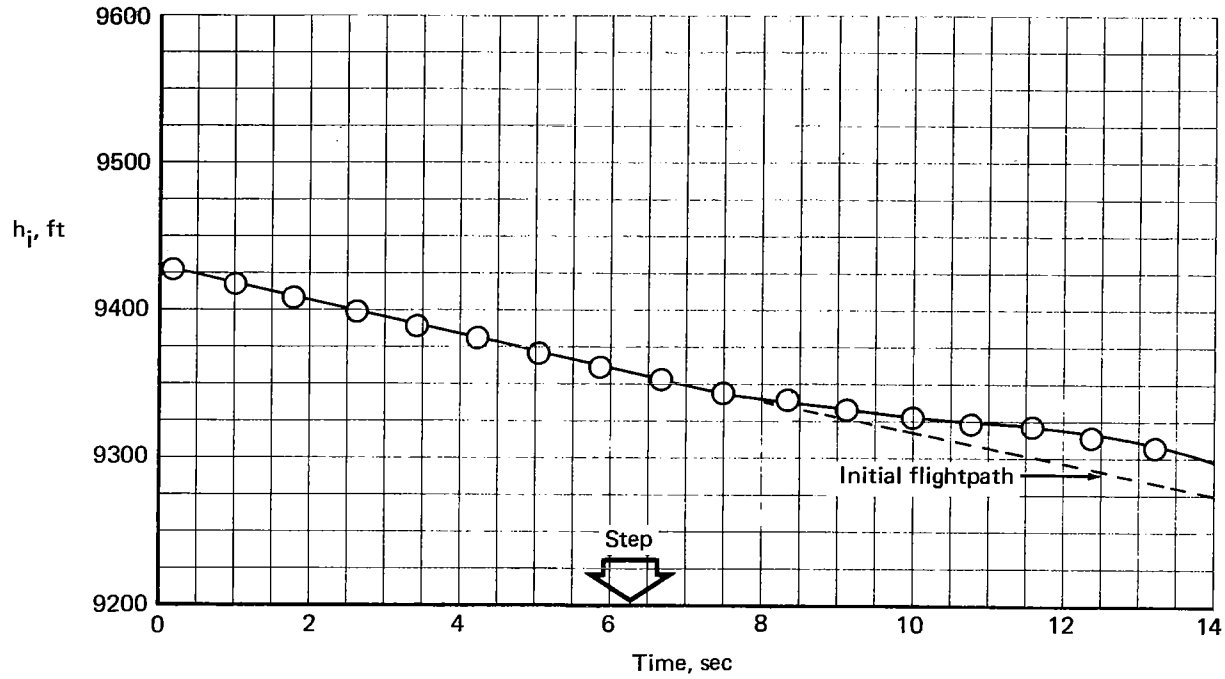

FIGURE 56.–ALTITUDE RESPONSE TO A 10° DOWN AUXILIARY FLAP STEP–40° MAIN FLAP AND 90% N_2 POWER; BLC ON

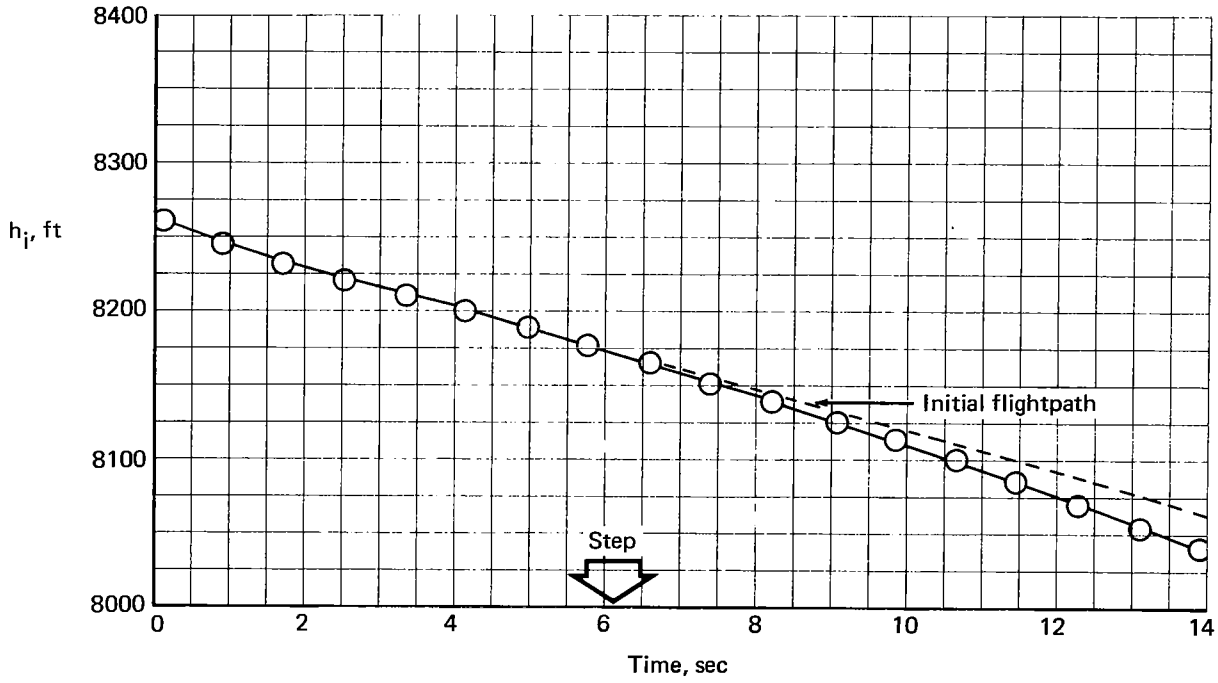

FIGURE 57.–ALTITUDE RESPONSE TO A 10° UP AUXILIARY FLAP STEP–40° MAIN FLAP AND 90% N_2 POWER; BLC ON

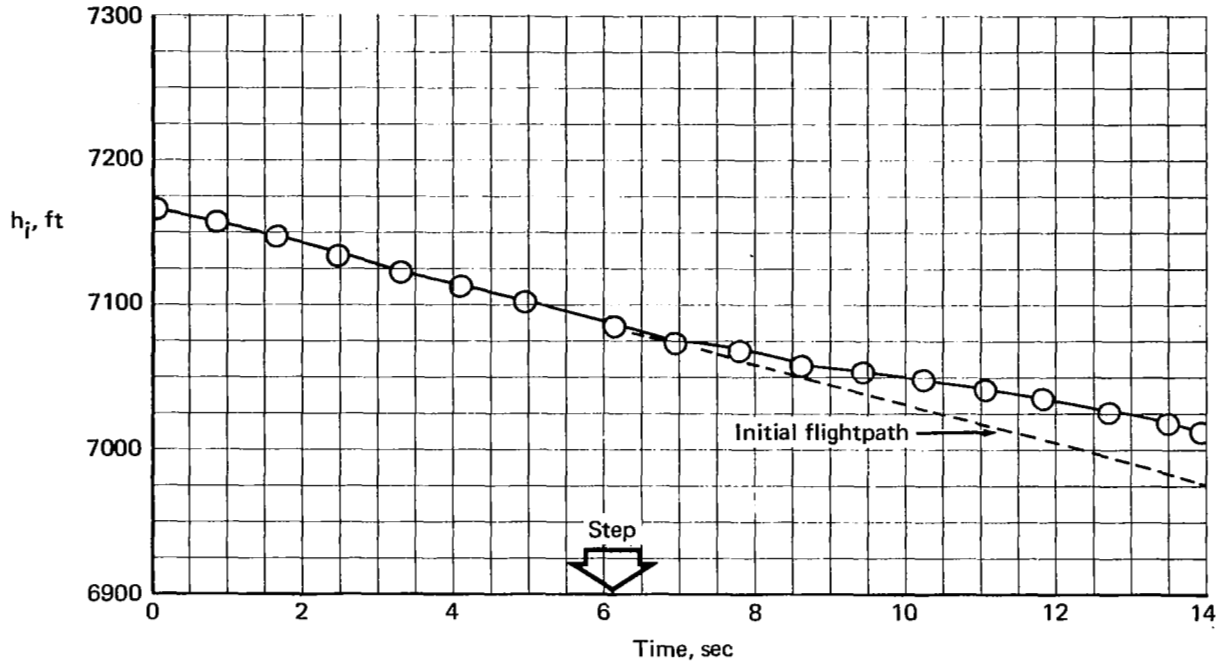

FIGURE 58.–ALTITUDE RESPONSE TO A 20° DOWN AUXILIARY FLAP STEP–40° MAIN FLAP AND 90% N_2 POWER; BLC ON

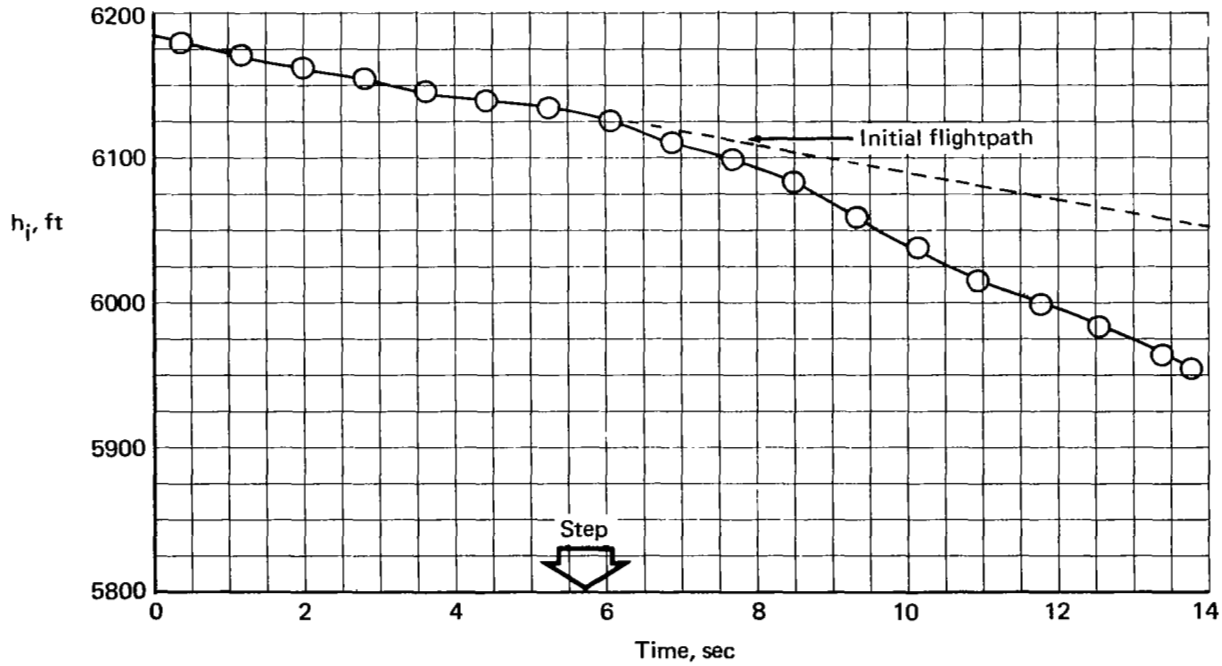

FIGURE 59.–ALTITUDE RESPONSE TO A 20° UP AUXILIARY FLAP STEP–40° MAIN FLAP AND 90% N_2 POWER; BLC ON

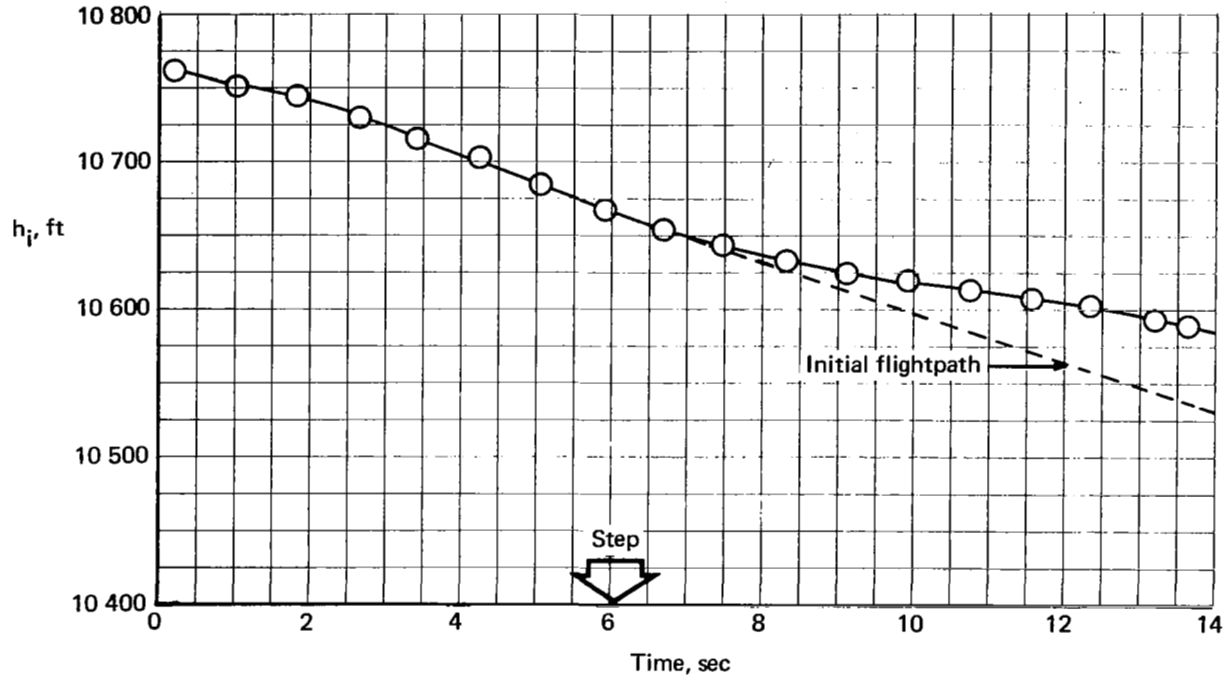

FIGURE 60.–ALTITUDE RESPONSE TO A 20° DOWN AUXILIARY FLAP STEP–50° MAIN FLAP AND 90% N_2 POWER; BLC ON

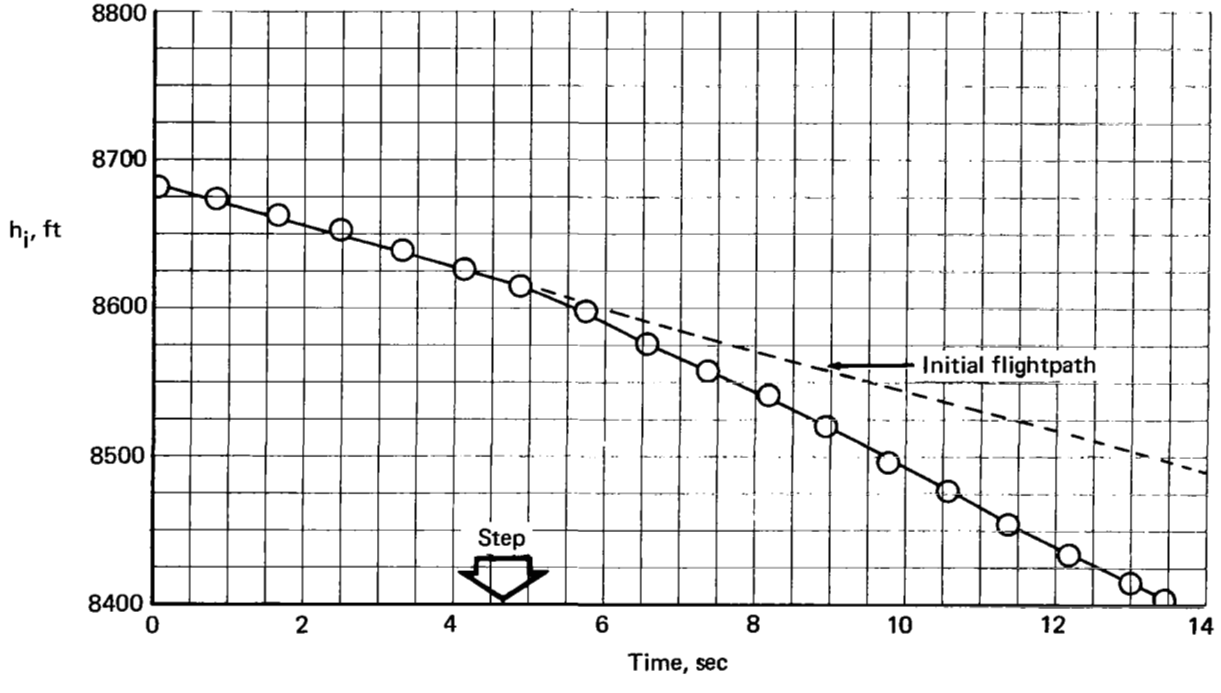

FIGURE 61.–ALTITUDE RESPONSE TO A 20° UP AUXILIARY FLAP STEP–50° MAIN FLAP AND 90% N_2 POWER; BLC ON

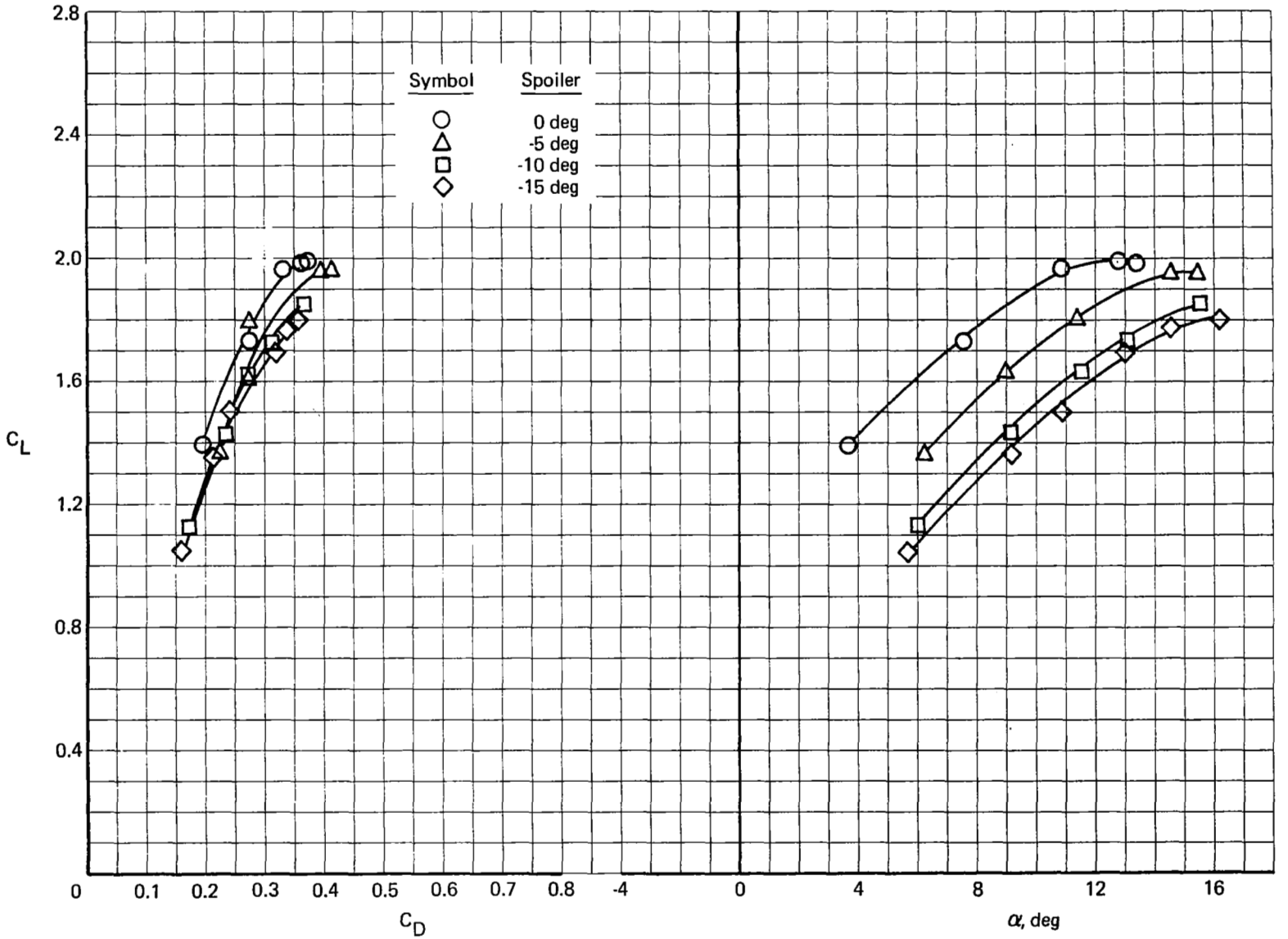

FIGURE 62.–DLC SPOILER CHARACTERISTICS–40° MAIN AND 10° AUXILIARY FLAPS AND 85% N_2 POWER; BLC ON

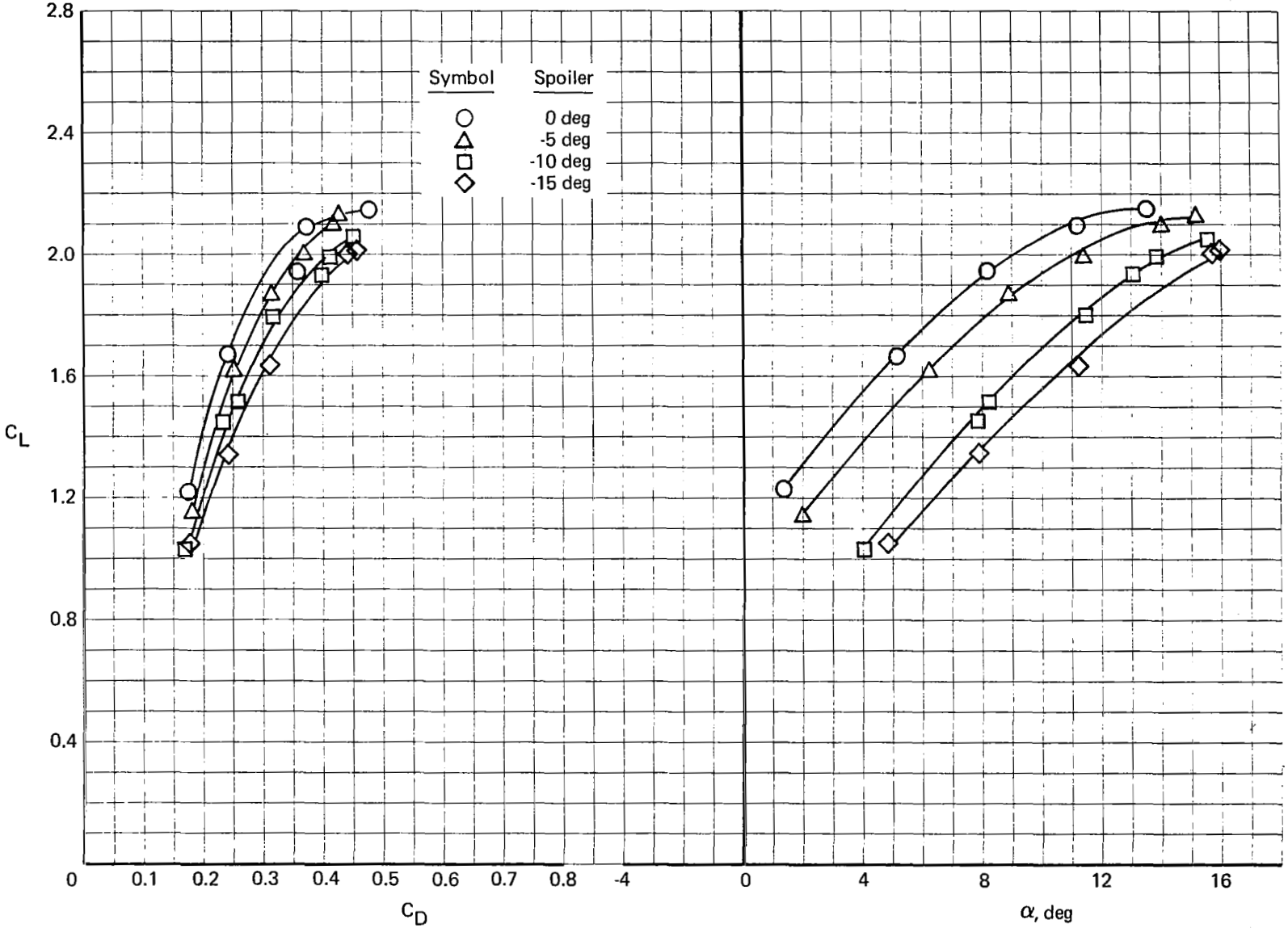

FIGURE 63.–DLC SPOILER CHARACTERISTICS–40° MAIN AND 10° AUXILIARY FLAPS AND 95% N_2 POWER; BLC ON

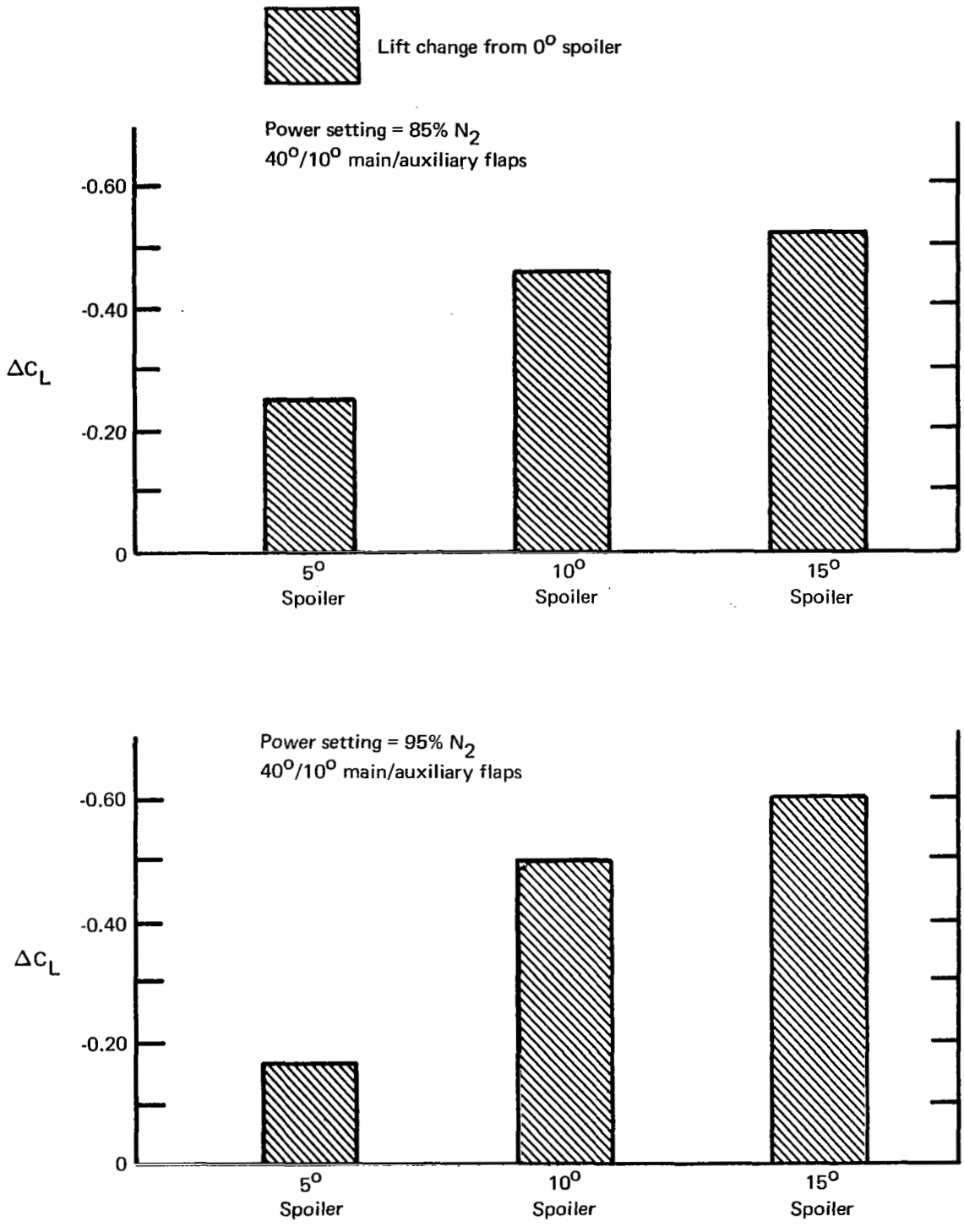

FIGURE 64.–TOTAL STEADY-STATE DLC SPOILER LIFT CAPABILITY AT CONSTANT ANGLES OF ATTACK FOR APPROACH

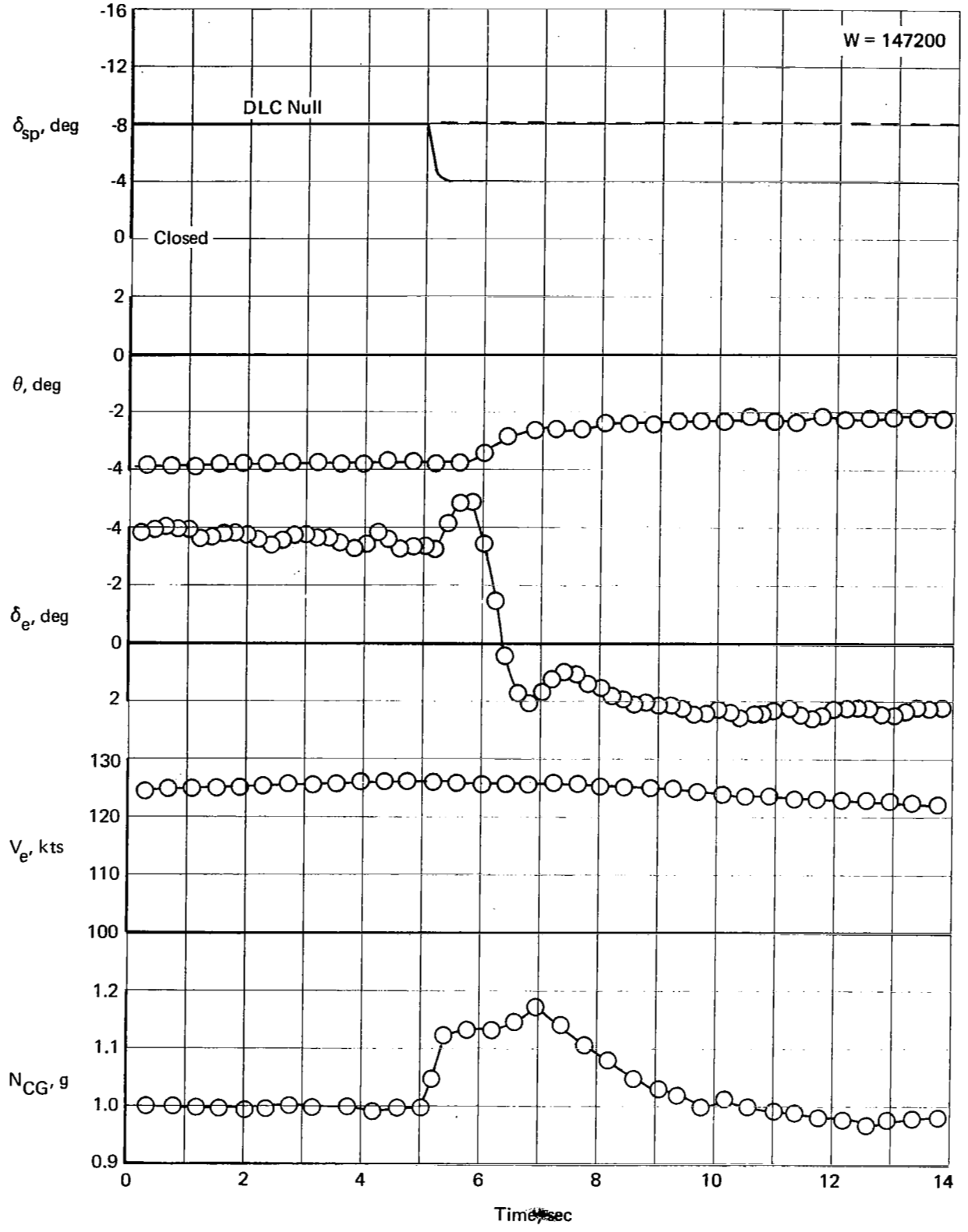

FIGURE 65.–AIRPLANE RESPONSE TO A 4° DOWN SPOILER STEP–40° MAIN AND 10° AUXILIARY FLAPS AND 90% N_2 POWER; BLC ON

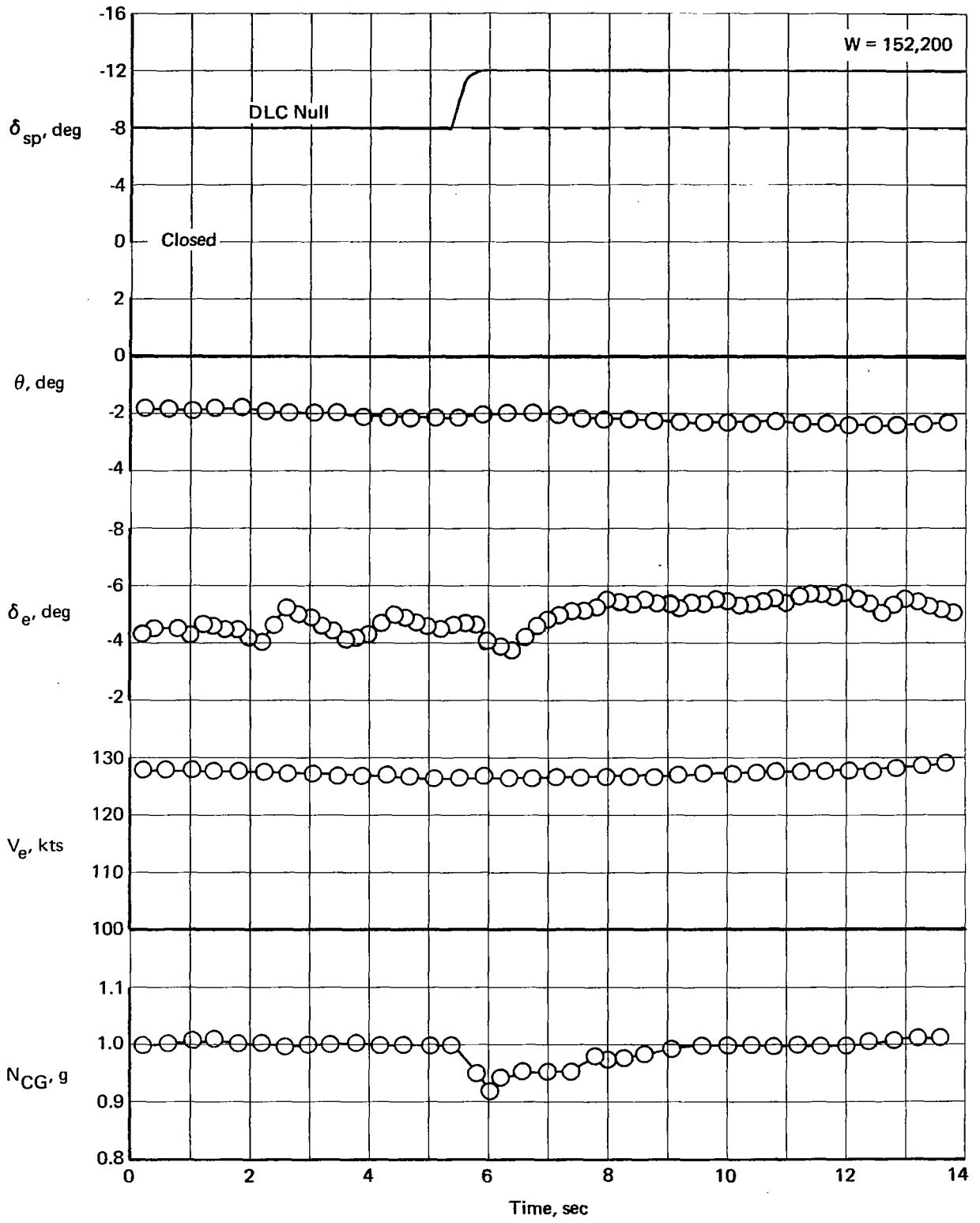

FIGURE 66.–AIRPLANE RESPONSE TO A 4° UP SPOILER STEP–40° MAIN AND 10° AUXILIARY FLAPS AND 90% N_2 POWER; BLC ON

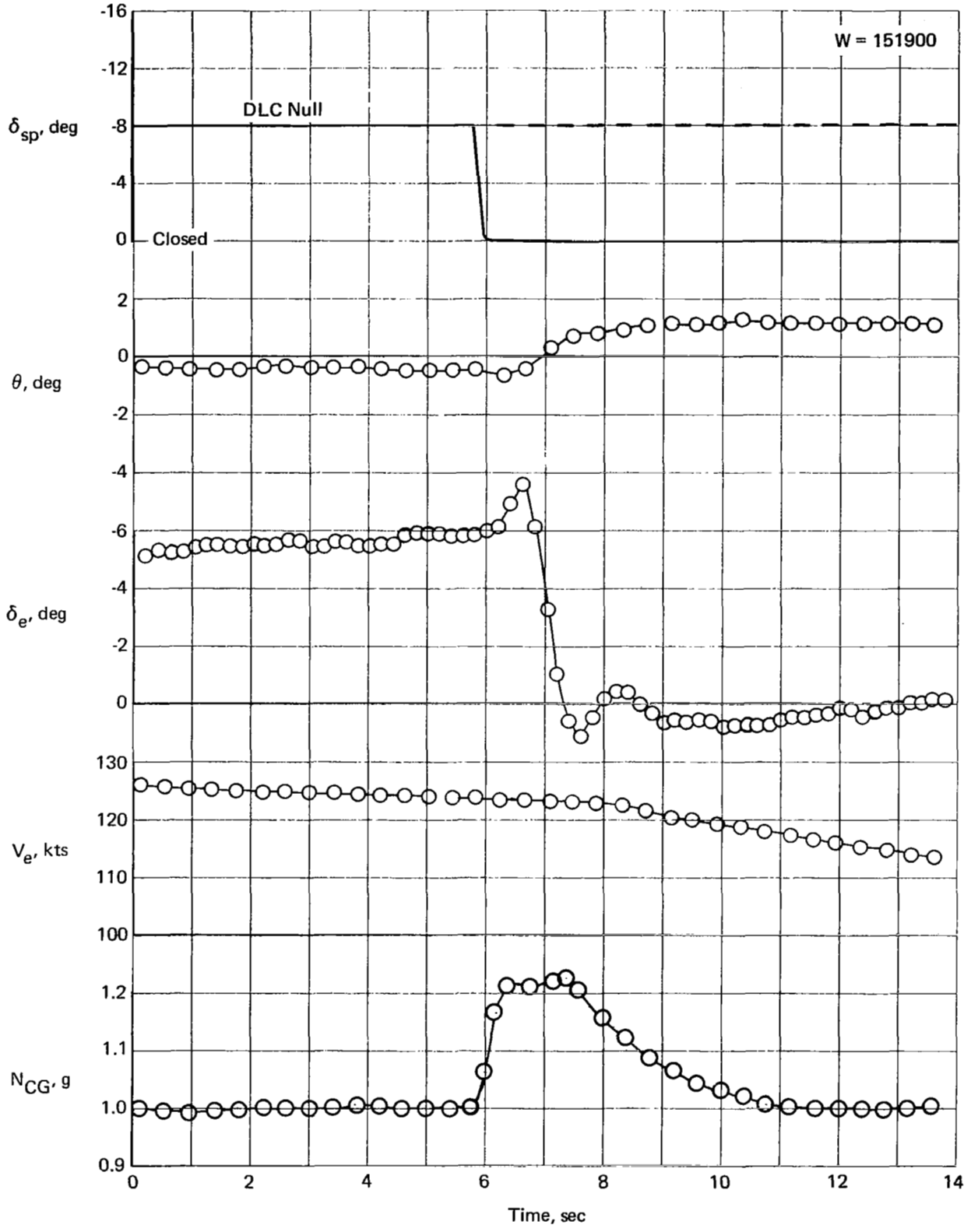

FIGURE 67.–AIRPLANE RESPONSE TO AN 8° DOWN SPOILER STEP–40° MAIN AND 10° AUXILIARY FLAPS AND 90% N_2 POWER; BLC ON

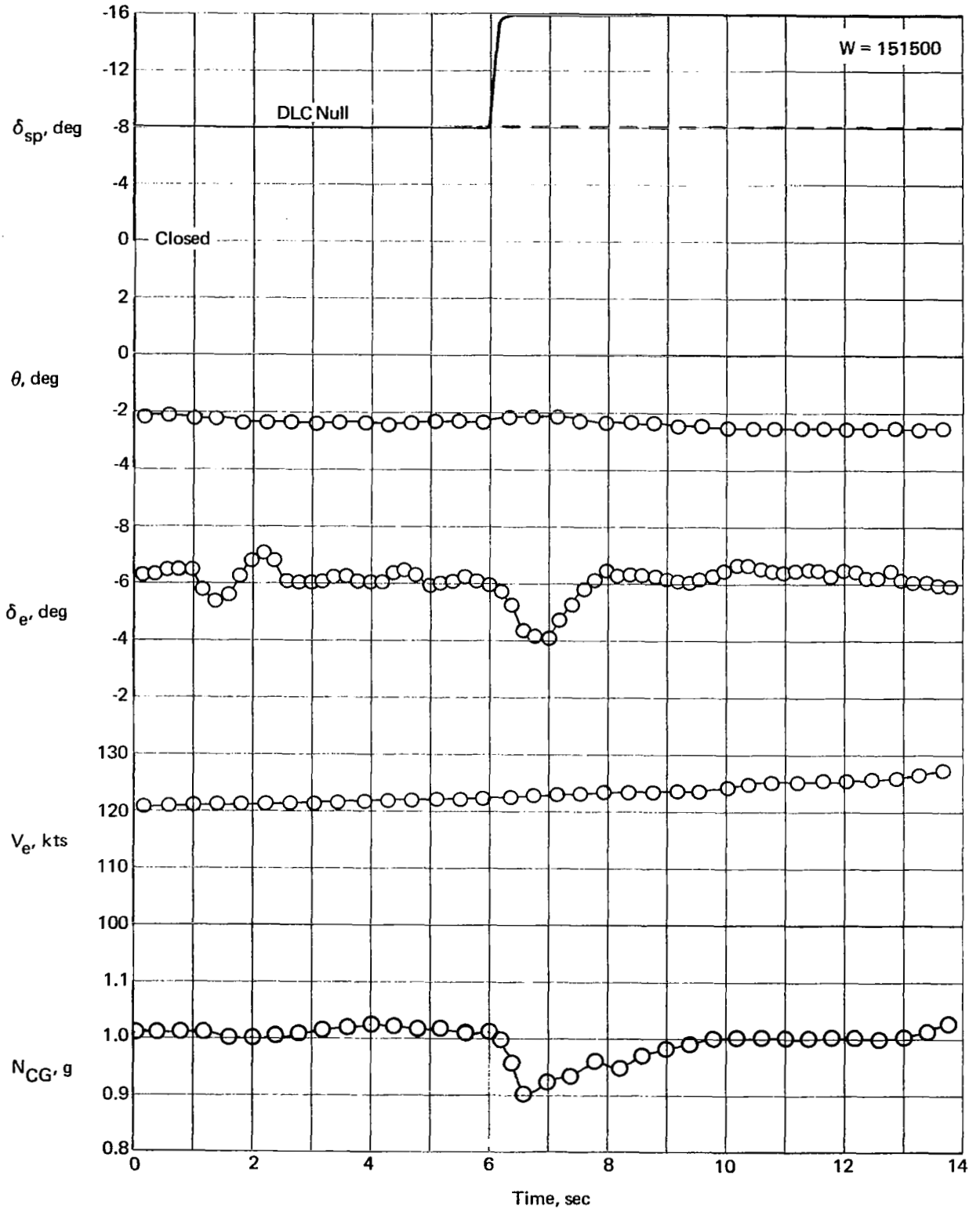

FIGURE 68.–AIRPLANE RESPONSE TO AN 8° UP SPOILER STEP–40° MAIN AND 10° AUXILIARY FLAPS AND 90% N_2 POWER; BLC ON

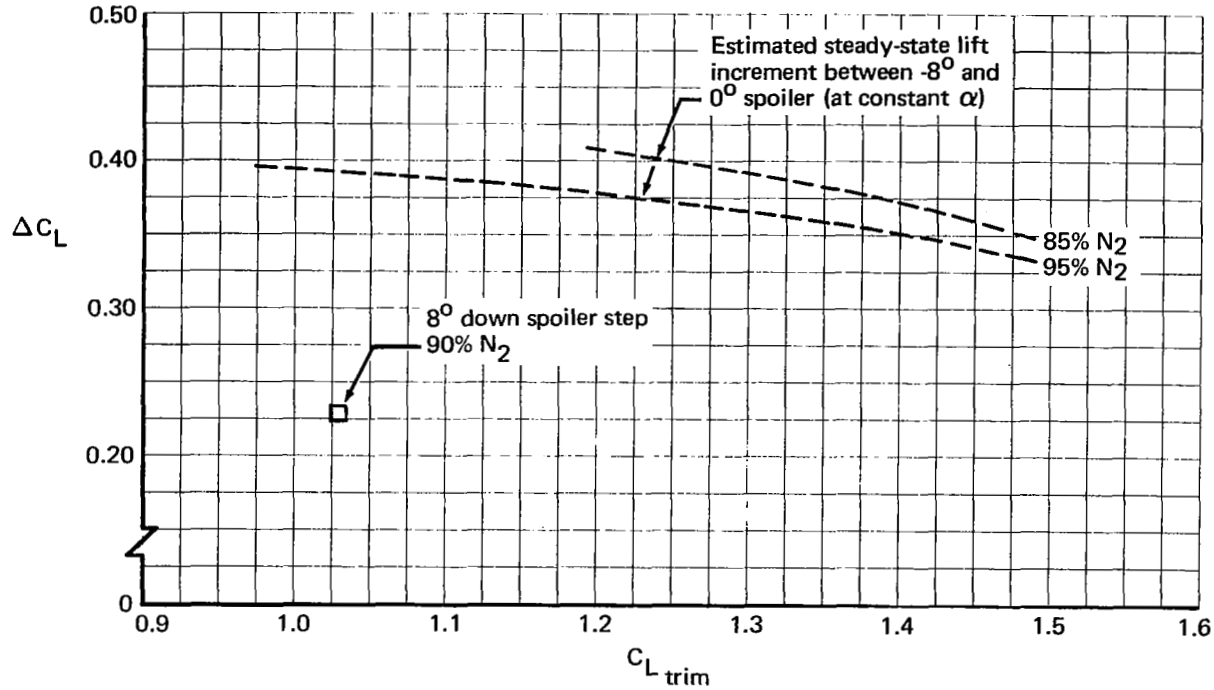

FIGURE 69.–COMPARISON OF DYNAMIC AND STEADY-STATE LIFT CHANGE WITH DOWN-SPOILER DEFLECTION–40° MAIN AND 10° AUXILIARY FLAPS; BLC ON

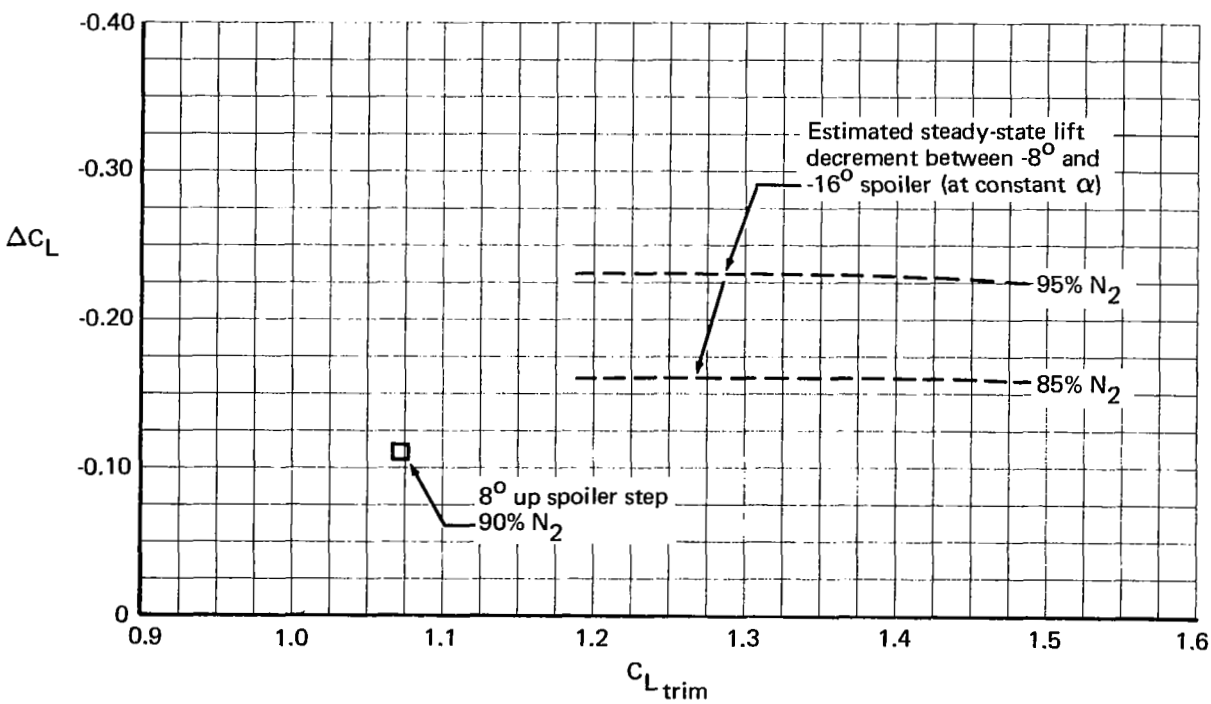

FIGURE 70.–COMPARISON OF DYNAMIC AND STEADY-STATE LIFT CHANGE WITH UP SPOILER DEFLECTION–40° MAIN AND 10° AUXILIARY FLAPS; BLC ON

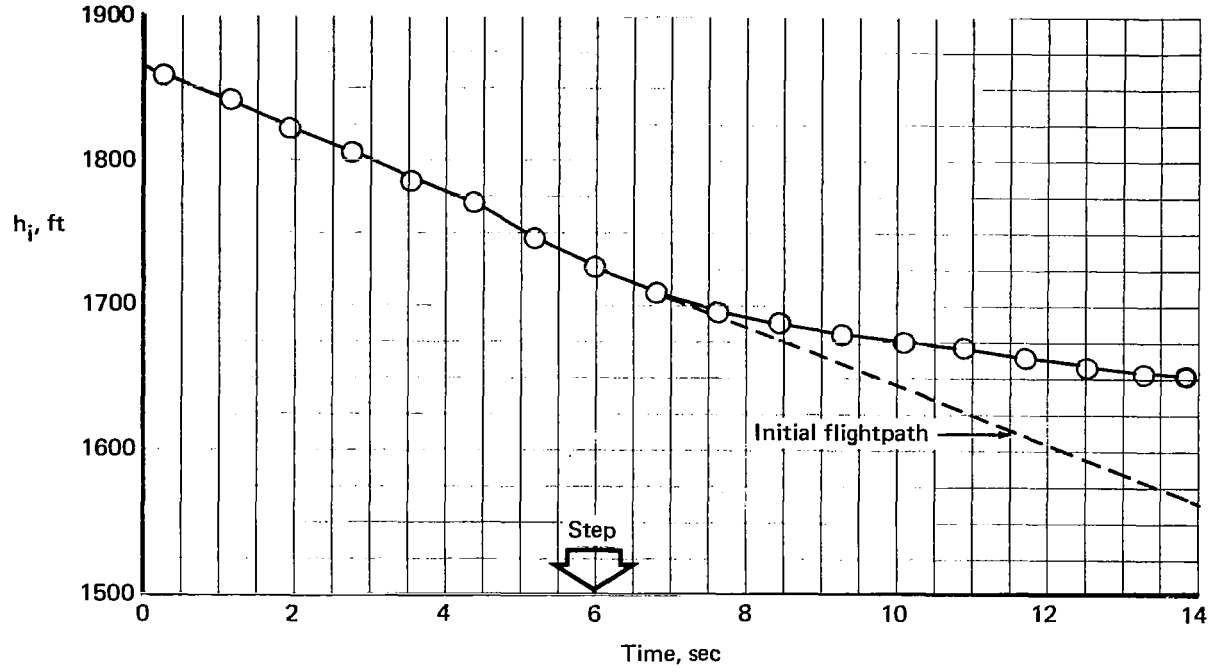

FIGURE 71.–ALTITUDE RESPONSE TO A 4° DOWN SPOILER STEP–40° MAIN AND 10° AUXILIARY FLAPS AND 90% N_2 POWER; BLC ON

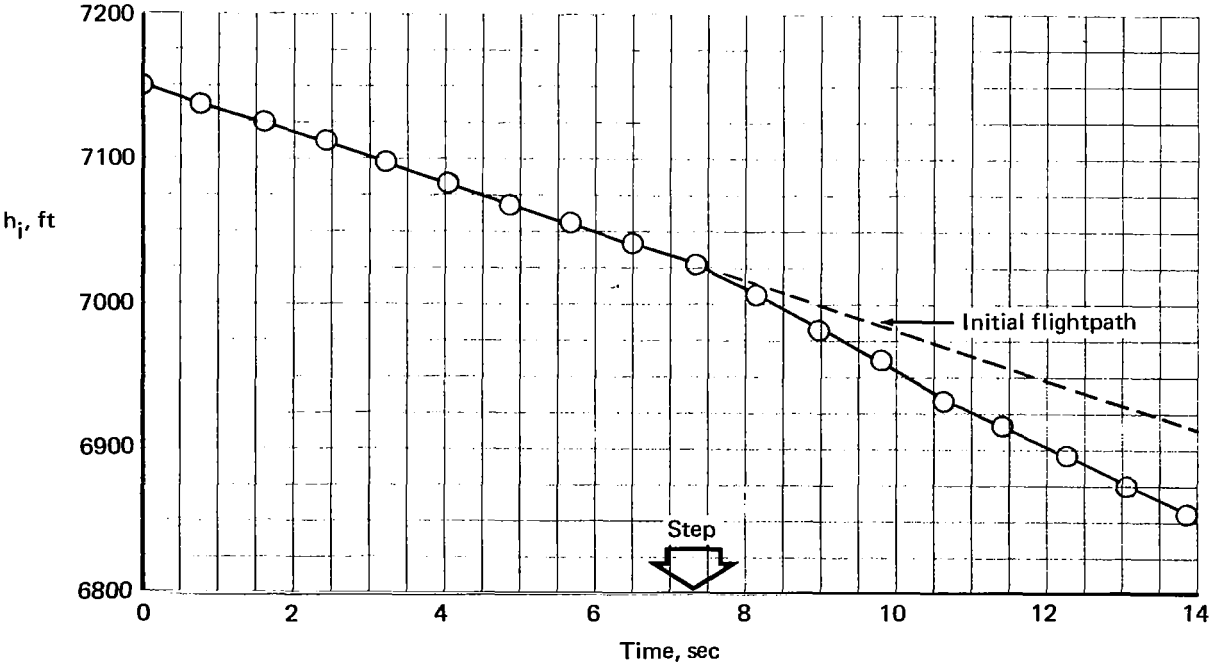

FIGURE 72.–ALTITUDE RESPONSE TO A 4° UP SPOILER STEP–40° MAIN AND 10° AUXILIARY FLAPS AND 90% N_2 POWER; BLC ON

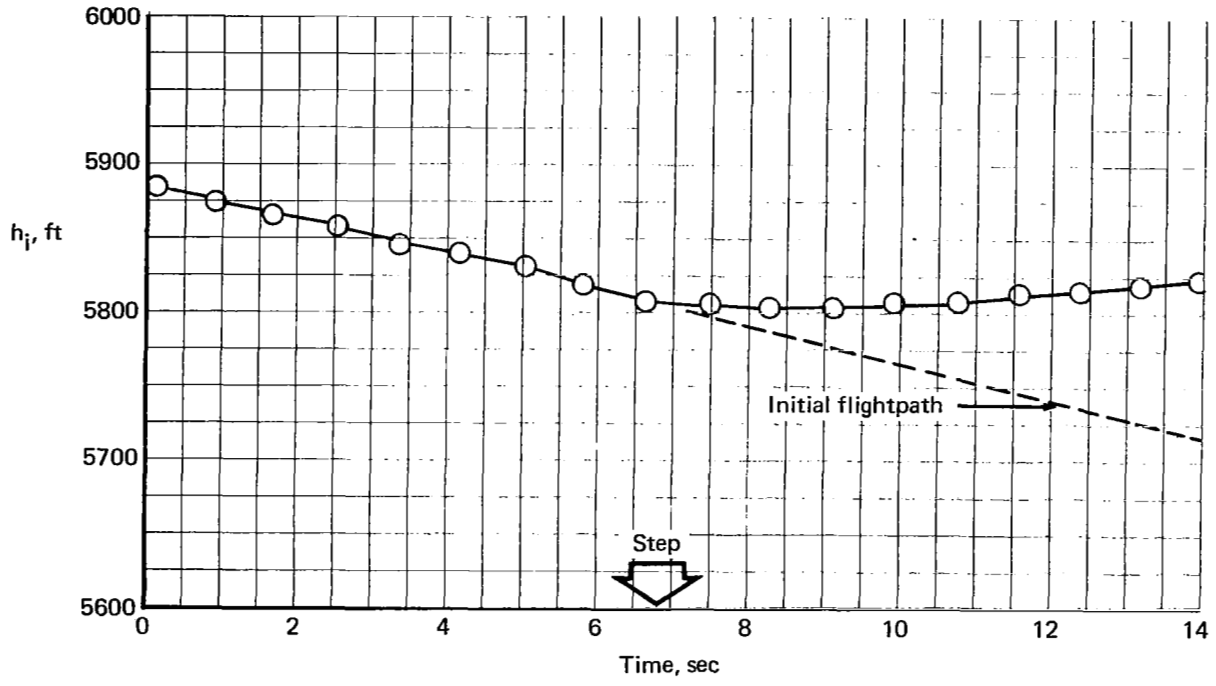

FIGURE 73.–ALTITUDE RESPONSE TO AN 8° DOWN SPOILER STEP–40° MAIN AND 10° AUXILIARY FLAPS AND 90% N_2 POWER; BLC ON

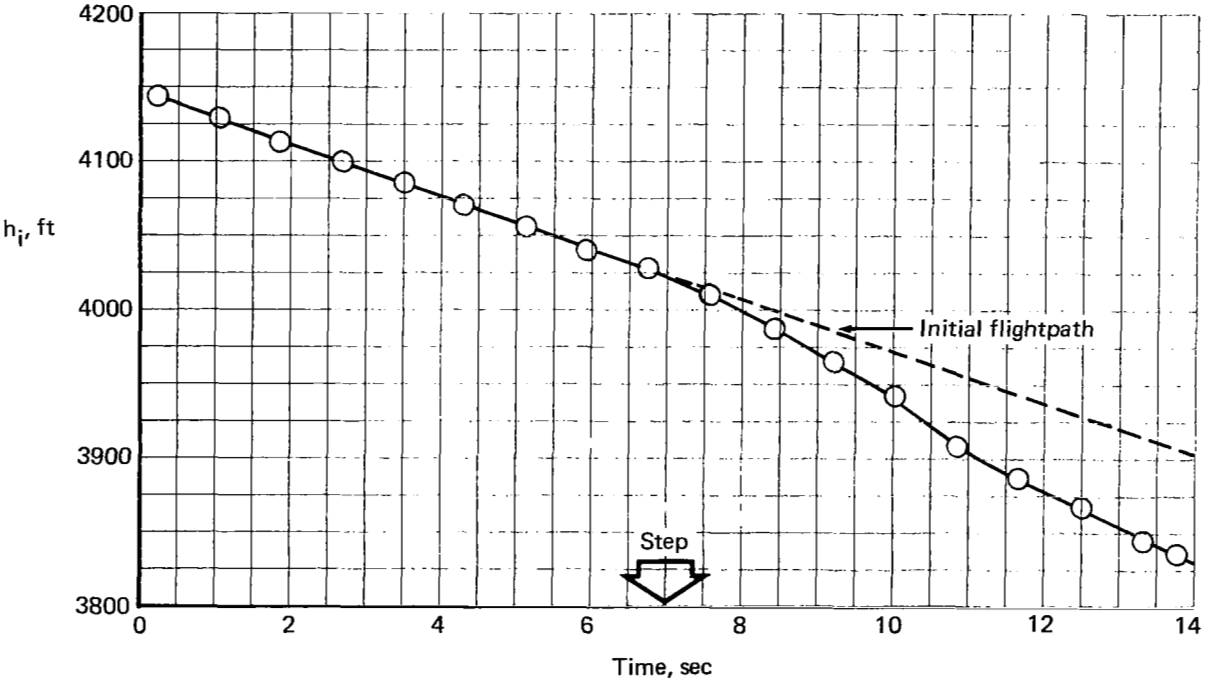

FIGURE 74.–ALTITUDE RESPONSE TO AN 8° UP SPOILER STEP–40° MAIN AND 10° AUXILIARY FLAPS AND 90% N_2 POWER; BLC ON

APPENDIX A

Engine Characteristics

Single engine thrust and airflow characteristics of the Pratt and Whitney JT3D-1 engine are presented in figs. A1 and A2. Data with and without BLC bleed are shown. The thrust and airflow values are referenced to the second-stage (high-pressure) compressor speed in terms of percentage of N_2, where 100 percent N_2 = 9655 rpm. Idle speed of the engine is about 57 percent N_2. The compressor speeds for MCT are dependent on exhaust gas temperature limits and, hence, outside air temperature, but are in general around the 95- to 98-percent N_2 level.

The thrust data are given in terms of gross thrust, i.e., the actual output of the engine. Net thrust, the propelling force on the airplane, is gross thrust less ram drag where ram drag is given by the equation

$$F_{ram} = 0.05245873 \ W_a \ V$$

where V = true airspeed (knots)
W_a = total airflow rate (lb/sec)

The airflow rate per engine may be determined from fig. A-2
where

$\sqrt{\theta_{t_2}}$ = square root of engine inlet temperature ratio

δ_{t_2} = engine inlet total pressure ratio

For general purposes, θ_{t_2} may be assumed equal to the ambient outside air temperature ratio, θ_{am}, while δ_{t_2} is nearly 1.0. The airflow rate decreases with BLC bleed because of a change in the speed ratio between the low- and high-pressure rotors.

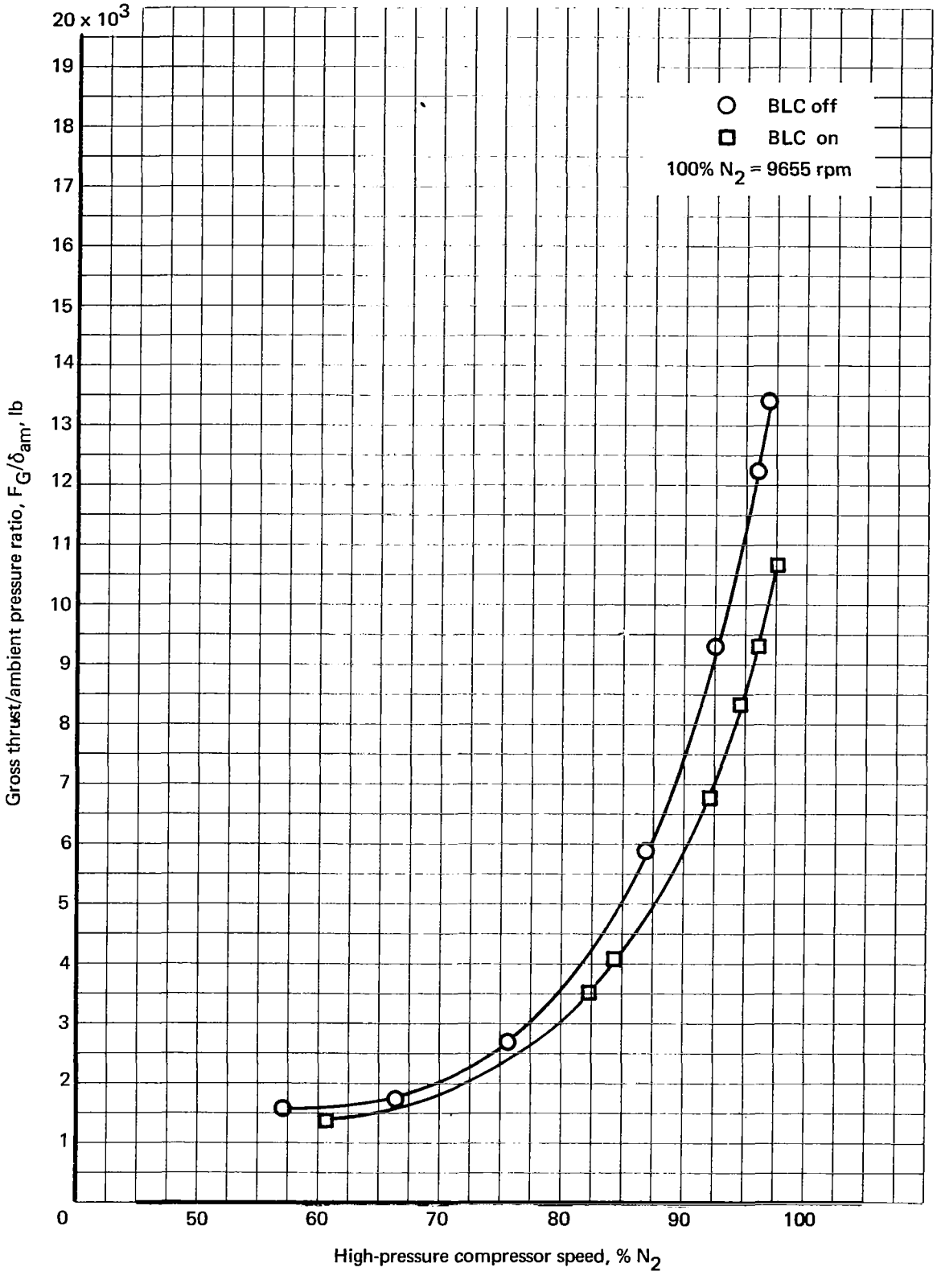

FIGURE A-1.–JT3D-1 ENGINE GROSS THRUST CHARACTERISTICS; BLC ON AND OFF

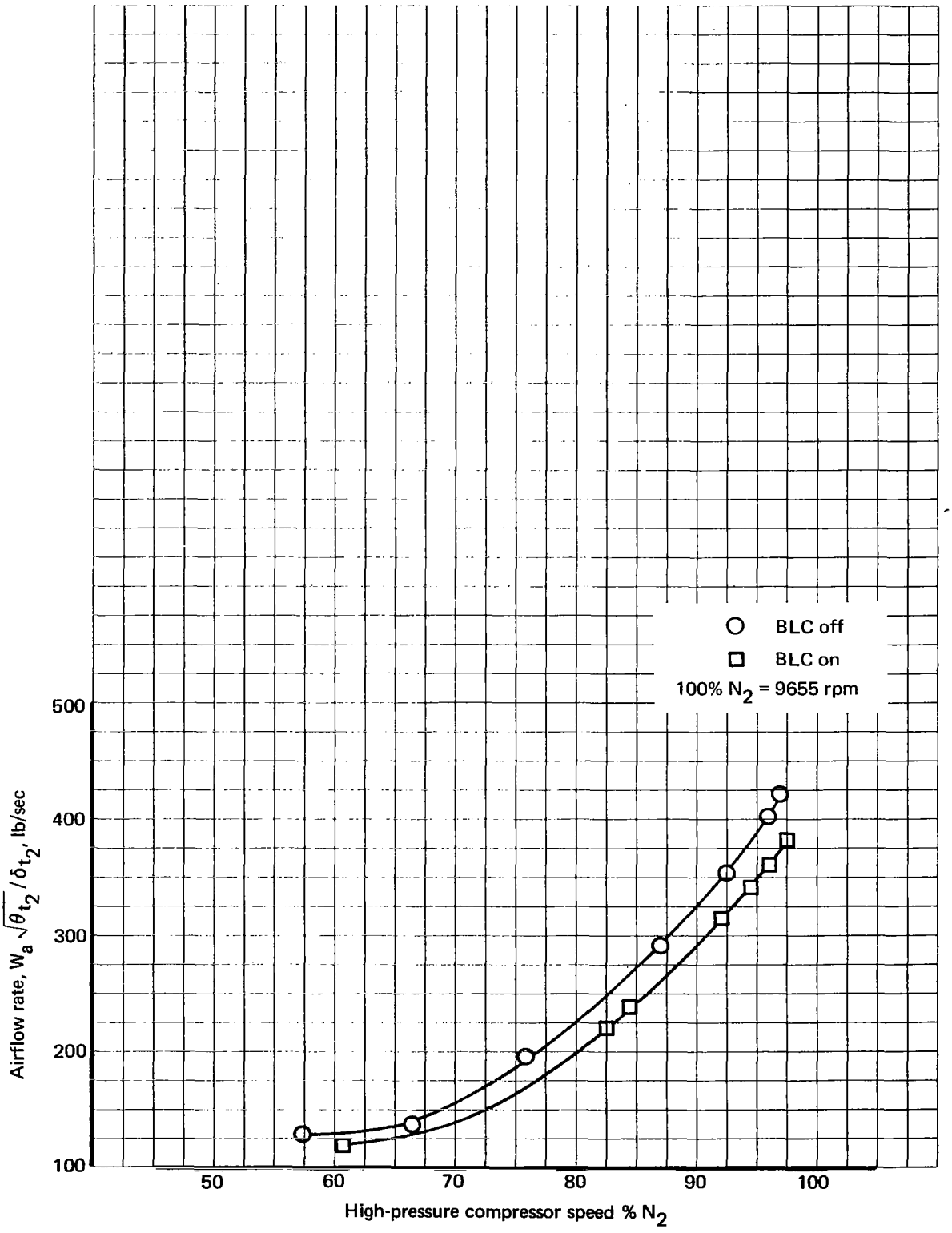

FIGURE A-2.–JT3D-1 ENGINE AIRFLOW CHARACTERISTICS; BLC ON AND OFF

APPENDIX B

Lift Coefficient Equation

Coefficient of lift values in the report were computed from the equation

$$C_L = \frac{W}{q_\infty S}\left[N\cos\alpha - \frac{\Sigma F_N \sin\alpha}{W}\right]$$

where
- N = normal acceleration (g units)
- q_∞ = freestream dynamic pressure (lb/sq ft)
- F_N = total airplane net thrust (lb)
- W = airplane gross weight (lb)
- S = wing area (sq ft)
- α = body angle of attack (deg)

Normal acceleration values were recorded at the airplane center of gravity by an accelerometer and were measured normal to the body axis. A pitot probe mounted at the top of the vertical fin measured static and total pressures for computation of dynamic pressure. The dynamic pressure values were corrected for compressibility effect, although this effect was almost negligible at the airspeeds tested. It may be noted that the above equation removes any thrust component acting in the lift direction but retains any BLC or impingement effect.

Drag Coefficient Equation

Coefficient of drag values were computed from the equations

$$D = \Sigma F_N \cos\alpha - \frac{W\,(dv/dt)}{g} - \frac{W\,(dh/dt)}{1.6878\,V}$$

and

$$C_D = \frac{D}{q_\infty S}$$

where
- V = true airspeed (knots)
- g = acceleration due to gravity (32.2 ft/sec^2)
- dv/dt = velocity change with time (ft/sec^2)
- dh/dt = tapeline altitude change with time (ft/sec)

The tapeline method of calculating dv/dt and dh/dt consisted of machine fitting a straight line to true airspeed and altitude versus time, respectively. The machine fit was made by connecting the first and last points of each test condition.

The above equations remove the direct net thrust component but include the indirect effects of impingement.

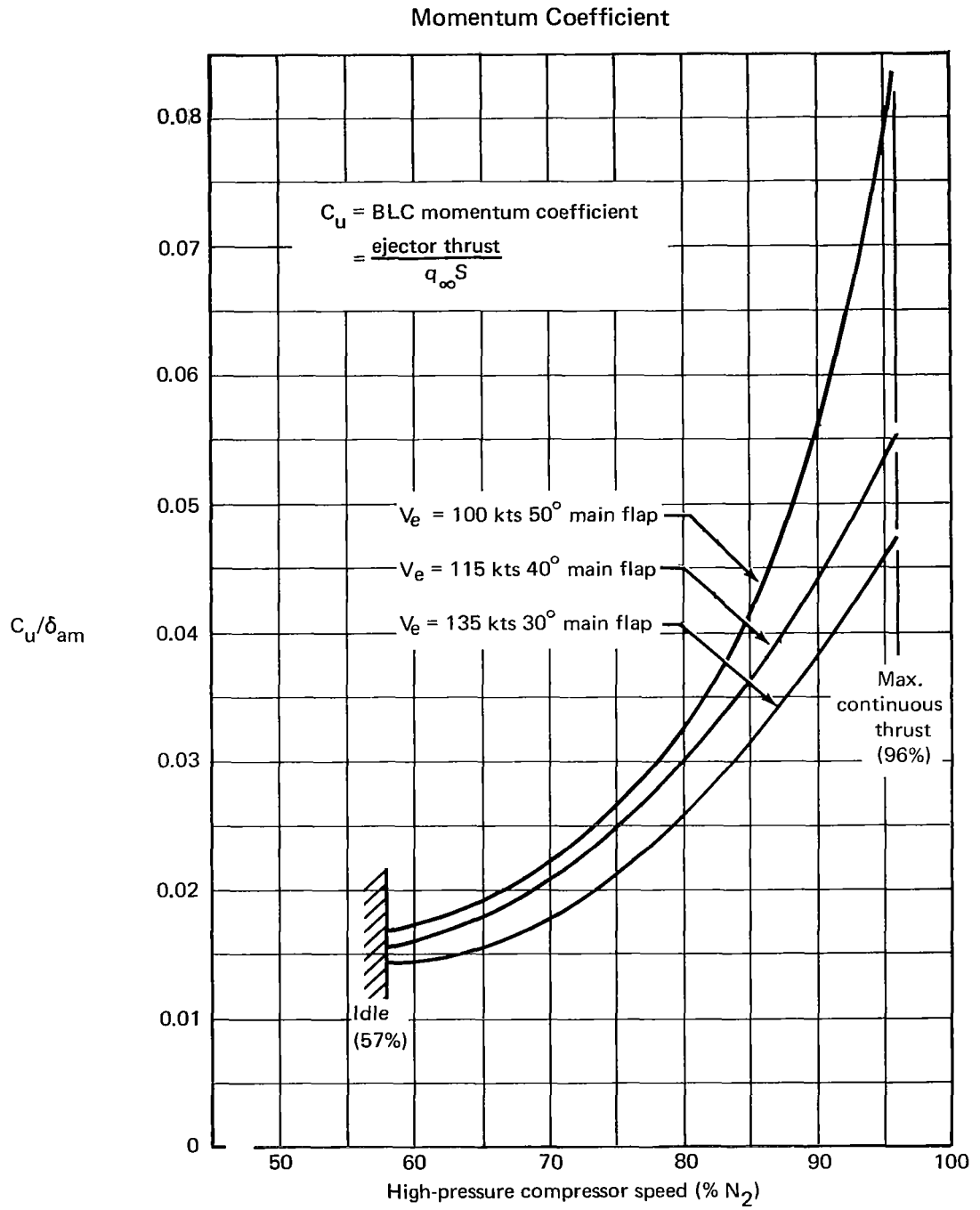

FIGURE B-1.–EFFECT ON MOMENTUM COEFFICIENT OF COMPRESSOR SPEED AND MAIN FLAP DEFLECTION

REFERENCES

1. Drake, Douglas E.: Direct Lift Control During Landing Approaches. AIAA Paper No. 65-316, July 26-29, 1965.

2. Nemoff, Commander Alfred J.: Direct Lift Control for the Landing Approach. The Society of Experimental Test Pilots Technical Review, Second Issue, Vol. 7, No. 4, 1965.

3. Flora, Clarence C.; Kriechbaum, Gerhard K.L.; and Willich, Wayne: A Flight Investigation of Systems Developed for Reducing Pilot Workload and Improving Tracking Accuracy During Noise Abatement Landing Approaches. NASA CR 1427 , 1969

4. Rolls, L. Stewart; Cook, Anthony M.; and Innis, Robert C.: Flight Determined Aerodynamic Properties of a Jet-Augmented, Auxiliary Flap, Direct-Lift-Control System Including Correlation with Wind-Tunnel Results. NASA TN D-5128, 1969.

5. Aoyagi, Kiyoshi; Dickinson, Stanley O.; and Soderman, Paul T.: Investigation of a .3-Scale Jet Transport Model Having a Jet-Augmented Boundary Layer Control Flap with Direct Lift Control. Proposed NASA TN D-5129,1969

6. Gratzer, L. B.; and O'Donnell, Thomas J.: Development of a BLC High Lift System for High Speed Airplanes. Journal of Aircraft, Vol. 2, No. 6, November-December, 1965, pp. 477-484.

7. Boeing -80 Project and Staff Engineering Group: Detail Design and Installation of a Direct-Lift Control Flap for the 367-80 Airplane. NASA CR-73292, 1969.